Dopaminergic modulation of *Drd1a-Cre+* neuronal network activity in the murine medial prefrontal cortex

A thesis presented by

Mohammed Abuelem

to

the Department of Physiology, Anatomy and Genetics

in fulfillment of the requirements

for the degree of

Master's in Science by Research

University of Oxford

St John's College

October 2024

Acknowledgements

Many notable individuals have generously supported me throughout this thesis project. I am grateful for the opportunity to learn from Prof. Edward Mann and Prof. Zoltán Molnár and conduct research under their mentorship. Thank you for taking me under your wing and guiding me as a young researcher. I truly appreciate all your academic and personal support. My research experience in your labs has refined my experimental and analytical skills, and it motivated me to pursue a PhD in neuroscience.

To all members of the Mann and Molnár labs, thank you for warmly welcoming me during my transition to Oxford and supporting me in my research efforts. I would like to especially thank Dr. Fernando Messore and Dr. Mohamed Ibrahim for their generosity and patience in guiding me as I learned new electrophysiology lab techniques. Your positivity, kindness, and humor really made my MSc experience enjoyable. I would also like to extend my appreciation to St. John's College and the Department of Physiology, Anatomy, and Genetics for providing a suitable environment to conduct my MSc studies.

I would also like to thank Prof. Armin Lak and Prof. Stephanie Cragg for conducting my Transfer of Status examination and providing helpful feedback on my thesis project, along with Prof. Armin Lak and Prof. Paul Anastasiades for agreeing to be my thesis examiners.

Finally, I am forever grateful for the tremendous love and support from my family and friends. I am deeply grateful for your presence in my life.

List of Contributions

This thesis project was jointly conceived by Prof. Z. Molnár and Prof. E. Mann, and designed by M. Abuelem, Dr. F. Messore, Prof. Z. Molnár, and Prof. E. Mann. Lab space and equipment was jointly provided by Prof. E. Mann and Prof. Z. Molnár at the University of Oxford Department of Physiology, Anatomy, and Genetics. Animal breeding and colonies were managed by Dr. F. Messore. All MEA and patch clamp experiments were conducted by M. Abuelem. Electrophysiological analyses and statistical analyses were done by M. Abuelem, and the Igor, MATLAB, and Python scripts were written by Prof. E. Mann, Dr. F. Messore, and M. Abuelem. Data and results were interpreted by M. Abuelem with assistance and guidance from Prof. E. Mann, Prof. Z. Molnár, and Dr. F. Messore.

Abstract

Cortical layer 6 (L6) neurons play an important role in driving cortical arousal via the higher-order corticothalamic system. In the murine somatosensory cortex, L6-Drd1a neurons (which express the dopamine D1 receptor) selectively project to higher-order thalamic nuclei and are highly sensitive to the wake-promoting neuropeptide orexin, likely playing an important role in cortical arousal, sensory valence processing, and anxiety behavior (Hoerder-Suabedissen et al., 2018; Zolnik et al., 2023). Whether these L6-Drd1a neurons play an analogous role in driving cortical arousal through a dopaminergic modulatory mechanism in the medial prefrontal cortex (mPFC) remains poorly understood. To test this hypothesis, we investigated the effects of 'silencing' L6-Drd1a neurons using a Snap25 conditional knockout mouse model (Drd1a-Cre$^{+/-}$;Snap25$^{fl/fl}$;tdTomato$^{STOPfl/fl}$) on the dopaminergic modulation of network activity in mPFC acute slices using high-density planar multielectrode arrays (MaxWell Biosystems) and whole-cell patch clamp recordings. We found that D1 receptor agonist SKF-81297 significantly increased broadband local field potential (LFP) activity in the infralimbic mPFC, which was eliminated upon chronic 'silencing' of L6-Drd1a neurons. On the other hand, D2 receptor agonist quinpirole only increased infralimbic network activity in L6-Drd1a 'silenced' slices. Subsequent whole-cell electrophysiological characterization of L6 neurons in the mPFC revealed that D1 receptor activation selectively increased L6-Drd1a intrinsic excitability and spontaneous synaptic potential amplitude, while D2 receptor activation non-selectively excited L6 neurons. Taken together, these results suggest a postsynaptic mechanism of D1 receptor activation that increases L6-Drd1a excitability to drive mPFC network arousal, along with a compensatory mechanism of D2 receptor activation in the functional absence of these L6-Drd1a neurons. Our findings

provide novel insight into the dopaminergic modulation of L6-Drd1a neurons in the mPFC that likely contributes to their orexinergic gating of cortical arousal, with relevant therapeutic implications for anxiety and stress-related disorders.

Table of Contents

Acknowledgements **2**

List of Contributions **3**

Abstract **4**

Table of Contents **6**

List of Figures **8**

Abbreviations **9**

I. General Introduction **11**

1.1 The transient cortical sublate 11

1.2 L6-Drd1a neurons drive cortical arousal through the higher-order corticothalamic system 15

1.3 Dopamine pathways and receptors 17

1.4 Dopamine signaling in the PFC 22

1.5 Hypothesis and specific aims 25

II. General Methods **27**

2.1 Transgenic animal breeding and housing 27

2.2 Acute slice preparation 29

2.3 Pharmacology 30

2.4 Statistical analyses 31

III. Chronically 'silencing' L6-Drd1a neurons alters dopaminergic modulation of local mPFC network activity **32**

3.1 Introduction 32

3.1.1 L6-Drd1a structural and functional connectivity *32*

3.1.2 L6b neuromodulation *35*

3.1.3 'Silencing' neurons via Snap25 conditional knockout *38*

3.2 Materials and Methods 40

3.2.1 Electrophysiology recordings and signal processing *40*

3.2.2 Data analysis *41*

3.3 Results 42

3.3.1 D1 receptor activation increases infralimbic mPFC network activity in the presence of functionally active L6-Drd1a neurons *42*

3.3.2 Chronically 'silencing' L6-Drd1a neurons eliminates network activity response to D1 receptor activation *44*

3.3.3 D2 receptor activation exerts no significant effects on local mPFC network activity in the presence of functionally active L6-Drd1a neurons *46*

3.3.4 Chronically 'silencing' L6-Drd1a neurons unmasks a D2 receptor-mediated increase in infralimbic mPFC network activity *48*

3.4 Discussion 50

3.4.1 The role of L6-Drd1a neurons in D1 receptor modulation of local mPFC network activity *51*

3.4.2 The role of L6-Drd1a neurons in D2 receptor modulation of local mPFC network activity *52*

3.4.3 Limitations and future directions *54*

IV. Dopaminergic modulation of L6-Drd1a and L6-non-Drd1a neurons in the mPFC 56

4.1 Introduction 56

4.1.1 L6b neuronal cell types and electrophysiological properties *56*

4.1.2 Dopaminergic modulation of PFC neurons in-vitro *61*

4.2 Materials and Methods 64

4.2.1 Electrophysiology recordings and signal processing *64*

4.2.2 Data analysis *66*

4.3 Results 67

4.3.1 D1 receptor activation selectively increases L6-Drd1a intrinsic neuronal excitability in the mPFC *68*

4.3.2 D2 receptor activation exerts non-selective effects on L6 intrinsic neuronal excitability in the mPFC ... *71*

4.3.3 D1 receptor activation selectively increases amplitude of spontaneous excitatory synaptic potentials in mPFC L6-Drd1a neurons *73*

4.3.4 D2 receptor activation does not significantly alter spontaneous synaptic potentials in mPFC L6 neurons *75*

4.4 Discussion 77

4.4.1 Dopaminergic modulation of L6 intrinsic neuronal excitability in the mPFC *77*

4.4.2 Dopaminergic modulation of L6 spontaneous synaptic potentials in the mPFC *79*

4.4.3 Limitations and future directions *80*

V. General Discussion 82

5.1 L6-Drd1a neurons mediate dopaminergic modulation of local mPFC network activity 83

5.2 D1 receptor activation selectively excites L6-Drd1a neurons while D2 receptor generally excites L6 neurons in the mPFC 85

5.3 Limitations and future directions 86

5.4 Conclusion 87

References 89

List of Figures

Figure 1.1. The subplate in the developing human and macaque cerebral cortex.

Figure 1.2. L6-Drd1a neurons selectively target higher-order thalamic nuclei and are sensitive to orexin.

Figure 1.3. Dopaminergic nuclei and pathways in the rodent brain.

Figure 1.4. Intracellular dopamine signaling mechanisms.

Figure 2.1. Drd1a-Cre$^{+/-}$;Snap25$^{fl/fl}$ conditional knockout mouse model genetic construct.

Figure 3.1. Summary of L6b anatomical and functional connectivity in S1.

Figure 3.2. *In-vitro* MEA experimental protocol.

Figure 3.3. D1 receptor activation significantly increases broadband LFP activity in the infralimbic mPFC in the presence of functionally active L6-Drd1a neurons.

Figure 3.4. Chronically 'silencing' L6-Drd1a neurons eliminates broadband LFP activity response to D1 receptor activation.

Figure 3.5. D2 receptor activation exerts no significant changes in local mPFC network activity in the presence of functionally active L6-Drd1a neurons.

Figure 3.6. Chronically 'silencing' L6-Drd1a neurons unmasks a D2 receptor-mediated increase in infralimbic mPFC network activity.

Figure 4.1. Morphological diversity among L6b excitatory neurons.

Figure 4.2. Summary of D1 and D2 receptor modulation in PFC circuits.

Figure 4.3. *In-vitro* whole-cell patch clamp experimental protocol.

Figure 4.4. D1 receptor activation selectively increases L6-Drd1a intrinsic neuronal excitability in the mPFC.

Figure 4.5. D2 receptor activation exerts non-selective effects on L6 intrinsic neuronal excitability in the mPFC.

Figure 4.6. D1 receptor selectively increases sEPSP amplitude in mPFC L6-Drd1a neurons.

Figure 4.7. D2 receptor activation does not significantly alter sEPSPs in mPFC L6 neurons.

Abbreviations

4-AP	4-aminopyridine
ACA	Anterior cingulate area (of the mPFC)
aCSF	Artificial cerebrospinal fluid
AMPA	α-amino-3-hydroxy-5-methyl-4-isoxazolepropionic acid
cAMP	Cyclic adenosine monophosphate
Ca_V1	N-type voltage-gated calcium channel
$Ca_V2.2$	L-type voltage-gated calcium channel
Cplx3	Complexin-3
Ctgf	Connective tissue growth factor
D1-D5	Dopamine receptor subtypes 1-5
DARPP-32	Dopamine and cAMP-regulated phosphoprotein
DAG	Diacylglycerol
DAT	Dopamine transporter
Drd1a	Dopamine receptor 1a
EPSP	Excitatory postsynaptic potential
ET	Extratelencephalic
GABA	γ-aminobutyric acid
GAD67	Glutamate decarboxylase 67
GIRK2	G protein-regulated inward-rectifier potassium channel 2
ILA	Infralimbic area (of the mPFC)
IP_3	Inositol triphosphate
IPSC	Inhibitory postsynaptic current
IPSP	Inhibitory postsynaptic potential
IT	Intratelencephalic
K_{ir}	Inwardly-rectifying potassium channel
L6/6b	Layer 6/6b
LFP	Local field potential
Lpar1	Lysophosphatidic acid receptor 1
M2	Secondary motor cortex
mAChR	Muscarinic acetylcholine receptor
MEA	Multielectrode array
mPFC	Medial prefrontal cortex
nAChR	Nicotinic acetylcholine receptor
NMDA	*N*-methyl-D-aspartate
NMDG	N-methyl-D-glucamine
NPY	Neuropeptide Y
Ntsr1	Neurotensin receptor 1
Nurr1	Orphan nuclear receptor Nr4a2
OX1R	Orexin receptor type 1
OX2R	Orexin receptor type 2
PCW	Postconception week
PFC	Prefrontal cortex

PKA	Protein kinase A
PKC	Protein kinase C
PL	Prelimbic area (of the mPFC)
PLC	Phospholipase C
POm	Posteromedial thalamus
PP1	Protein phosphatase 1
PP2B	Protein phosphatase 2B
PV	Parvalbumin
Rbp4	Retinol binding protein-4
S1	Primary somatosensory cortex
sEPSP	Spontaneous excitatory postsynaptic potential
SN	Substantia nigra
Snap5	Synaptosomal-associated protein 25
SST	Somatostatin
Tbr1	T-box brain transcription factor 1
TH	Tyrosine hydroxylase
TRN	Thalamic reticular nucleus
t-SNARE	Target membrane-bound SNARE
TTX	Tetrodotoxin
VIP	Vasoactive intestinal peptide
v-SNAPRE	Vesicle-bound SNARE
VTA	Ventral tegmental area

I. General Introduction

The dynamic processes that govern cortical circuit development offer valuable insights into the functional modulation of cortical network activity and the etiology and pathogenesis of related neurodevelopmental disorders. The mammalian cerebral cortex is a laminar structure composed of six layers, with the deepest layer resembling the earliest generated cortical neurons involved in thalamocortical and intracortical circuit development. The prefrontal cortex (PFC) in particular plays an important role in higher cognitive functioning and emotional processing, and PFC circuits are highly responsive to dopamine (Miller & Cohen, 2001; Seamans & Yang, 2004). In this thesis, we investigate the dopaminergic modulation of a subpopulation of neurons in these deep layers of the PFC that selectively project to higher-order thalamic nuclei (Hoerder-Suabedissen et al., 2018; Zolnik et al., 2020, 2023), which we hypothesize is likely contributing to their selective response to the wake-promoting neuropeptide orexin in driving cortical arousal (Bayer et al., 2004; Zolnik et al., 2023; Messore et al., 2024).

1.1 The transient cortical sublate

The laminar structure of the mammalian cerebral cortex generally develops in an inside-first, outside-last manner. The earliest stage of corticogenesis involves the preplate, which contains differentiated neurons superficial to the asymmetrically-dividing radial glial progenitor cells in the ventricular zone (Kostovic & Rakic, 1990; Allendoerfer & Shatz, 1994). As neural precursors in the ventricular zone differentiate into postmitotic neurons, they migrate vertically along the radial glial progenitors to form the cortical plate such that the earliest postmitotic neurons settle in the deepest layers of the cortical plate. This process splits the preplate into the

superficial marginal zone above the cortical plate and the subplate zone below (Marin-Padilla, 1971; Allendoerfer & Shatz, 1994). Notably, the marginal zone contains Cajal-Retzius cells that express reelin, which is a secreted molecule essential for normal cortical lamination (Caviness & Sidman, 1973).

The subplate zone contains some of the earliest generated cortical neurons involved in the establishment of thalamocortical and intracortical circuits. Subplate neurons are the first cortical neurons to project axons across the pallial-subpallial boundary and form a "handshake" with incoming thalamocortical axons (McConnell et al., 1989; De Carlos & O'Leary, 1992; Molnár & Blakemore, 1995; López-Bendito & Molnár, 2003), which is necessary for these thalamic afferents to then cross the pallial-subpallial boundary (Kanold & Luhmann, 2010; Magnani et al., 2013; Hevner et al., 2001; Doyle et al., 2021). Within the cortex, subplate neurons are essential for correct thalamic axonal targeting and patterning of primary sensory areas (Ghosh et al., 1990; Kanold & Luhmann, 2010).

Subplate neurons are also heterogeneous and exhibit molecular diversity. Postnatal subplate markers include connective tissue growth factor (Ctgf), the presynaptic protein complexin-3 (Cplx3), the orphan nuclear receptor Nr4a2 (Nurr1), and the G protein-coupled lysophosphatidic acid receptor 1 (Lpar1/Edg2) (Heuer et al., 2003; Arimatsu et al., 2003; Hoerder-Suabedissen et al., 2009; Hoerder-Suabedissen & Molnár, 2013). Furthermore, more than one-quarter of subplate neurons are derived from symmetrically-dividing intermediate progenitor cells in the subventricular zone, distinct from the asymmetrically-dividing radial glial progenitors in the underlying ventricular zone (Vasistha et al., 2014). Inhibitory interneurons generated from the ganglionic eminences also tangentially migrate through the subplate before reaching their final cortical destinations (Anderson et al., 1997). This diversity is also evidenced

by little overlap in the expressed subplate genes at embryonic and postnatal stages, highlighting the changing roles of the subplate throughout development and the importance of studying developmental-specific mechanisms in the pathophysiology of neurodevelopmental disorders associated with the subplate (Hoerder-Suabedissen et al., 2009; Hoerder-Suabedissen & Molnár, 2013; Osheroff & Hatten, 2009; Oeschger et al., 2012; McKellar & Shatz, 2009).

The transient subplate is largely an embryonic structure. It forms around 12-15 post-conception weeks (PCWs) in humans and embryonic day E54-E59 in monkeys. During this formation stage, a thin and cell sparse lower subplate can be distinguished from a thicker and denser upper subplate, and both can be distinguished from the very cell dense cortical plate above (Hoerder-Suabedissen & Molnár, 2015). From 15-35 PCWs in humans and E59-E120 in monkeys, the subplate expands in size and becomes a waiting compartment for ingrowing thalamocortical axons, basal forebrain cholinergic afferents, and corticocortical afferents (Figure 1.1) (Hoerder-Suabedissen & Molnár, 2015). Acetylcholinesterase staining further highlights a clear boundary between the subplate and intermediate zone (Hoerder-Suabedissen & Molnár, 2015). After 35 PCWs in humans and E120 in monkeys, most subplate neurons decline in number, with the rate of decline varying across brain regions and faster underneath sulci compared to gyri (Hoerder-Suabedissen & Molnár, 2015). This dissolution stage is concurrent with the secondary gyrification of the brain. The subplate neurons that survive into adulthood become interstitial white matter neurons (Kostovic & Rakic, 1980, 1990; Marx et al., 2017; Hoerder-Suabedissen & Molnár, 2015; Feldmeyer, 2023). In rodents, subplate neurons form during a short time window from E10.5-E12.5, but they are not easily identifiable until E16 because they lack a clear boundary with the intermediate zone (Hoerder-Suabedissen & Molnár, 2015). From birth, the subplate is clearly delineated from the overlying layer 6a and underlying

intermediate zone and white matter, and the subplate neurons that survive into adulthood maintain this dense compact cortical layer 6b (L6b) (Marx et al., 2017; Hoerder-Suabedissen & Molnár, 2013).

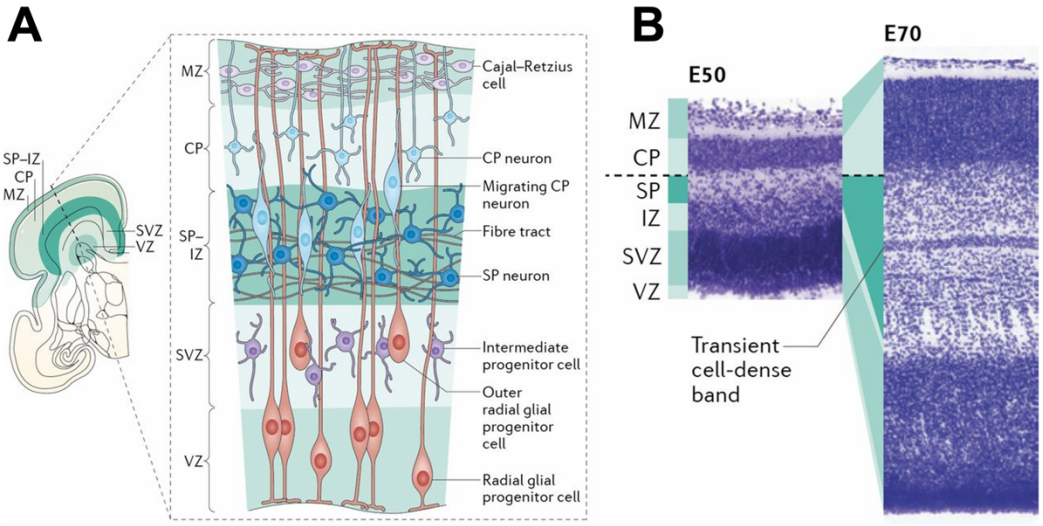


Figure 1.1. The subplate in the developing human and macaque cerebral cortex.
(Adapted from Hoerder-Suabedissen & Molnár, 2015).
(**A**) Coronal section of the developing human cortex at the peak of neurogenesis and migration at 26 PCWs. A magnified view of the cellular composition of the transient developmental zones shows the subplate (SP) located between the overlying cortical plate (CP) and marginal zone (MZ) and the underlying subventricular zone (SVZ) and ventricular zone (VZ). The boundary between the intermediate zone (IZ) and the SP can be difficult to discern, although the IZ contains denser fiber tracts while the SP contains more postmitotic neurons with distinguishable processes.
(**B**) Nissl-stained coronal sections from the macaque visual cortex at E50 and E70 show the prominent increase of the subplate zone during this midfetal period. Notably, at E70, a transient cell-dense band separates the subplate into upper and lower layers in the primary visual cortex.

Subplate neurons have important clinical implications as they are likely involved in neurodevelopmental conditions such as schizophrenia and autism (Kostovic, 2024). Postmortem human brain tissue from individuals with schizophrenia reveal an altered distribution of interstitial white matter neurons identified by nicotinamide adenine dinucleotide phosphate diaphorase staining in the dorsolateral PFC and temporal lobe (Akbarian et al. 1993a, 1993b). In autism, postmortem analysis documents heterotopias and an increased number of interstitial

neurons in the white matter, along with indistinct grey-white matter boundary, suggesting abnormalities in subplate and deep-layer neurons (Bailey et al., 1998; Wegiel et al., 2010; Avino & Hutsler, 2010; McFadden & Minshew, 2013). Furthermore, co-expression network analysis in humans implicates deep-layer cortical projection neurons during the midfetal gestational period in the pathogenesis of autism by identifying several high-confidence autism risk genes such as T-box brain transcription factor 1 (Tbr1) as highly expressed in midfetal deep-layer PFC projection neurons (Willsey et al., 2013).

1.2 L6-Drd1a neurons drive cortical arousal through the higher-order corticothalamic system

The working definition of L6b in rodents varies across the literature, with some citing anatomical constraints and others referencing laminar-specific expression patterns. Anatomically, L6b is generally considered to be the bottom 30% of L6 or within ~100 μm of the underlying white matter (Feldmeyer, 2023; Hay et al., 2015; Marx & Feldmeyer, 2013; Zolnik et al., 2023). Laminar-specific genetic markers of L6b have also been used, notably the subplate markers Ctgf and Cplx3. In the mouse primary somatosensory cortex (S1), two L6b subpopulations have been characterized using specific Cre driver lines: Drd1a-Cre+ neurons (which express the dopamine D1 receptor) and Ctgf-dgCre+ neurons (which express connective tissue growth factor during adulthood). Drd1a neurons and Ctgf neurons represent 25-40% and 25% of S1 L6b neurons, respectively (Hoerder-Suabedissen et al., 2018; Zolnik et al., 2020). Notably, Drd1a-Cre+ expression is largely restricted to L6b in primary sensory areas but more widespread across deep layers in the PFC. Roughly one-third of Drd1a neurons co-express the subplate markers Ctgf, Cplx3, or Neuroserpin, whereas none express Lpar1 (Hoerder-

Suabedissen et al., 2018; Zolnik et al., 2020). In terms of cell-type and morphology, both Drd1a and Ctgf neurons are excitatory as they are not immunoreactive to glutamate decarboxylase 67 (GAD67), but Drd1a neurons can be pyramidal or non-pyramidal whereas Ctgf neurons are almost exclusively non-pyramidal (Zolnik et al., 2020). In S1, both L6b subpopulations receive local intracortical excitatory input from all layers, especially L6a, L5, and L2/3, along with inhibitory input mostly from L6a. Around 95% of their long-range input is intracortical, including both ipsilateral and contralateral, and they receive little subcortical input, with the most prominent exception being the higher-order posteromedial thalamus (POm) (Zolnik et al., 2020).

L6-Drd1a neurons are particularly interesting because their thalamic projections almost exclusively target higher-order nuclei such as the POm with small boutons and without collaterals in the thalamic reticular nucleus (TRN) (Figure 1.2A) (Hoerder-Suabedissen et al., 2018). On the other hand, L6a projections form TRN collaterals and target both primary and higher-order thalamic nuclei, and L5 projections exclusively target higher-order nuclei but with significantly larger boutons and collaterals to the superior colliculus and spinal cord (Hoerder-Suabedissen et al., 2018; Sherman & Guillery, 2002). Furthermore, L6b is the only cortical layer responsive to the wake-promoting neuropeptide orexin (Figure 1.2C) (Bayer et al., 2004), and Drd1a neurons are the only projection neurons in L6 that respond to orexin (Figure 1.2D), suggesting that these neurons are likely modulated by orexinergic neurons from the lateral hypothalamus and play an important role in cortical arousal via the higher-order thalamocortical system (Bayer et al., 2004; Zolnik et al., 2023; Messore et al., 2024). It should be noted that other D1 receptor-expressing neurons in the PFC include pyramidal projections to contralateral cortex, claustrum, and striatum, along with superficial VIP interneurons (Anastasiades et al., 2019), but L6-specific Drd1a neurons display unique orexin sensitivity and higher-order thalamic

targeting, and they could even reflect Drd1a expression at an earlier time in development. Despite extensive anatomical and electrophysiological characterization of L6-Drd1a neurons in S1, their anatomical connections and electrophysiological modulation in the medial prefrontal cortex (mPFC) throughout development remains poorly understood.

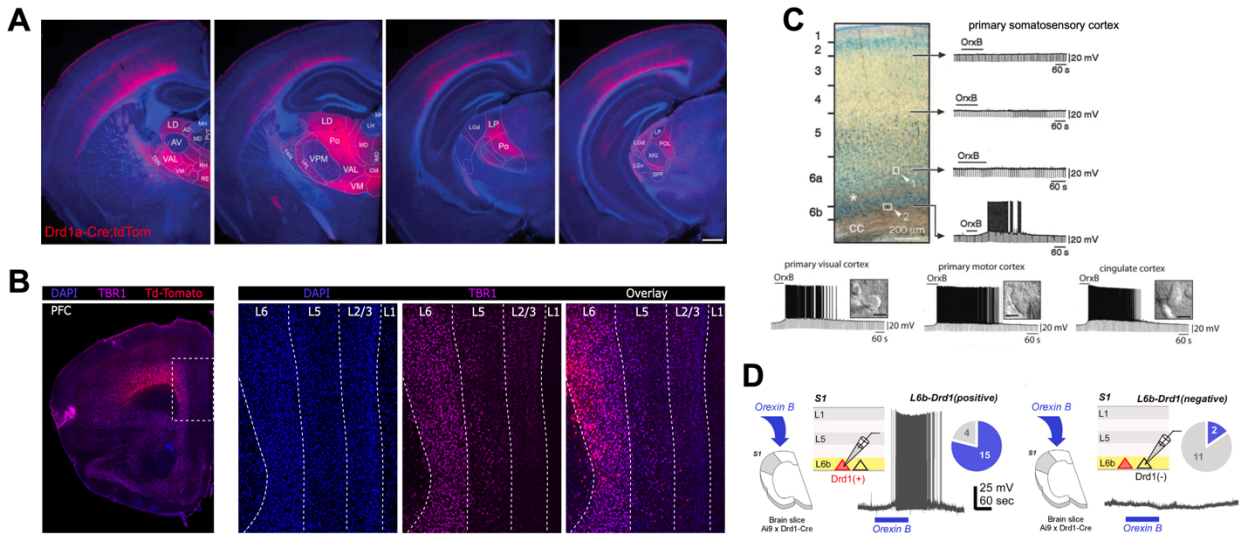


Figure 1.2. L6-Drd1a neurons selectively target higher-order thalamic nuclei and are sensitive to orexin.
(Adapted from Hoerder-Suabedissen et al., 2018 (**A**); Messore et al., 2024 (**B**); Bayer et al., 2004 (**C**); Zolnik et al., 2023 (**D**)).
(**A**) Drd1a neurons labeled with tdTomato (red) are largely restricted to L6b in the adult S1 and target higher-order thalamic nuclei (posterior nucleus (Po), lateral dorsal (LD), ventral anterior lateral (VAL), and ventral medial (VM)) while largely avoiding ventral posterior-medial (VPM), anterior ventral (AV), lateral geniculate (LGd), medial geniculate (MG), habenula, and paraventricular nucleus. Fibers pass through the thalami reticular nucleus (TRN) and ventral posterior lateral nucleus (VPL) without branching. Scale bar: 500 µm.
(**B**) Drd1a neurons labeled with tdTomato (red) are largely restricted to L6 in the adult mPFC. DAPI (blue) is a general neuronal marker used to delineate L1, L2/3, and L5 boundaries, and TBR1 (purple) is a cortical L6 marker used to delineate the L5/L6 boundary.
(**C**) Orexin B selectively activates L6b in the primary somatosensory, primary visual, primary motor, and cingulate cortices.
(**D**) Within L6b in S1, orexin B selectively activates Drd1a-Cre+ neurons.

1.3 Dopamine pathways and receptors

Because L6-Drd1a neurons highly express D1 receptor, their dopaminergic modulation may play a synergistic role with orexin in driving cortical arousal. Dopamine is a catecholamine, which is a monoamine neurotransmitter synthesized from the amino acid tyrosine (Ayano, 2016).

The rate-limiting step in dopamine synthesis is the formation of L-dopa from tyrosine, which is catalyzed by the enzyme tyrosine hydroxylase (TH). L-dopa is then rapidly converted to dopamine by aromatic amino acid decarboxylase, also known as dopa decarboxylase (Ayano, 2016). Interestingly, dopa decarboxylase is also highly expressed in a subplate neuronal population in the white matter (Hoerder-Suabedissen et al., 2009; Wang et al., 2011). The dopamine transporter DAT and TH are used as markers for dopaminergic neurons, although it should be noted that not all TH-positive neurons contain dopamine, especially in the hypothalamus, and the level of TH expression in dopaminergic neurons changes over time and in response to functional demand or hormonal changes (Björklund & Dunnett, 2007).

There are nine main dopaminergic neuronal groups in the mammalian brain classified as A8-A16 across different species, with the majority of dopaminergic neurons located in the ventral tegmental area (VTA) (A10) and substantia nigra (SN) (A9) (Figure 1.3A) (Björklund & Dunnett, 2007). Some of the other groups include the retrorubral field (A8), arcuate nucleus of the hypothalamus (A12), and olfactory bulb (A16) (Björklund & Dunnett, 2007). There are also four main dopaminergic pathways in the mammalian brain: mesolimbic, mesocortical, nigrostriatal/mesostriatal, and tuberoinfundibular (Figure 1.3A). The latter pathway involves dopaminergic neurons in the arcuate nucleus of the hypothalamus projecting to the pituitary gland and inhibiting prolactin release (Ayano, 2016). The mesostriatal pathway is primarily involved in motor function, whereas the mesolimbic pathway is involved in reward-related cognition, pleasure, and addiction. The mesocortical pathway is involved in executive functions, cognition, attention, and learning (Ayano, 2016). The mesolimbic, mesocortical, and mesostriatal pathways involve dopaminergic neurons dispersed throughout the midbrain that are generally separated into a dorsal and ventral tier based on their connectivity and morphology (Figure

1.3B). The dorsal tier includes round or fusiform, calbindin-positive neurons located in the dorsal areas of the VTA, SN, and retrorubral field projecting to ventral striatal, limbic, and cortical areas, along with the matrix compartment of the dorsal striatum (Bentivoglio & Morelli, 2005; Gerfen et al., 1987; Lynd-Balta & Haber, 1994). On the other hand, the ventral tier includes densely packed angular neurons located in the ventral areas of the VTA and SN projecting almost exclusively to the patch compartment of the dorsal striatum. These ventral tier neurons are calbindin-negative but are immunopositive for the G protein-gated inwardly rectifying potassium channel GIRK2 (Gerfen et al., 1987; Prensa & Parent, 2001). As such, the dorsal tier represents a mixed population of midbrain dopaminergic neurons in the mesolimbic, mesocortical, and mesostriatal pathways, whereas the ventral tier represents a dense population of midbrain dopaminergic neurons primarily involved in the mesostriatal pathway.

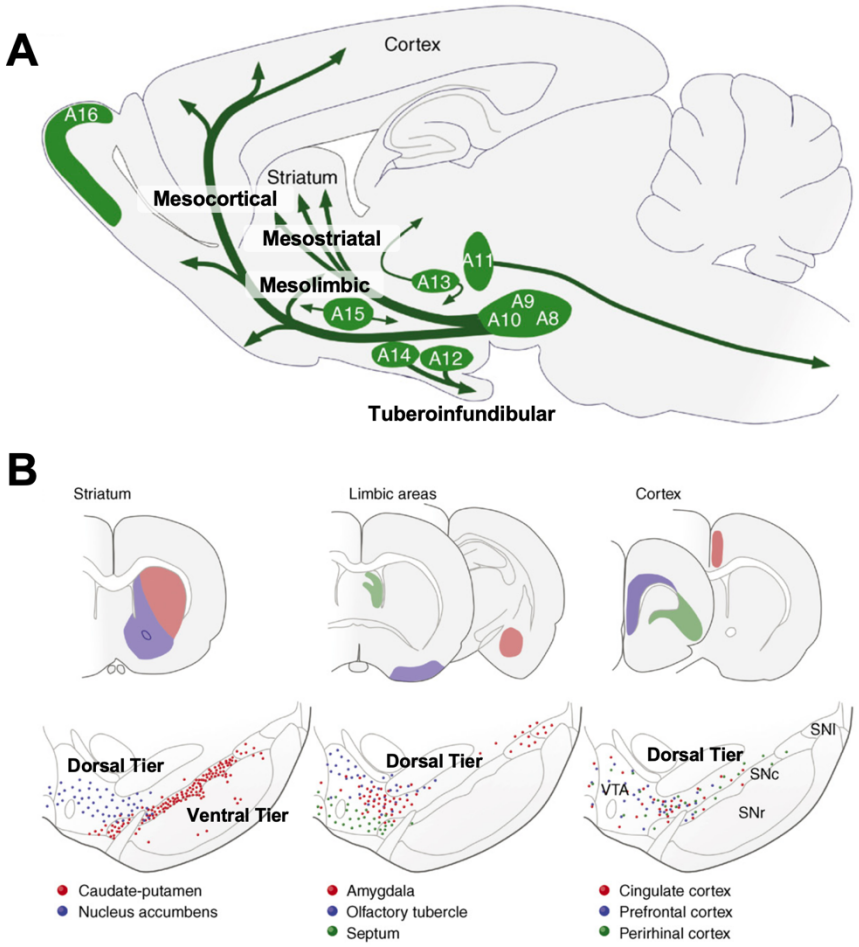


Figure 1.3. Dopaminergic nuclei and pathways in the rodent brain.
(Modified from Björklund & Dunnett, 2007).
(**A**) Sagittal view of an adult rodent brain displays the nine main dopaminergic neuronal groups classified as A8-A16, along with their pathways. The majority of dopaminergic neurons located in the ventral tegmental area (VTA) (A10), substantia nigra (SN) (A9), retrorubral field (A8), and arcuate nucleus of the hypothalamus (A12) The four main dopaminergic pathways are also shown: mesolimbic, mesocortical, nigrostriatal/mesostriatal, and tuberoinfundibular.
(**B**) Coronal slices of an adult rodent brain show the distribution of midbrain dorsal tier and ventral tier dopaminergic neurons and their projections. Neurons in the ventral tier of the substantia nigra pars compacta (SNc) mostly innervate the sensorimotor caudate-putamen. Neurons in the dorsal tier project widely to striatal, limbic, and cortical targets.
Abbreviations: substantia nigra pars compacta (SNc); substantia nigra pars reticulata (SNr); substantia nigra pars lateralis (SNl); ventral tegmental area (VTA).

There are five subtypes of G protein-coupled dopamine receptors: D1, D2, D3, D4, and D5. These subtypes are divided into two classes: D1-like receptors (D1 and D5) and D2-like receptors (D2, D3, and D4). D1-like receptors are $G_{s/olf}$-coupled receptors that stimulate cyclic adenosine monophosphate (cAMP) production leading to protein kinase A (PKA) that

phosphorylates voltage-gated potassium, sodium, and calcium channels (Di Domenico & Mapelli, 2023). PKA also activates the dopamine and cAMP-regulated phosphoprotein DARPP-32, which inhibits protein phosphatase 1 (PP1) to ultimately amplify PKA signaling. On the other hand, D2-like receptors are $G_{i/o}$-coupled receptors that inhibit cAMP production and PKA activity, along with its downstream signaling targets (Di Domenico & Mapelli, 2023). D2-like receptors can also modulate phospholipase C (PLC) activity. PLC stimulates diacylglycerol (DAG) production, which activates protein kinase C (PKC) signaling, and PLC also activates inositol triphosphate (IP_3), which increases intracellular calcium levels leading to protein phosphatase 2B (PP2B) activation that inhibits DARPP-32 signaling (Tritsch & Sabatini, 2012). The liberation of the Gßγ protein subunits upon activation of D2-like receptors also directly activates inward-rectifying potassium channels (K_{ir}) and inhibit L-type ($Ca_V2.2$) and N-type (Ca_V1) voltage-gated calcium channels (Tritsch & Sabatini, 2012). Both D1-like and D2-like receptors can also modulate GABA (γ-aminobutyric acid) receptors and glutamatergic NMDA (*N*-methyl-D-aspartate) and AMPA (α-amino-3-hydroxy-5-methyl-4-isoxazolepropionic acid) receptors through PKA/IP_3 signaling or direct protein-protein interactions (Figure 1.4) (Di Domenico & Mapelli, 2023).

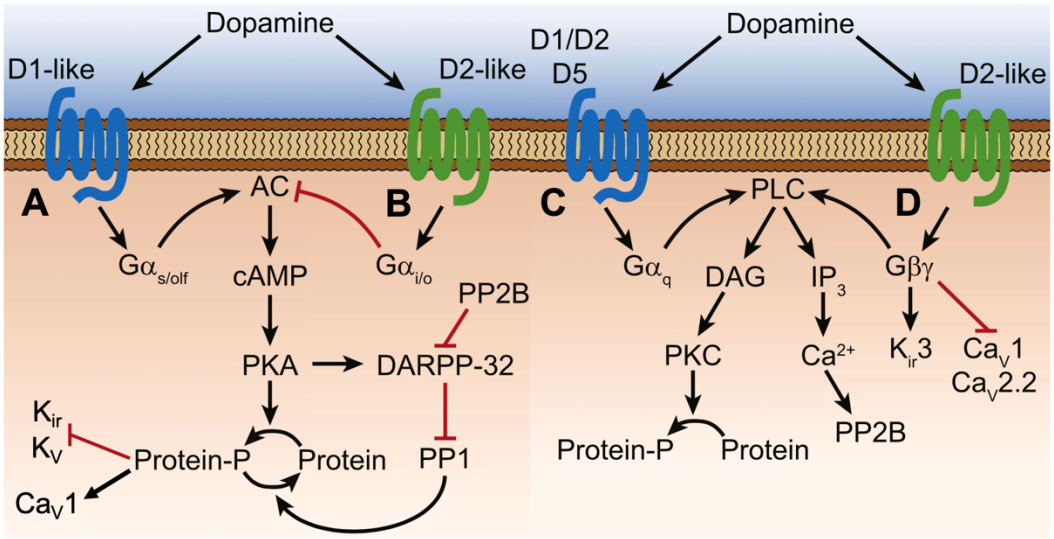


Figure 1.4. Intracellular dopamine signaling mechanisms.
(Modified from Tritsch & Sabatini, 2012).
(**A**) D1-like receptors couple with $G_{s/olf}$ proteins to activate the cAMP/PKA pathway, which activates voltage-gated calcium channels (Ca_V1) and inhibits voltage-gated potassium channels (K_V) and inward rectifiers (K_{ir}). PKA signaling is also amplified through DARPP-32 activation.
(**B**) D2-like receptors couple with $G_{i/o}$ proteins to inhibit the cAMP/PKA pathway, which yields the opposite effect of D1-like receptor activation.
(**C**) D1/D2 receptors can form a heterodimer that couples with G_q proteins to activate the PLC pathway, which activates PKC signaling and PP2B, which can inhibit DARPP-32.
(**D**) D2-like receptors can also couple with G_q proteins to activate the PLC pathway, which through PP2B can also inhibit DARPP-32 components of the PKA pathway. Upon activation of D2-like receptors, the liberation of the Gßγ protein subunits can also directly activate K_{ir} and inhibit L-type ($Ca_V2.2$) and N-type (Ca_V1) voltage-gated calcium channels.
Abbreviations: adenylyl cyclase (AC); cyclic adenosine monophosphate (cAMP); protein kinase A (PKA); dopamine and cAMP-regulated phosphoprotein (DARPP-32); protein phosphatase 1 (PP1); phospholipase C (PLC); diacylglycerol (DAG); protein kinase C (PKC); inositol triphosphate (IP_3); protein phosphatase 2B (PP2B); voltage-gated potassium channel (K_V); inwardly-rectifying potassium channel (K_{ir}); N-type voltage-gated calcium channel (Ca_V1); L-type voltage-gated calcium channel ($Ca_V2.2$).

1.4 Dopamine signaling in the PFC

The PFC is involved in executive and cognitive functions such as flexible decision making, working memory, stimulus selection, and goal-directed behavior, and PFC circuits are highly responsive to neuromodulators like dopamine (Miller & Wallis, 2009; Miller & Cohen, 2001; Seamans & Yang, 2004). Pharmacological or optogenetic manipulation of PFC dopamine signaling in rodents and primates modulates performance on delayed-response working memory tasks, gating of sensory signals, response to aversive stimuli, and neuronal rule coding (Sawaguchi & Goldman-Rakic, 1994; Vander Weele et al., 2018; Popescu et al., 2016; Abe et

al., 2024; Ott et al., 2014). Dopaminergic networks between the VTA and mPFC also play an important role in decision-based reward learning by differentially encoding confidence-dependent predicted value and prediction error (Lak et al., 2020). Moreover, enhanced working memory performance requires an optimal level of D1 receptor activation in the PFC. Low levels of D1 receptor antagonists in the primate PFC enhanced delay period activity in a working memory task, whereas high levels of D1 receptor antagonists suppressed activity, indicating a bell-shaped relationship between D1 receptor activity and cognitive performance (Williams & Goldman-Rakic, 1995).

A feedforward inhibition model of dopamine action involving synaptic triads has been proposed by Goldman-Rakic and colleagues to explain the biphasic action of D1 receptor activity in the PFC (Goldman-Rakic et al., 2000). The spines of cortical pyramidal neurons receive paired input from dopaminergic and glutamatergic axon terminals, as evidenced by D1 receptor localization in close proximity to asymmetric synapses, presumably glutamatergic, on the same pyramidal dendritic spine (Goldman-Rakic et al., 1989). Fast-spiking parvalbumin interneurons also exhibit spatially tuned activity to their adjacent pyramidal neurons (Rao et al., 1999), and D1 receptor expression in these interneurons is localized in presynaptic axon terminals and in the distal dendrites near excitatory asymmetric synapses (Muly et al., 1998). As such, moderate levels of dopamine release primarily enhance glutamatergic inputs onto pyramidal neurons, which improves working memory performance, whereas high dopamine levels enhance glutamatergic inputs onto both pyramidal neurons and inhibitory interneurons (ultimately reducing pyramidal neuron output by feedforward inhibition) and low dopamine levels fail to enhance either glutamatergic inputs.

Within the PFC, D1-like receptors are more abundant than D2-like receptors, and D1-like receptors are highly expressed in deep layers of the PFC in rodents and primates (Berger et al., 1991). In rats, D1 receptors are prominently expressed in L5/6 and D2 receptors in L5 of the mPFC, agranular insular cortex, claustrum, and endopiriform nucleus (Santana et al., 2009). Notably, D1 but not D2 receptor expression is also localized to the tenia tecta and piriform cortex. In the mPFC, L6 contains the highest proportion of pyramidal (VGLUT1-positive, 38%) and GABAergic (GAD65/67-positive, 38%) neurons expressing D1 receptor mRNA (Santana et al., 2009). However, for D2 receptor mRNA expression, L5 contains the highest proportion of pyramidal neurons (25%) and L6 contains the highest proportion of GABAergic neurons (17%) (Santana et al., 2009). These distribution patterns suggest that D1 and D2 receptors may differentially modulate PFC activity in a laminar-specific manner. Mouse brain transcriptomics confirm that D1 receptors are highly expressed in a subtype of cortical L6b, unlike D2 receptors (Allen Brain Map Single-cell Transcriptomics, 2020), but the dopaminergic modulatory mechanisms involving L6-Drd1a neurons remain poorly understood. By investigating the effects of D1and D2 receptor activation on network-level and neuronal-level activity in the mPFC, we hope to provide valuable insights into the contribution of dopamine to cortical arousal driven by L6-Drd1a neurons, with significant implications for anxiety and stress disorders, along with dopamine-related disorders such as schizophrenia.

1.5 Hypothesis and specific aims

In the mouse S1 cortex, Drd1a-Cre+ neurons are a subpopulation of L6b that selectively project to higher-order thalamic nuclei and are highly sensitive to the wake-promoting neuropeptide orexin, likely playing an important role in cortical arousal, sensory valence processing, and anxiety behavior (Hoerder-Suabedissen et al., 2018; Zolnik et al., 2023; Messore et al., 2024). Dopamine modulation in the PFC plays an important role in cognition, motivation, and sensory valence processing, with relevant implications in schizophrenia, autism, and anxiety-related disorders (Miller & Cohen, 2001; Vander Weele et al., 2018; Popescu et al., 2016; Abe et al., 2024). Given the layer-specific enrichment of D1 receptor expression in L6 and the role of L6-Drd1a neurons in orexin-mediated cortical arousal, whether these L6-Drd1a neurons play an analogous role in cortical arousal through a dopaminergic modulatory mechanism in the mPFC remains poorly understood.

Layer-specific neuronal populations can be 'silenced' through Cre-mediated cell type-specific conditional knockout of the presynaptic SNARE protein SNAP25, which abolishes action potential-evoked neurotransmitter release while initially developing normal axonal projections (Hoerder-Suabedissen et al., 2019). Different cortical projection populations (L5-Rbp4, L6a-Ntsr1, and L6-Drd1a) have differential sensitivity to Snap25-mediated 'silencing,' with some exhibiting disrupted synaptic maturation, altered myelination, and axon degeneration (Hoerder-Suabedissen et al., 2019; Hayashi et al., 2021; Korrell et al., 2019). Notably, L6-Drd1a neurons do not display these drastic changes in response to Snap25 conditional knockout, making it a suitable model for manipulating their activity. Thus, this thesis investigates the effects of chronically 'silencing' L6-Drd1a neurons in a Snap25 conditional knockout mouse

model (Drd1a-Cre$^{+/-}$;Snap25$^{fl/fl}$;tdTomato$^{STOPfl/fl}$) on the dopaminergic modulation of network activity in mPFC acute slices. Our specific aims are:

1. Investigate D1 and D2 receptor modulation of local mPFC network activity in functionally active L6-Drd1a slices and 'silenced' L6-Drd1a slices using *in-vitro* high-density planar multielectrode array (MEA) recordings.
2. Characterize D1 and D2 receptor modulation of L6-Drd1a and L6-non-Drd1a intrinsic neuronal excitability and spontaneous synaptic potentials in the mPFC using *in-vitro* whole-cell patch clamp recordings.

We hypothesize that D1 receptor agonist will increase local network activity in the mPFC due to higher cortical expression of D1 receptors compared to D2 receptors, along with the stimulatory signaling of D1-like receptors compared to the inhibitory signaling of D2-like receptors. We expect to blunt D1 receptor agonist-induced activity in the mPFC upon chronic 'silencing' of L6-Drd1a neurons. We also hypothesize that D1 receptor agonist selectively excites L6-Drd1a neurons compared to other L6 neurons in the mPFC, with a non-selective effect of D2 receptor agonist.

II. General Methods

2.1 Transgenic animal breeding and housing

Transgenic mice were bred and housed on a temperature-controlled 12-hour light/dark cycle with ad libitum access to food and water at the University of Oxford Biomedical Sciences Building. All procedures involving transgenic animals were performed in accordance with the UK Animals (Scientific Procedures) Act 1986. We maintained three mouse colonies: Drd1a-Cre$^{+/-}$;tdTom$^{STOPfl/fl}$, Snap25$^{fl/fl}$;tdTom$^{STOPfl/fl}$, and Drd1a-Cre$^{+/-}$;Snap25$^{fl/fl}$;tdTom$^{STOPfl/fl}$. For the Drd1a-Cre$^{+/-}$;tdTom$^{STOPfl/fl}$ colony, Tg(Drd1a-Cre)FK164Gsat/Mmucd (Drd1a-Cre) mice were obtained from Mutant Mouse Regional Resource Centre (MMRRC) and crossed with C57BL6;129S6-Gt(ROSA)26Sortm14(CAG-tdTomato)Hze/J (Ai14) mice such that the STOP sequence of the fluorescent reporter tdTomato is floxed and excised in a Cre-dependent manner, allowing for visualization of Drd1a-Cre+ neurons (Figure 2.1A2) (Hoerder-Suabedissen et al., 2018). For the Snap25$^{fl/fl}$;tdTom$^{STOPfl/fl}$ colony, C57BL6-Snap25tm3mcw (Snap25$^{fl/fl}$) mice were obtained from the University of New Mexico and crossed with C57BL6;129S6-Gt(ROSA)26Sortm14(CAG-tdTomato)Hze/J (Ai14) mice such that exon 5a/5b of Snap25 is floxed and excised in a Cre-dependent manner, rendering a truncated dysfunctional SNAP25 protein and abolishing action potential-evoked neurotransmitter release, with Cre-dependent tdTomato expression allowing for visualization of 'silenced' neurons (Figure 2.1A1) (Hoerder-Suabedissen et al., 2019; Hayashi et al., 2021). Finally, for the Drd1a-Cre$^{+/-}$;Snap25$^{fl/fl}$;tdTom$^{STOPfl/fl}$ colony, Snap25$^{fl/fl}$;tdTom$^{STOPfl/fl}$ mice were crossed with Tg(Drd1a-Cre)FK164Gsat/Mmucd (Drd1a-Cre) mice from MMRRC such that Drd1a-Cre+ neurons are 'silenced' and visualized (Figure 2.1A1). This colony was maintained by crossing Drd1a-Cre$^{+/-}$

;Snap25$^{fl/fl}$;tdTom$^{STOPfl/fl}$ females with Snap25$^{fl/fl}$;tdTom$^{STOPfl/fl}$ males (Hoerder-Suabedissen et al., 2019). Animal genotype was determined using polymerase chain reaction from ear clips in-house or through Transnetyx (Transnetyx Inc.) and further confirmed by assessing tdTomato expression in ~P14 animals with fluorescent goggles in the animal facility.

For the MEA experimental cohort, the Drd1a-Cre$^{+/-}$;Snap25$^{fl/fl}$;tdTom$^{STOPfl/fl}$ colony was used such that control animals were Drd1a-Cre$^{-/-}$ and 'silenced' animals were Drd1a-Cre$^{+/-}$ (Figure 2.1B1). For the patch clamp experimental cohort, Drd1a-Cre$^{+/-}$ animals from the Drd1a-Cre$^{+/-}$;tdTom$^{STOPfl/fl}$ colony were used to distinguish between fluorescing L6-Drd1a neurons and non-fluorescing L6-non-Drd1a neurons (Figure 2.1B2).

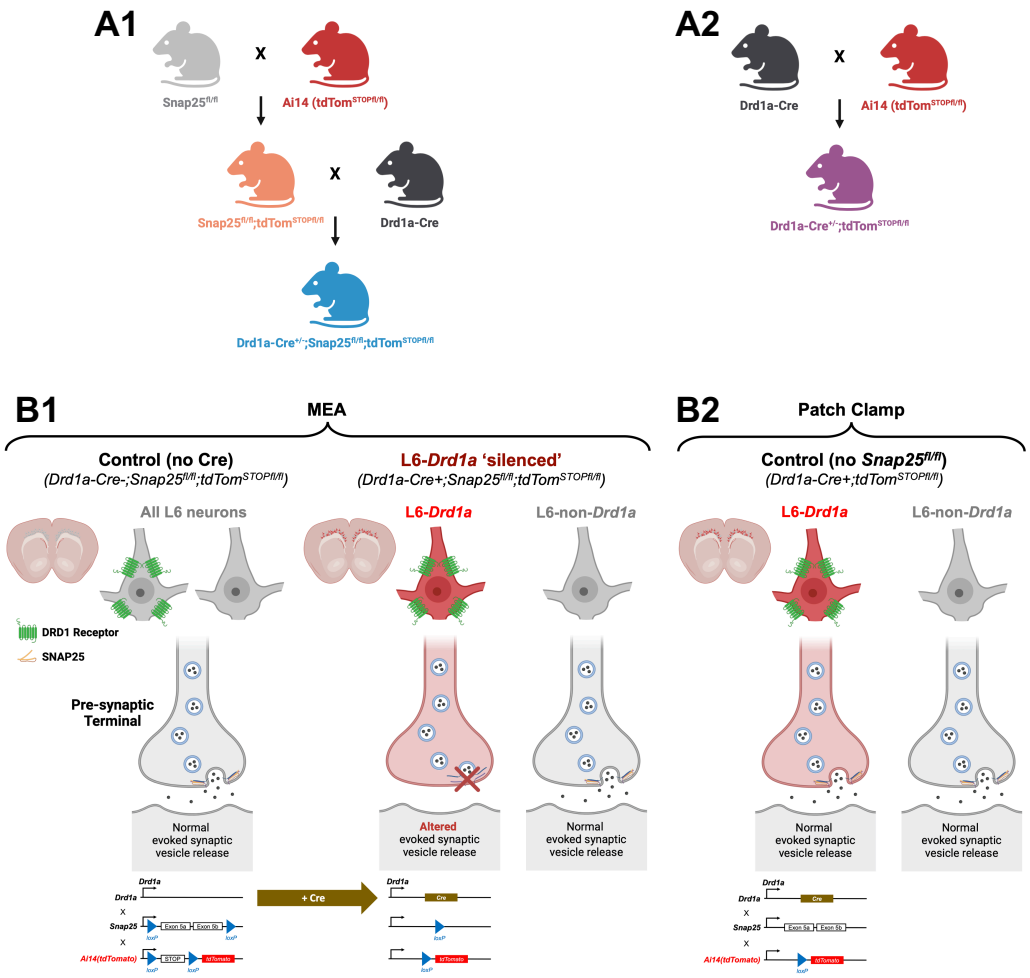


Figure 2.1. Drd1a-Cre$^{+/-}$;Snap25$^{fl/fl}$ conditional knockout mouse model genetic construct.
(**A1**) Colony breeding design that generates Drd1a-Cre$^{+/-}$;Snap25$^{fl/fl}$;tdTom$^{STOPfl/fl}$ mice, which were used for the MEA experiments.
(**A2**) Colony breeding design that generates Drd1a-Cre$^{+/-}$;tdTom$^{STOPfl/fl}$ mice, which were used for the patch clamp experiments.
(**B1**) Genetic construct of the Drd1a-Cre$^{+/-}$;Snap25$^{fl/fl}$;tdTom$^{STOPfl/fl}$ mouse colony for the MEA experiments, which yields control mice without Cre expression and L6-Drd1a 'silenced' mice with Cre expression that renders a nonfunctional truncated SNAP25 protein in Drd1a-expressing neurons.
(**B2**) Genetic construct of the Drd1a-Cre$^{+/-}$;tdTom$^{STOPfl/fl}$ mouse colony for the patch clamp experiments, from which we used the offspring with Cre expression that labels Drd1a-expressing neurons with tdTomato fluorescence.

2.2 Acute slice preparation

For MEA experiments, adult (5-20 weeks old) Drd1a-Cre$^{+/-}$;Snap25$^{fl/fl}$;tdTom$^{STOPfl/fl}$ mice of both sexes were anesthetized with 4% isoflurane and decapitated, and coronal slices (250 µm) were prepared using a Leica Vibratome VT1200S in ice-cold (~4ºC) sucrose cutting solution containing (in mM): 150 sucrose, 40 NaCl, 3 KCl, 15 glucose, 7.4 $MgSO_4 \cdot 7H_2O$, 1 $CaCl_2 \cdot 6H_2O$,

1.25 $NaH_2PO_4•H_2O$, and 25 $NaHCO_3$; osmolality 300 ± 10 mOsmol/kg. The slices were then cut into two hemispheres and transferred to an interface chamber containing room temperature aCSF (in mM: 126 NaCl, 3.5 KCl, 10 glucose, 1 $MgSO_4•7H_2O$, 1.2 $CaCl_2•6H_2O$, 1.25 $NaH_2PO_4•H_2O$, and 26 $NaHCO_3$; osmolality 300 ± 10 mOsmol/kg) to recover for at least one hour. All solutions were bubbled with carbogen gas (95% O_2, 5% CO_2).

For whole-cell patch clamp experiments, adult (5-20 weeks old) Drd1a-$Cre^{+/-}$;$Snap25^{fl/fl}$;$tdTom^{STOPfl/fl}$ mice of both sexes were anesthetized with 4% isoflurane and decapitated, and coronal slices (350 μm) were prepared using a Leica Vibratome VT1200S in ice-cold (~4ºC) N-methyl-D-glucamine (NMDG)-HEPES cutting solution containing (in mM): 92 NMDG, 2.5 KCl, 25 glucose, 2 thiourea, 5 sodium ascorbate, 3 sodium pyruvate, 10 $MgSO_4•7H_2O$, 0.5 $CaCl_2•6H_2O$, 1.2 $NaH_2PO_4•H_2O$, 30 $NaHCO_3$, and 20 HEPES; pH adjusted to 7.3-7.4 with HCl; osmolality 300 ± 10 mOsmol/kg. The slices were then cut into two hemispheres and transferred to an interface chamber containing 34ºC NMDG-HEPES solution for 10 minutes followed by room temperature aCSF to recover for at least one hour. All solutions were bubbled with carbogen gas (95% O_2, 5% CO_2).

2.3 Pharmacology

By bath application, we blocked voltage-gated potassium channels with 4-aminopyradine (4-AP) (200 μM, Sigma-Aldrich #275875) (only for MEA recordings), activated D1 receptors with the D1 receptor agonist SKF-81297 (2 μM, Tocris #1447), and activated D2 receptors with the D2 receptor agonist quinpirole (2 μM, Tocris #1061) (Lancon et al., 2021; Stagkourakis et al., 2016; Clark & Bracci, 2018).

2.4 Statistical analyses

All statistical analyses were performed using GraphPad Prism software. Datasets were analyzed for significance using two-way or three-way ANOVA or mixed-effects analysis with Bonferroni multiple comparisons post-hoc tests. All data are presented as mean +/- s.e.m., using *$p < 0.05$, **$p < 0.01$, and ***$p < 0.001$. Sample sizes were chosen on the basis of previous studies using the Drd1a-Cre mouse line (Messore et al., 2024). Further details on specific statistical analyses are included in the results section and figures for each dataset.

III. Chronically 'silencing' L6-Drd1a neurons alters dopaminergic modulation of local mPFC network activity

3.1 Introduction

This chapter addresses the first aim of this thesis: investigating D1 and D2 receptor modulation of local mPFC network activity in functionally active L6-Drd1a slices and 'silenced' L6-Drd1a slices using *in-vitro* high-density planar MEA recordings. Given the cortical layer-specific enrichment of D1 receptor expression in L6 (Berger et al., 1991; Hoerder-Suabedissen et al., 2018; Allen Brain Map Single-cell Transcriptomics, 2020), and the role of L6-Drd1a neurons in arousing mPFC local network activity in response to orexin (Messore et al., 2024), we hypothesize that these L6-Drd1a neurons play an analogous role in cortical arousal through a dopaminergic modulatory mechanism in the mPFC. Specifically, we expect that D1 receptor agonist will increase mPFC local network activity due to higher cortical expression of D1 receptors compared to D2 receptors, along with the stimulatory signaling of D1-like receptors compared to the inhibitory signaling of D2-like receptors. We further expect chronic 'silencing' of L6-Drd1a via Snap25 conditional knockout to blunt D1 receptor agonist-induced activity in the mPFC.

3.1.1 L6-Drd1a structural and functional connectivity

Although poorly understood in the mPFC, the structural and functional connectivity of L6-Drd1a neurons in S1 has been well-characterized. As described in Chapter 1, Drd1a neurons represent 25-40% of L6b neurons in S1, but their distribution is more widespread across deep layers in the PFC (Hoerder-Suabedissen et al., 2018; Zolnik et al., 2020; Messore et al., 2024).

L6-Drd1a neurons are excitatory as they are not immunoreactive to GAD67, and their morphology can be pyramidal or non-pyramidal (Zolnik et al., 2020). In fact, the pyramidal neurons project to the POm and L5, and the non-pyramidal ones project to L1, forming two distinct L6-Drd1a subcircuits in S1 (Figure 3.1C) (Zolnik et al., 2023). The L5-projecting Drd1a neurons target L5 extratelencephalic (ET) and intratelencephalic (IT) pyramidal neurons, evoking facilitating input to their proximal dendrites. The L1-projecting Drd1a neurons target the apical tuft dendrites of L5-ET neurons, triggering NMDA-dependent dendritic spikes (Zolnik et al., 2023). Interestingly, L6-Drd1a neurons target similar cortical layers as higher-order thalamic afferents and functionally excite the cortico-thalamo-cortical loop between L5 and the higher-order thalamus in a topographic manner. L6-Drd1a neurons also subcortically project to higher-order thalamic nuclei in a selective manner, eliciting strong synaptic facilitation in the POm (Hoerder-Suabedissen et al., 2018; Zolnik et al., 2023). This suggests that L6-Drd1a neurons activate the thalamocortical system, specifically in a unidirectional manner due to the lack of direct input from the cortico-thalamo-cortical loop to L6-Drd1a neurons (Figure 3.1D) (Zolnik et al., 2023).

Regarding their input, L6-Drd1a neurons in S1 receive local intracortical excitatory input from all layers (most prominently L6a, L5, and L2/3), along with inhibitory input mostly from L6a (Figure 3.1A,B). Over 95% of long-range input to L6-Drd1a neurons is intracortical, primarily from L5 in the ipsilateral motor cortex and L6a in the contralateral S1 (Zolnik et al., 2020). L6-Drd1a neurons receive little subcortical input, with the most prominent exception being the POm. Functionally, the main local excitatory input that elicits powerful excitatory postsynaptic potentials (EPSPs) in L6-Drd1a neurons is from L2/3 L4, and L5 corticocortical neurons (Zolnik et al., 2020). Distant ipsilateral and contralateral sensorimotor regions also elicit

powerful direct excitatory input to L6-Drd1a neurons. Although L6-Drd1a neurons project to and facilitate higher-order thalamic nuclei, they do not respond to direct thalamocortical excitation, nor are they excited by L5 corticothalamic collaterals.

Within L6, fast-spiking parvalbumin (PV) interneurons and non-fast-spiking somatostatin (SST) interneurons receive strong functional input from L6-Drd1a neurons, exhibiting short-term depression (Zolnik et al., 2023). L6-Drd1a neurons elicit inhibitory postsynaptic potentials (IPSPs) that suppress L6b neuronal firing likely through a disynaptic mechanism (Zolnik et al., 2020). This feedback inhibitory mechanism is mediated by PV or SST interneurons through GABA-A receptors. Notably, vasoactive intestinal peptide (VIP) interneuron-mediated disinhibition in L6b through L6a interneurons (which represent most of the inhibitory input onto L6b) is not significant (Zolnik et al., 2020). However, the local functional circuitry involving L6-Drd1a neurons in the mPFC remains poorly understood.

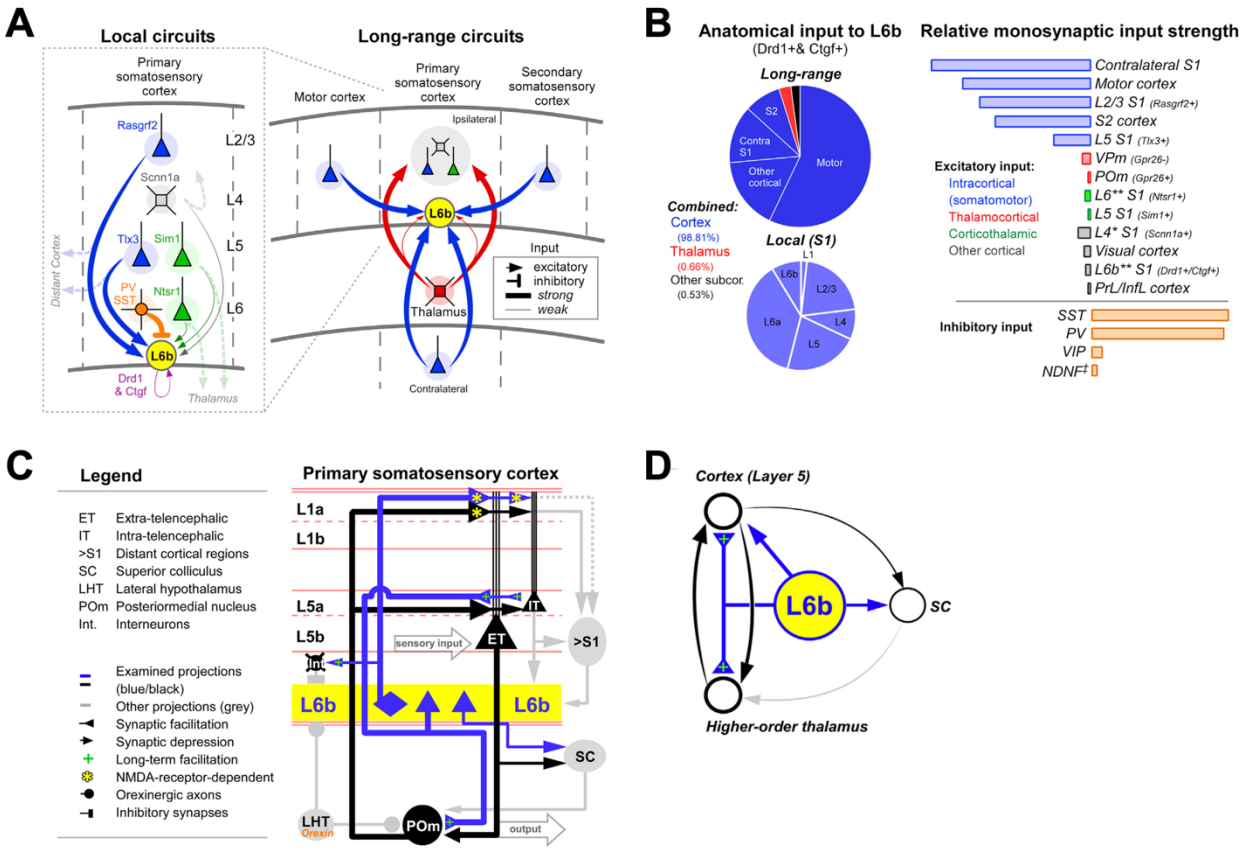


Figure 3.1. Summary of L6b anatomical and functional connectivity in S1.
(Adapted from Zolnik et al., 2020 (**A, B**), 2023 (**C, D**)).
(**A**) Schematic summarizing the functional input onto L6b-Drd1a and L6b-Ctgf neurons in S1.
(**B**) Relative distribution of local and long-range anatomical input to L6b in S1, along with the relative monosynaptic strength of intracortical, thalamocortical, corticothalamic, and inhibitory inputs.
(**C**) Detailed summary of the circuitry and physiology of L6b projections (blue lines) in S1, with the thick black lines indicating components of the higher-order cortico-thalamo-cortical loop.
(**D**) Simplified circuit diagram of L6b's role in activating higher-order cortico-thalamo-cortical loops.

3.1.2 L6b neuromodulation

L6b strongly responds to numerous neuromodulators with arousal functions, synergistically driving cortical arousal and behavior involving attention, sensory gating, and sleep. The most prominent neuromodulator that strongly and selectively activates L6b is the wake-promoting neuropeptide orexin/hypocretin, which is involved in appetite regulation, arousal, and wakefulness (De Lecea et al., 1998; Jones, 2008). Orexinergic neurons located in the lateral hypothalamus project across the cortex, and their optogenetic stimulation promotes the

transition from sleep to wakefulness (Adamantidis et al., 2007). There are two orexin peptides (orexin-A and orexin-B) that bind to two types of G protein-coupled receptors: orexin receptor type 1 (OX1R) and orexin receptor type 2 (OX2R). OX1R has a higher affinity for orexin-A, and it is coupled to G_q proteins, which activate PKC and IP_3 signaling through PLC. On the other hand, OX2R has a similar affinity for orexin-A and orexin-B, and it is coupled to G_q and $G_{i/o}$ proteins, the latter of which inhibit PKA signaling (Tsujino & Sakurai, 2013). OX2R is highly expressed in L6b excitatory neurons in sensory, motor, and prefrontal cortices, and *in-vitro* orexin-B elicits strong depolarizing responses in both pyramidal and non-pyramidal L6b neurons that is potentiated by nicotinic acetylcholine receptor activation (Bayer et al., 2004; Hay et al., 2015; Combremont et al., 2016a, 2016b). In the PFC, orexin-A depolarizes L2/3 and L5 pyramidal neurons (Yan et al., 2012; Li et al., 2010).

Within L6b in S1, Drd1a neurons respond to orexin-B *in-vitro*, and optogenetic photoactivation of S1 L6-Drd1a neurons *in-vivo* increases neuronal spiking, suppresses sub-gamma power (1-30 Hz, sleep-like slow waves), increases high-gamma power (80-140 Hz, wake-like fast oscillations), and increases distant activity in the frontal cortex (Zolnik et al., 2023). This shift toward fast cortical oscillations is likely mediated through local excitatory-inhibitory feedback loops with PV and SST interneurons in L6. In the mPFC, *in-vitro* OX2R agonist administration increased L6-Drd1a intrinsic excitability, and *in-vivo* orexin administration in deep mPFC layers increased slow-wave activity (0.5-8 Hz) (Messore et al., 2024). Taken together, these findings suggest that orexin-sensitive L6-Drd1a neurons control brain state and cortical arousal by modulating both local and long-range cortical communication via the higher-order corticothalamic system.

Orexin modulation in L6b is potentiated by acetylcholine, which is a neurotransmitter involved in arousal and attention that is released from cholinergic neurons in the basal forebrain. There are two types of acetylcholine receptors: nonselective excitatory ionotropic nicotinic receptors (nAChRs) and metabotropic muscarinic receptors (mAChRs) that are coupled to G_q and $G_{i/o}$ proteins (Picciotto et al., 2012). L6b neuronal response to orexin-B is potentiated by nAChRs, and fast-spiking PV interneurons in L6b can be directly activated by acetylcholine (Hay et al., 2015; Combremont et al., 2016a).

Neurotensin also excites slow-bursting non-pyramidal neurons and fast-spiking PV interneurons in L6b (Combremont et al., 2016a, 2016b). Neurotensin is another neuropeptide involved in homeostatic behaviors like sleep regulation, appetite, body temperature, and locomotion. The neurotensin G protein-coupled receptor NTSR1 is highly expressed in L6 corticothalamic neurons (Olsen et al., 2012), and neurotensin colocalizes with orexinergic and dopaminergic neurons, suggesting a synergistic role among orexin, dopamine, and neurotensin in gating cortical arousal through L6 (Furutani et al., 2013; Case et al., 2017).

Dopamine also functionally modulates L6b neuronal activity, especially slow-bursting non-pyramidal neurons (Combremont et al., 2016b). As described in Chapter 1, D1-like receptors are highly expressed in deep layers of the PFC (Berger et al., 1991), and mouse brain transcriptomics confirm that the D1 receptor is highly expressed in a subtype of cortical L6b (Allen Brain Map Single-cell Transcriptomics, 2020). As such, a Drd1a-Cre mouse line has been developed to target a subpopulation of L6 excitatory neurons in the cortex that are sensitive to orexin and project to higher-order thalamic nuclei (Hoerder-Suabedissen et al., 2018; Zolnik et al., 2023; Messore et al., 2024). Notably, this Drd1a-Cre line displays minimal striatal expression as it selectively labels cortical L6 neurons, but it does not necessarily label all D1 receptor-

expressing cortical neurons (Hoerder-Suabedissen et al., 2018). Other D1 receptor-expressing neurons in the PFC include pyramidal projections to contralateral cortex, claustrum, and striatum, along with superficial VIP interneurons (Anastasiades et al., 2019). The dopaminergic modulatory mechanisms involving L6-specific Drd1a neurons in mediating cortical arousal through higher-order cortico-thalamo-cortical loops remain poorly understood, particularly in the mPFC.

3.1.3 'Silencing' neurons via Snap25 conditional knockout

In order to study the functional role of L6-Drd1a neurons on the dopaminergic modulation of mPFC network activity, we chronically 'silenced' these neurons using a L6-Drd1a-Cre-mediated functional knockout of the presynaptic SNARE protein SNAP25 (synaptosomal-associated protein 25) (Hoerder-Suabedissen et al., 2019). The onset of Drd1a-Cre expression occurs shortly after birth, and a considerable proportion of cortical L6b express Cre by the end of the first postnatal week (Hoerder-Suabedissen et al., 2019). The SNARE complex includes vesicle-bound SNARE (v-SNARE) proteins and target membrane-bound SNARE (t-SNARE) proteins that mediate synaptic vesicle fusion to the presynaptic membrane. Normally, depolarization of the presynaptic neuron activates voltage-gated calcium channels in the presynaptic terminal, leading to an influx of calcium ions that bind to v-SNAREs. In the presence of calcium, v-SNAREs interact with t-SNAREs in order to facilitate vesicle fusion to the presynaptic membrane and neurotransmitter release into the synaptic cleft (Söllner et al., 1993; Rizo & Südhof, 2012). SNAP25 is a t-SNARE protein that mediates evoked synaptic vesicle fusion by forming a complex with the v-SNARE protein synaptobrevin and the t-SNARE protein syntaxin-1 (Hanson et al., 1997; Poirier et al., 1998; Sutton et al., 1998).

Snap25 expression is essential for action potential-evoked neurotransmitter release (Washbourne et al., 2002; Bronk et al., 2007). Global Snap25 homozygous knockout mice die at birth, but heterozygous mice display normal development, targeting, and synaptic formation of cortical and thalamic axons, along with spontaneous neurotransmitter release (Molnár et al., 2002; Washbourne et al., 2002). Layer-specific Snap25 knockout in L5 (Rbp4-Cre), L6a (Ntsr1-Cre), and L6b (Drd1a-Cre) across the cortical mantle has been validated to reduce evoked neurotransmitter release while displaying normal initial axonal development and synaptic formation (Hoerder-Suabedissen et al., 2019; Hayashi et al., 2021). However, subsequent inflammation and axon degeneration occurs around 8-9 months of age in mice, with L5-Rbp4 neurons being the most vulnerable. 'Silenced' L5-Rbp4 corticothalamic projection neurons display significantly altered synaptic structural maturation in the POm, and 'silenced' L6a-Ntsr1 neurons display reduced postnatal myelination (Hayashi et al., 2021; Korrell et al., 2019). However, 'silenced' L6-Drd1a neurons do not exhibit these drastic changes. Chronically 'silencing' L6-Drd1a neurons blocks orexin receptor-mediated increases in mPFC network excitability and decreases anxiety behavior, while 'silencing' L5-Rbp4 neurons does not alter this orexin response (Messore et al., 2024). This suggests that L6-Drd1a neurons selectively gate the orexinergic activation of the mPFC and help sustain cortical arousal through higher-order cortico-thalamo-cortical loops (Messore et al., 2024; Zolnik et al., 2023).

In this chapter, we investigated the functional role of L6-Drd1a neurons in the dopaminergic modulation of *in-vitro* mPFC network activity, and how dopamine may contribute to gating cortical arousal through these L6-Drd1a neurons.

3.2 Materials and Methods

3.2.1 Electrophysiology recordings and signal processing

For MEA recordings, slices were transferred to a submerged high-density planar MEA (MaxOne, MaxWell Biosystems) and superfused at 3-5 ml/min with carbogenated aCSF containing 200 µM 4-AP (Sigma-Aldrich) at 33-35ºC. An average of 4-5 slices were used from each animal. The 3.85 mm x 2.10 mm MEA provides 26,400 electrodes with a pitch of 17.5 µm, allowing for the simultaneous recording of up to 1,024 channels (Figure 3.2B). For each slice, three 5-minute recordings were obtained at baseline and repeated for either 2 µM SKF-81297 (Tocris) or 2 µM quinpirole (Tocris), with a 15-minute wait period after first administering the agonist (Figure 3.2A,C). All recordings were obtained with a sampling rate of 20 kHz and a gain of 1,024. The recordings were extracted and processed using custom-written procedures in MATLAB. The signal was decimated to 1 kHz, low-pass filtered at 800 Hz, and band-stop filtered at 50 Hz.

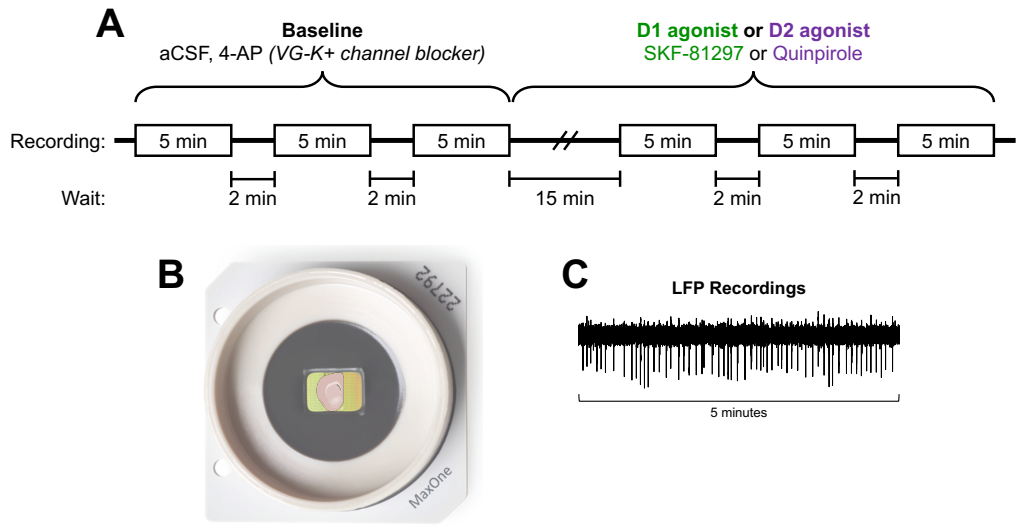


Figure 3.2. *In-vitro* MEA experimental protocol.
(**A**) Experimental timeline for MEA recordings included three 5-minute baseline LFP recordings with aCSF and the voltage-gated potassium channel blocker 4-AP, followed by three 5-minute LFP recordings with D1 receptor agonist SKF-81297 or D2 receptor agonist quinpirole (with a 15-minute waiting period after initial drug administration).
(**B**) Schematic of an MEA chip (MaxWell Biosystems) with one hemisphere of a coronal mPFC slice.
(**C**) Schematic of a 5-minute LFP recording trace.

3.2.2 Data analysis

Data analysis was performed using custom-written procedures in MATLAB and Python. To remove artifact signals from the MEA channels, the median signal across all channels was subtracted from the signal in each individual channel. We then analyzed LFP properties (event frequency, interevent interval, amplitude, and half-width), carried out a short-time Fourier transform to analyze signal frequency distribution over time per channel, and carried out a fast Fourier transform using a Hanning window and power spectral density analysis to analyze the spatial distribution of individual frequency band powers. The LFP event detection threshold was 6 median absolute deviations from the median and a minimum event duration of 10 ms. For the power spectral density analysis, we defined delta frequency as 0.5-4 Hz, theta as 4-8 Hz, alpha as 8-12 Hz, beta as 12-35 Hz, and gamma as 35-100 Hz. We referenced the Allen Brain Atlas for anatomical region mapping.

3.3 Results

Because L6-Drd1a neurons highly express the D1 receptor and play an important functional role in arousing mPFC network activity in response to orexin, we sought to investigate D1 and D2 receptor modulation of mPFC local network activity, and the effects of 'silencing' L6-Drd1a neurons on this dopaminergic modulation.

3.3.1 D1 receptor activation increases infralimbic mPFC network activity in the presence of functionally active L6-Drd1a neurons

We first examined how D1 receptor activation modulates local network activity in control mPFC slices with functionally active L6-Drd1a neurons. We bath-applied the voltage-gated potassium blocker 4-AP for all recordings in order to detect local field potentials (LFPs) in the mPFC (Messore et al., 2024), and we recorded network activity at baseline and after D1 receptor agonist SKF-81297 administration. We found that D1 receptor activation significantly increased LFP event frequency in the infralimbic area (ILA) of the mPFC compared to other mPFC regions (prelimbic (PL) and anterior cingulate area (ACA)) and the secondary motor cortex (M2) (Figure 3.3A,B1). We also examined the distribution of interevent interval, amplitude, and half-width of LFP events in the ILA and found a decrease in interevent interval and half-width and an increase in amplitude, further supporting increased network activity (Figure 3.3B2-B4). To further characterize the frequency components of the D1 receptor-induced increase in ILA activity, we carried out a short-time Fourier transform for each recording and observed an increase in broadband activity for most LFP events after D1 receptor activation (Figure 3.3C). We then carried out a fast Fourier transform and power spectral density analysis to compare individual

frequency bands across different regions of the mPFC and M2 before and after D1 receptor agonist administration. We found that D1 receptor activation significantly increased delta, alpha, beta, and gamma power in the ILA (Figure 3.3D1-D5). Taken together, these results suggest that D1 receptor activation increases broadband infralimbic network activity in the mPFC that is likely due to excitement of L6-Drd1a neurons. Event analysis and fast Fourier transform suggest that these are network bursts with broadband power, rather than oscillations in the delta-gamma range. Future wavelet analysis will be used to discern the frequency spectrum of individual events and current source density to resolve laminar distribution.

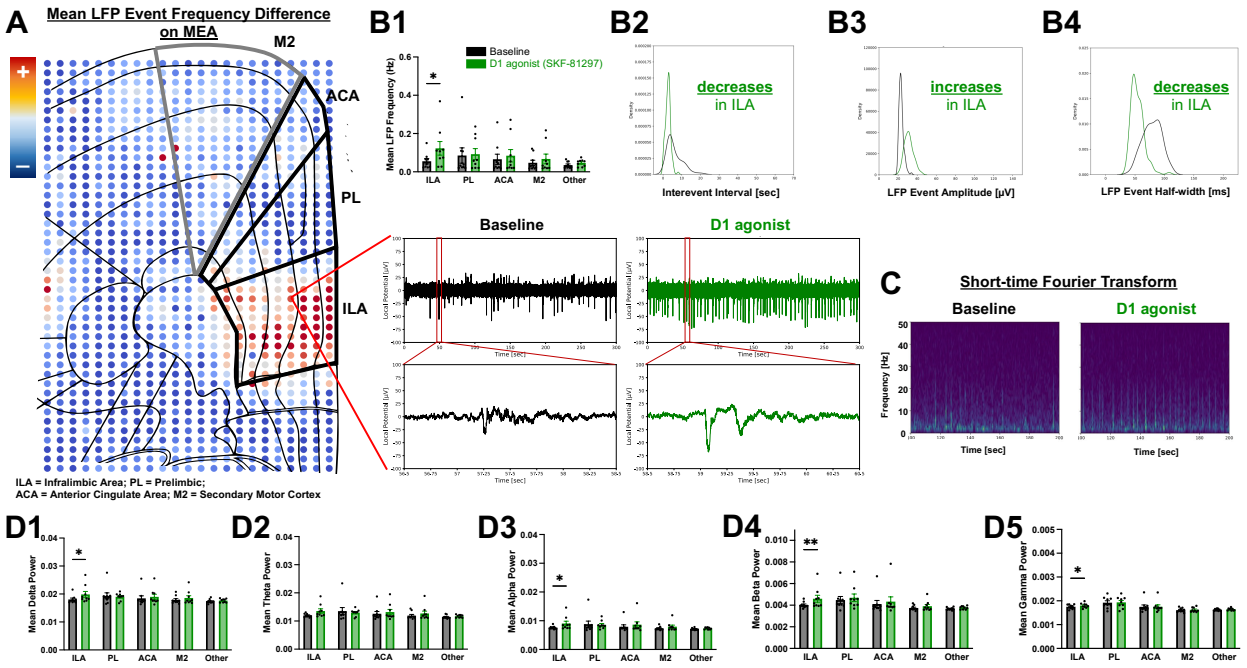


Figure 3.3. D1 receptor activation significantly increases broadband LFP activity in the infralimbic mPFC in the presence of functionally active L6-Drd1a neurons.
(**A**) Schematic of one hemisphere of a coronal mPFC slice taken from the Allen Brain Atlas on top of the MEA chip, along with a baseline trace (black) and SKF-81297 trace (green) from one electrode in the infralimbic mPFC. The MEA diagram displays the mean LFP event frequency difference (SKF-81297 minus baseline), with red resembling a positive difference and blue resembling a negative difference. SKF-81297 increases mean LFP event frequency compared to baseline in the infralimbic mPFC. ILA: infralimbic area; PL: prelimbic; ACA: anterior cingulate area; M2: secondary motor cortex.
(**B1**) Significant increase in mean LFP event frequency with SKF-81297 (green) compared to baseline (black) in the infralimbic mPFC, with a significant drug effect (two-way ANOVA; drug: $F(1,40) = 6.783$, $p = 0.0129$) (Bonferroni multiple comparisons post-hoc test; $p = 0.0151$).

(**B2**) Distribution of interevent intervals across the electrodes in the infralimbic mPFC shows a decrease in interevent intervals with SKF-81297 (green) compared to baseline (black).
(**B3**) Distribution of LFP event amplitudes across the electrodes in the infralimbic mPFC shows an increase in LFP event amplitudes with SKF-81297 (green) compared to baseline (black).
(**B4**) Distribution of LFP event half-widths across the electrodes in the infralimbic mPFC shows a decrease in LFP event half-widths with SKF-81297 (green) compared to baseline (black).
(**C**) Short-time Fourier transform of a baseline and SKF-81297 trace from one electrode in the infralimbic mPFC reveals an increase in broadband activity with SKF-81297 compared to baseline.
(**D1**) Fast Fourier transform reveals a significant increase in mean delta power with SKF-81297 (green) compared to baseline (black) in the infralimbic mPFC, with a significant drug effect (two-way ANOVA; drug: $F(1,40) = 5.940$, $p = 0.0193$) (Bonferroni multiple comparisons post-hoc test; $p = 0.0118$).
(**D2**) Fast Fourier transform reveals no significant difference in mean theta power between SKF-81297 (green) and baseline (black) across the mPFC and M2.
(**D3**) Fast Fourier transform reveals a significant increase in mean alpha power with SKF-81297 (green) compared to baseline (black) in the infralimbic mPFC, with a significant drug effect (two-way ANOVA; drug: $F(1,40) = 6.197$, $p = 0.0171$) (Bonferroni multiple comparisons post-hoc test; $p = 0.0357$).
(**D4**) Fast Fourier transform reveals a significant increase in mean beta power with SKF-81297 (green) compared to baseline (black) in the infralimbic mPFC, with a significant drug effect (two-way ANOVA; drug: $F(1,40) = 13.00$, $p = 0.0009$) (Bonferroni multiple comparisons post-hoc test; $p = 0.0032$).
(**D5**) Fast Fourier transform reveals a significant increase in mean gamma power with SKF-81297 (green) compared to baseline (black) in the infralimbic mPFC, with a significant drug effect (two-way ANOVA; drug: $F(1,40) = 7.378$, $p = 0.0097$) (Bonferroni multiple comparisons post-hoc test; $p = 0.0161$).
For all plots, data are presented as mean +/- s.e.m. ($n = 9$ control slices (Drd1a-Cre-;Snap25$^{fl/fl}$;tdTom$^{STOPfl/fl}$)). Baseline is shown in black, and SKF-81297 is shown in green. Significance is denoted as follows: *$p < 0.05$, **$p < 0.01$, and ***$p < 0.001$ (two-way ANOVA with Bonferroni multiple comparisons tests).

3.3.2 Chronically 'silencing' L6-Drd1a neurons eliminates network activity response to D1 receptor activation

To test whether L6-Drd1a neurons mediate the increase in infralimbic LFP activity in response to D1 receptor agonist, we repeated the above experiment on acute mPFC slices with chronically 'silenced' L6-Drd1a neurons via Snap25 conditional knockout. Indeed, we found that chronically 'silencing' L6-Drd1a neurons eliminated the D1 receptor-induced network activity in the mPFC (Figure 3.4A). This was evidenced by no significant differences in LFP event frequency, interevent interval, amplitude, or half-width before and after D1 receptor agonist administration or across mPFC regions and M2 (Figure 3.4B1-B4). Moreover, there was no significant difference in broadband activity pattern or individual frequency band power (Figure 3.4C,D1-D5). Interestingly, the baseline network activity in the 'silenced' slices was lower than baseline activity in the control slices, suggesting that 'silencing' L6-Drd1a neurons not only

eliminates network activity response to D1 receptor activation but also lowers baseline activity levels in the mPFC.

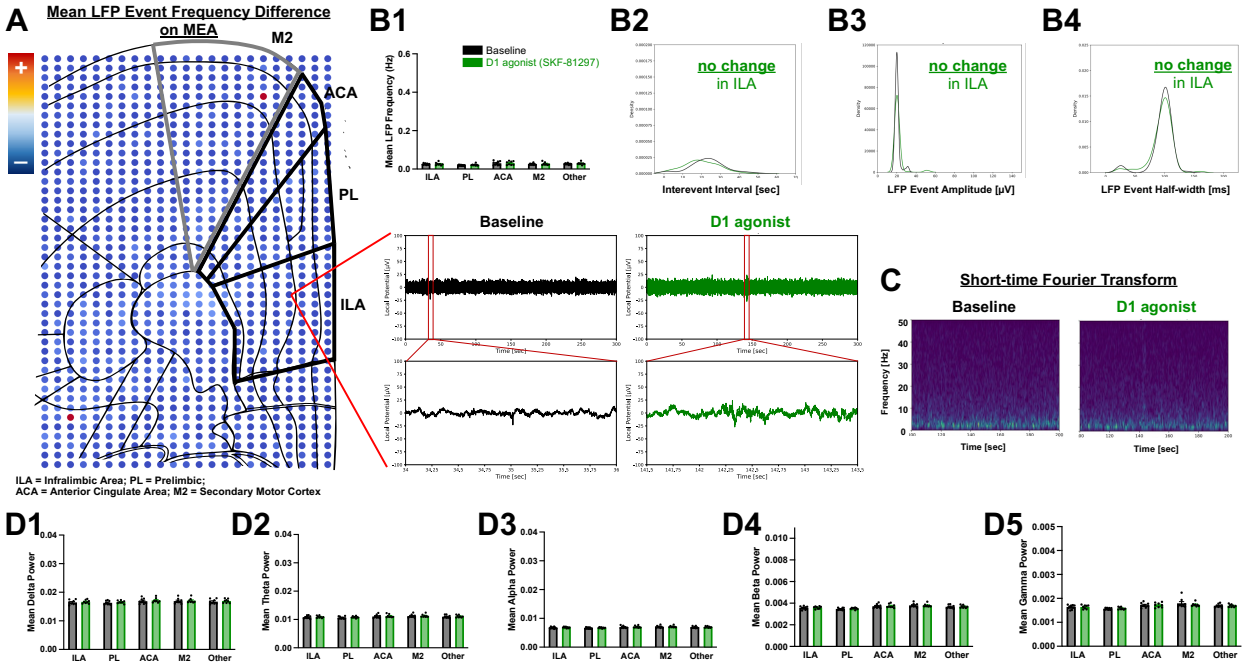


Figure 3.4. Chronically 'silencing' L6-Drd1a neurons eliminates broadband LFP activity response to D1 receptor activation.

(**A**) Schematic of one hemisphere of a coronal mPFC slice taken from the Allen Brain Atlas on top of the MEA chip, along with a baseline trace (black) and SKF-81297 trace (green) from one electrode in the infralimbic mPFC. The MEA diagram displays the mean LFP event frequency difference (SKF-81297 minus baseline), with red resembling a positive difference and blue resembling a negative difference. There is no difference in mean LFP event frequency between SKF-81297 and baseline across the mPFC and M2. ILA: infralimbic area; PL: prelimbic; ACA: anterior cingulate area; M2: secondary motor cortex.

(**B1**) No Significant difference in mean LFP event frequency between SKF-81297 (green) and baseline (black) across the mPFC and M2.

(**B2**) Distribution of interevent intervals across the electrodes in the infralimbic mPFC shows no difference in interevent intervals between SKF-81297 (green) and baseline (black).

(**B3**) Distribution of LFP event amplitudes across the electrodes in the infralimbic mPFC shows no difference in LFP event amplitudes between SKF-81297 (green) and baseline (black).

(**B4**) Distribution of LFP event half-widths across the electrodes in the infralimbic mPFC shows no difference in LFP event half-widths between SKF-81297 (green) and baseline (black).

(**C**) Short-time Fourier transform of a baseline and SKF-81297 trace from one electrode in the infralimbic mPFC reveals no difference in broadband activity between SKF-81297 and baseline.

(**D1**) Fast Fourier transform reveals no significant difference in mean delta power between SKF-81297 (green) and baseline (black) across the mPFC and M2.

(**D2**) Fast Fourier transform reveals no significant difference in mean theta power between SKF-81297 (green) and baseline (black) across the mPFC and M2.

(**D3**) Fast Fourier transform reveals no significant difference in mean alpha power between SKF-81297 (green) and baseline (black) across the mPFC and M2.

(**D4**) Fast Fourier transform reveals no significant difference in mean beta power between SKF-81297 (green) and baseline (black) across the mPFC and M2.

(**D5**) Fast Fourier transform reveals no significant difference in mean gamma power between SKF-81297 (green) and baseline (black) across the mPFC and M2.
For all plots, data are presented as mean +/- s.e.m. (n = 8 L6-Drd1a 'silenced' slices (Drd1a-Cre+;Snap25$^{fl/fl}$;tdTom$^{STOPfl/fl}$)). Baseline is shown in black and SKF-81297 is shown in green. Significance is determined using two-way ANOVA with Bonferroni multiple comparisons tests.

3.3.3 D2 receptor activation exerts no significant effects on local mPFC network activity in the presence of functionally active L6-Drd1a neurons

The differential laminar distribution and cell-type expression patterns of D1 (predominately L6 pyramidal and GABAergic neurons) and D2 receptors (predominately L5 pyramidal neurons and L6 GABAergic neurons) (Santana et al., 2009), along with their different downstream signaling pathways, prompted us to investigate how D2 receptor activation contributes to the overall dopaminergic modulation of local network activity in the mPFC. We found that D2 receptor agonist quinpirole administration did not significantly change LFP event frequency, interevent interval, amplitude, or half-width (Figure 3.5A,B1-B4). There was also no significant difference in broadband activity pattern or individual frequency band power (Figure 3.5C,D1-D5). These findings suggest that D2 receptor activation may equally activate excitatory and inhibitory networks in the mPFC to yield no significant differences in overall network activity, unlike D1 receptors which are more abundant in the PFC and are highly expressed in L6 pyramidal neurons (Berger et al., 1991; Santana et al., 2009; Allen Brain Map Single-cell Transcriptomics, 2020).

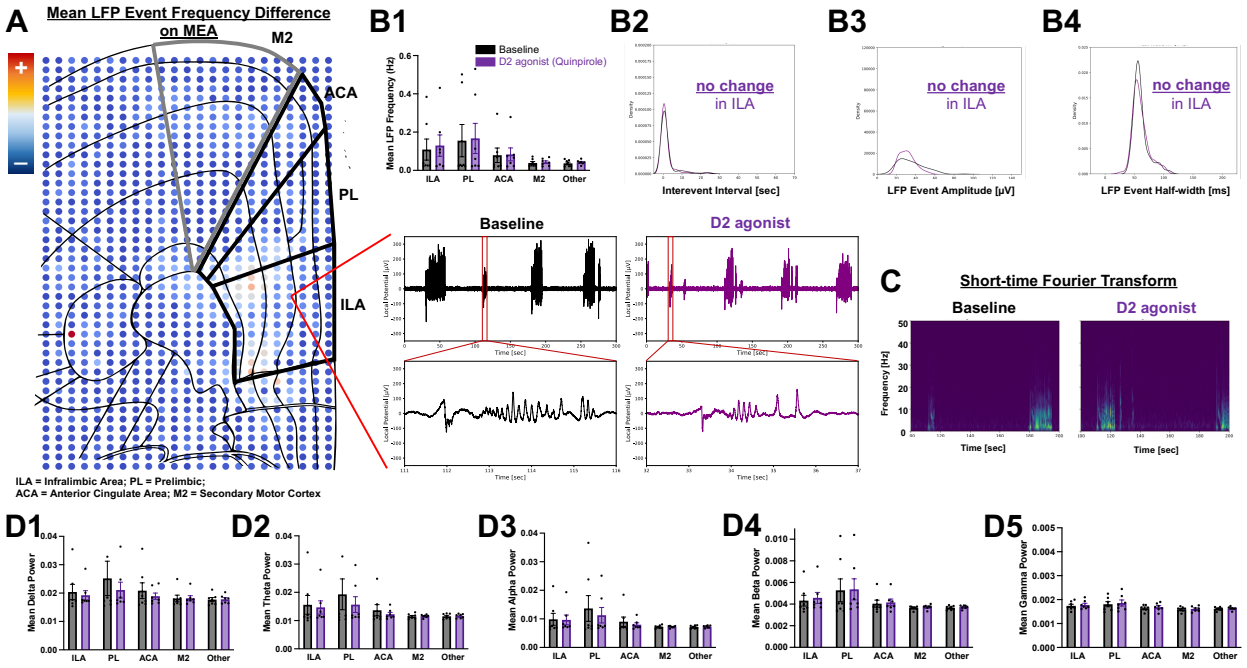


Figure 3.5. D2 receptor activation exerts no significant changes in local mPFC network activity in the presence of functionally active L6-Drd1a neurons.

(**A**) Schematic of one hemisphere of a coronal mPFC slice taken from the Allen Brain Atlas on top of the MEA chip, along with a baseline trace (black) and quinpirole trace (purple) from one electrode in the infralimbic mPFC. The MEA diagram displays the mean LFP event frequency difference (quinpirole minus baseline), with red resembling a positive difference and blue resembling a negative difference. There is no difference in mean LFP event frequency between quinpirole and baseline across the mPFC and M2. ILA: infralimbic area; PL: prelimbic; ACA: anterior cingulate area; M2: secondary motor cortex.

(**B1**) No Significant difference in mean LFP event frequency between quinpirole (purple) and baseline (black) across the mPFC and M2.

(**B2**) Distribution of interevent intervals across the electrodes in the infralimbic mPFC shows no difference in interevent intervals between quinpirole (purple) and baseline (black).

(**B3**) Distribution of LFP event amplitudes across the electrodes in the infralimbic mPFC shows no difference in LFP event amplitudes between quinpirole (purple) and baseline (black).

(**B4**) Distribution of LFP event half-widths across the electrodes in the infralimbic mPFC shows no difference in LFP event half-widths between quinpirole (purple) and baseline (black).

(**C**) Short-time Fourier transform of a baseline and quinpirole trace from one electrode in the infralimbic mPFC reveals no difference in broadband activity between quinpirole and baseline.

(**D1**) Fast Fourier transform reveals no significant difference in mean delta power between quinpirole (purple) and baseline (black) across the mPFC and M2.

(**D2**) Fast Fourier transform reveals no significant difference in mean theta power between quinpirole (purple) and baseline (black) across the mPFC and M2.

(**D3**) Fast Fourier transform reveals no significant difference in mean alpha power between quinpirole (purple) and baseline (black) across the mPFC and M2.

(**D4**) Fast Fourier transform reveals no significant difference in mean beta power between quinpirole (purple) and baseline (black) across the mPFC and M2.

(**D5**) Fast Fourier transform reveals no significant difference in mean gamma power between quinpirole (purple) and baseline (black) across the mPFC and M2.

For all plots, data are presented as mean +/- s.e.m. (n = 7 control slices (Drd1a-Cre-;Snap25$^{fl/fl}$;tdTom$^{STOPfl/fl}$)). Baseline is shown in black and quinpirole is shown in purple. Significance is determined using two-way ANOVA with Bonferroni multiple comparisons tests.

3.3.4 Chronically 'silencing' L6-Drd1a neurons unmasks a D2 receptor-mediated increase in infralimbic mPFC network activity

To study the specific interaction between L6-Drd1a neurons and D2 receptor activation, we chronically 'silenced' L6-Drd1a neurons via Snap25 conditional knockout and examined the effects of D2 receptor activation on local network activity in the mPFC. Surprisingly, we found that D2 receptor agonist quinpirole significantly and paradoxically increased LFP event frequency in the ILA compared to other mPFC regions and M2 in the L6-Drd1a 'silenced' slices, along with decreasing interevent interval and increasing amplitude (Figure 3.6A,B1-B4). A short-time Fourier transform revealed an increase in broadband activity patterns in the ILA upon D2 receptor activation, and a fast Fourier transform and power spectral density analysis further revealed significant increases in delta, theta, alpha, and beta power in the ILA (Figure 3.6C,D1-D5). Notably, these results matched the network response to D1 receptor activation in control slices (Figure 3.3), suggesting that L6-Drd1a neurons functionally mediate the fine-tuned balance between D1 and D2 receptor modulation in local mPFC networks.

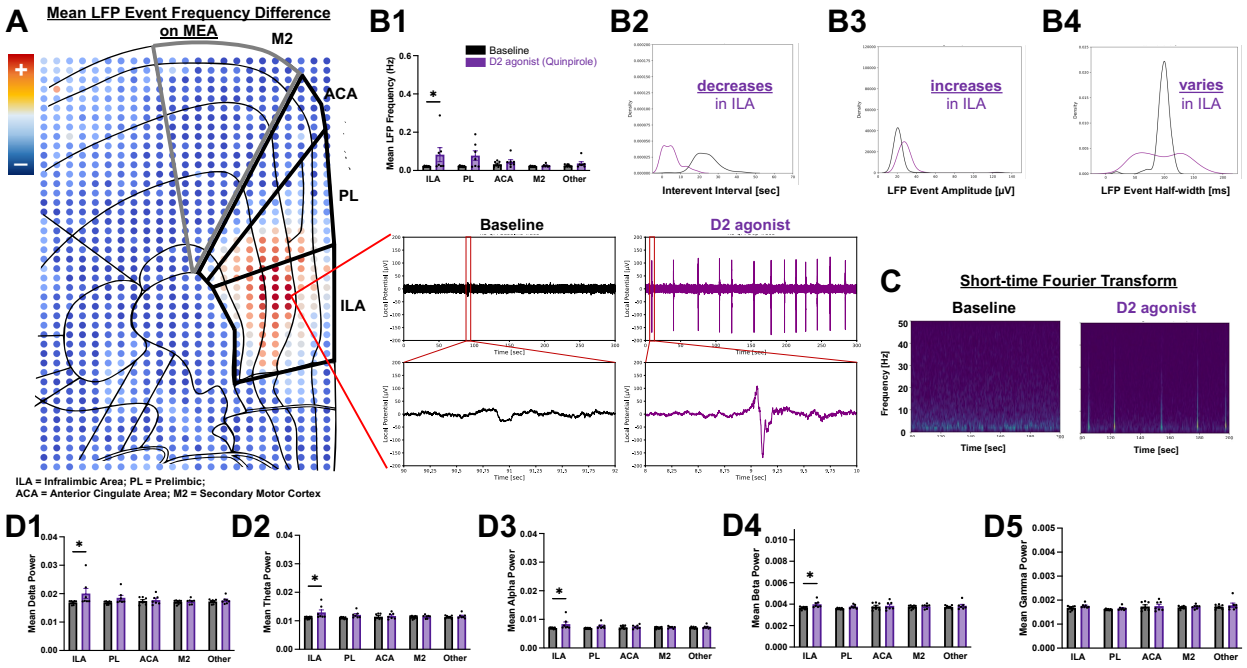


Figure 3.6. Chronically 'silencing' L6-Drd1a neurons unmasks a D2 receptor-mediated increase in infralimbic mPFC network activity.

(**A**) Schematic of one hemisphere of a coronal mPFC slice taken from the Allen Brain Atlas on top of the MEA chip, along with a baseline trace (black) and quinpirole trace (purple) from one electrode in the infralimbic mPFC. The MEA diagram displays the mean LFP event frequency difference (quinpirole minus baseline), with red resembling a positive difference and blue resembling a negative difference. Quinpirole increases mean LFP event frequency compared to baseline in the infralimbic mPFC. ILA: infralimbic area; PL: prelimbic; ACA: anterior cingulate area; M2: secondary motor cortex.

(**B1**) Significant increase in mean LFP event frequency with quinpirole (purple) compared to baseline (black) in the infralimbic mPFC, with a significant drug effect (two-way ANOVA; drug: $F(1,30) = 10.06$, $p = 0.0035$) (Bonferroni multiple comparisons post-hoc test; $p = 0.0286$).

(**B2**) Distribution of interevent intervals across the electrodes in the infralimbic mPFC shows a decrease in interevent intervals with quinpirole (purple) compared to baseline (black).

(**B3**) Distribution of LFP event amplitudes across the electrodes in the infralimbic mPFC shows an increase in LFP event amplitudes with quinpirole (purple) compared to baseline (black).

(**B4**) Distribution of LFP event half-widths across the electrodes in the infralimbic mPFC varies with quinpirole (purple) compared to baseline (black).

(**C**) Short-time Fourier transform of a baseline and quinpirole trace from one electrode in the infralimbic mPFC reveals an increase in broadband activity with quinpirole compared to baseline.

(**D1**) Fast Fourier transform reveals a significant increase in mean delta power with quinpirole (purple) compared to baseline (black) in the infralimbic mPFC, with a significant drug effect (two-way ANOVA; drug: $F(1,30) = 6.087$, $p = 0.0195$) (Bonferroni multiple comparisons post-hoc test; $p = 0.0258$).

(**D2**) Fast Fourier transform reveals a significant increase in mean theta power with quinpirole (purple) compared to baseline (black) in the infralimbic mPFC, with a significant drug effect (two-way ANOVA; drug: $F(1,30) = 8.088$, $p = 0.0079$) (Bonferroni multiple comparisons post-hoc test; $p = 0.0120$).

(**D3**) Fast Fourier transform reveals a significant increase in mean alpha power with quinpirole (purple) compared to baseline (black) in the infralimbic mPFC, with a significant drug effect (two-way ANOVA; drug: $F(1,30) = 7.327$, $p = 0.0111$) (Bonferroni multiple comparisons post-hoc test; $p = 0.0176$).

(**D4**) Fast Fourier transform reveals a significant increase in mean beta power with quinpirole (purple) compared to baseline (black) in the infralimbic mPFC, with a significant drug effect (two-way ANOVA; drug: $F(1,30) = 10.57$, $p = 0.0028$) (Bonferroni multiple comparisons post-hoc test; $p = 0.0118$).

(**D5**) Fast Fourier transform reveals no significant difference in mean gamma power between quinpirole (purple) and baseline (black) across the mPFC and M2.

For all plots, data are presented as mean +/- s.e.m. (n = 7 L6-Drd1a 'silenced' slices (Drd1a-Cre+;Snap25$^{fl/fl}$;tdTom$^{STOPfl/fl}$)). Baseline is shown in black, and quinpirole is shown in purple. Significance is denoted as follows: *$p < 0.05$, **$p < 0.01$, and ***$p < 0.001$ (two-way ANOVA with Bonferroni multiple comparisons tests).

3.4 Discussion

It is generally recognized that L6 primarily functions as an output layer sending corticothalamic projections, with L6b sharing developmental origins from the transient subplate that is involved in establishing the earliest corticothalamic connections (Hoerder-Suabedissen & Molnár, 2015). The functional role of L6b in primary sensory areas has been extensively characterized as modulating cortical arousal through the orexin-sensitive L6-Drd1a neuronal subpopulation that subcortically targets higher-order thalamic nuclei and intracortically shares laminar-specific targets with thalamocortical afferents (Hoerder-Suabedissen et al., 2018; Zolnik et al., 2023). Furthermore, L6b is driven by long-range intracortical inputs, forms extensive local networks with inhibitory interneurons in L6, and is strongly activated by arousal neuromodulators such as orexin, acetylcholine, neurotensin, dopamine, and noradrenaline (Zolnik et al., 2020; Bayer et al., 2004; Hay et al., 2015; Combremont et al., 2016a, 2016b).

In anterior neocortical association areas such as the mPFC, the functional connectivity and modulation of these L6-Drd1a neurons remain poorly understood. Messore and colleagues have shown that orexin receptor-mediated increases in infralimbic mPFC network excitability is eliminated upon chronic 'silencing' of L6-Drd1a neurons, and that orexin selectively excites L6-Drd1a neurons compared to other L6 neurons in the mPFC (Messore et al., 2024). In this chapter, we directed our attention to the dopaminergic modulation of local mPFC network activity because we were interested in whether dopamine plays an analogous role to orexin in arousing local mPFC network activity through these L6-Drd1a neurons. Given the different stimulatory and inhibitory downstream signaling pathways of D1 and D2 receptors, respectively, we

specifically compared network modulation by D1 and D2 receptors in control and L6-Drd1a 'silenced' mPFC slices. We speculate that L6-Drd1a neurons fine-tune local network activity in the mPFC by balancing D1 and D2 receptor modulation to gate cortical arousal alongside orexin.

3.4.1 The role of L6-Drd1a neurons in D1 receptor modulation of local mPFC network activity

To test the above claim, we began by bath-applying D1 receptor agonist to acute mPFC slices *in-vitro* on a high-density planar MEA and carried out LFP recordings in control and L6-Drd1a 'silenced' slices. We observed that D1 receptor agonist SKF-81297 strongly activated LFP activity in the infralimbic mPFC in control slices, which is eliminated upon chronic 'silencing' of L6-Drd1a neurons (Figure 3.3, 3.4). This localized L6-Drd1a-mediated response in the ILA was also observed with OX2R agonist YNT-185 (Messore et al., 2024), suggesting that D1 and orexin neuromodulators likely converge on L6-Drd1a neurons in activating local mPFC networks to drive cortical arousal. However, the mechanism by which D1 receptor and OX2R activate these networks seems to be nuanced. While OX2R activation significantly increases slow-wave delta power (Messore et al., 2024), we showed that D1 receptor activation significantly increased broadband activity. We speculate that D1 receptor and OX2R may differentially activate components of the higher-order cortico-thalamo-cortical loop through L6-Drd1a neurons, with D1 receptor modulating its salience. Future analysis will need to compare how the frequency, morphology, and laminar distribution of individual events change during dopaminergic and orexinergic neuromodulation.

Interestingly, baseline mPFC network activity decreases upon chronic 'silencing' of L6-Drd1a neurons, indicating that they play a prominent role in sustaining local network activity. Although these L6-Drd1a neurons are primarily driven by long-range intracortical input, they are

known to form extensive local excitatory-inhibitory loops within L6, and thus the effect of their 'silencing' can be detected on the MEA. Given the functional demand of these L6-Drd1a neurons in driving cortical arousal, we expected that their chronic 'silencing' yields an overall decrease in network activity. This decrease in baseline network activity upon L6-Drd1a 'silencing' may also explain the diminished effect of D1 receptor activation, since dopamine can exert different effects at different network activity levels (Seamans & Yang, 2004).

3.4.2 The role of L6-Drd1a neurons in D2 receptor modulation of local mPFC network activity

Given the complex signaling interactions between D1 and D2 receptors in the PFC, we sought to examine how L6-Drd1a neurons also mediate D2 receptor modulation of local mPFC network activity. We found that D2 receptor agonist quinpirole exerted no significant changes in LFP activity in control mPFC slices, but chronically 'silencing' L6-Drd1a neurons unmasked a significant D2 receptor-mediated increase in infralimbic mPFC network activity (Figure 3.5, 3.6). This activity was similar to what was observed with D1 receptor activation in control slices (Figure 3.3). There a few likely explanations for these findings. The lack of network response to D2 receptor agonist in control slices is likely due to a balanced activation of excitatory-inhibitory loops in the mPFC. Unlike D1 receptor, which is predominately expressed in L6 excitatory pyramidal neurons, D2 receptor is expressed in a smaller proportion of pyramidal neurons that are mostly in L5, and its predominant L6 expression is in inhibitory GABAergic neurons (Santana et al., 2009). As such, D2 receptor activation likely does not elicit the same prominent level of mPFC network excitation as does D1 receptor activation.

The paradoxical D2 receptor-mediated increase in network activity upon chronically 'silencing' L6-Drd1a neurons is likely due to a compensatory shift in network activation

patterns. D1 and D2 receptors can form heterodimers that couple to a PLC signaling pathway (Lee et al., 2004). Coactivation of D1 and D2 receptors in the lateral orbitofrontal cortex potentiates NMDA-dependent synaptic transmission (Thompson et al., 2016). If D2 receptors are co-expressed in L6-Drd1a neurons, chronically 'silencing' these L6-Drd1a neurons will likely potentiate other excitatory D2-expressing neurons to compensate for this functional 'silencing'.

Another likely explanation for these findings is that the fine-tuned balance of D1 and D2 receptor modulation in the mPFC involves disynaptic inhibition mechanisms through GABAergic interneurons that may underlie the biphasic time-dependent nature of dopamine activity. During dopamine application, D2 receptor activation in the PFC initially reduces spike firing, but after 10-15 minutes, D1 receptor activation elicits a prolonged increase in evoked spiking (Gulledge & Jaffe, 1998; Gorelova & Yang, 2000; Seamans et al., 2001b). Furthermore, L6-Drd1a neurons form excitatory-inhibitory feedback loops with local interneurons in L6 and suppress L6b firing activity through a disynaptic mechanism (Zolnik et al., 2020, 2023). Thus, the biphasic pattern of dopamine signaling in the PFC may be due to D1 receptor-expressing neurons inhibiting D2 receptor-expressing neurons over time through GABAergic interneurons. In our study, we noticed that the D2 receptor-mediated increase in network activity in the L6-Drd1a 'silenced' slices was only evident 15 minutes after D2 receptor agonist administration. Therefore, by chronically 'silencing' L6-Drd1a neurons, D2 receptor-expressing neurons likely become disinhibited over time, which explains why we observed an increase in network activity 15 minutes after D2 receptor agonist administration.

3.4.3 Limitations and future directions

Although our results offer valuable insight into the dopaminergic modulation of local mPFC network activity, they do not capture the long-range functional connectivity of L6-Drd1a neurons due to our *in-vitro* acute coronal slice preparation. In order to investigate the dopaminergic modulation of L6-Drd1a long-range intracortical inputs or higher-order thalamic projections, we would need to carry out acute cortico-cortico or corticothalamic slices recordings, or *in-vivo* mPFC recordings. Additionally, although the voltage-gated potassium channel blocker 4-AP is generally used to detect *in-vitro* cortical LFP activity, its bath application in our experimental context may confound the observed effects of D1 receptor activation since one of the mechanisms by which D1 receptors excite PFC pyramidal neurons is by reducing voltage-gated potassium currents (Yang & Seamans, 1996).

Regarding the Drd1a-Cre mouse model, it should be noted that the onset of cortical Cre expression driven by the Drd1a promoter occurs shortly after birth with considerable expression by postnatal day P8, and thus Snap25 is conditionally knocked out in Drd1a-Cre+ neurons around the first postnatal week (Hoerder-Suabedissen et al., 2018). Moreover, although the Drd1a-Cre line that we used targets cortical L6b in primary sensory areas and L6 in the mPFC with relative specificity, it includes some off-target expression in the ventral hippocampus and cerebellum (Hoerder-Suabedissen et al., 2018). Thus, some hippocampal-mPFC connections may also be functionally 'silenced' in our experimental model, which could have a confounding effect on mPFC network activity. Furthermore, while Snap25 conditional knockout abolishes action potential-evoked neurotransmission, spontaneous synaptic vesicle release still occurs (Washbourne et al., 2002; Bronk et al., 2007). Nonetheless, synaptic transmission is predominately disrupted in the cortical L6-Drd1a neuronal subpopulation, and previous studies

have reported significant behavioral and physiological phenotypes using this Snap25 conditional knockout model (Messore et al., 2024; Krone et al., 2021).

As a follow-up to this study, we would like to investigate how the coactivation of orexin and dopamine agonists modulates mPFC network activity in control and L6-Drd1a 'silenced' slices, since both neuromodulators independently arouse local mPFC networks and activate L6-Drd1a neurons (Messore et al., 2023). Moreover, given the differential regulation of PFC glutamatergic (Law-Tho et al., 1994; Momiyama et al., 1996; Seamans et al., 2001a; Wang & O'Donnell, 2001) and GABAergic networks by D1 and D2 receptors (Gorelova et al., 2002; Gulledge & Jaffe, 2001; Seamans et al., 2001b), we would also like to test D1 and D2 receptor modulation of mPFC network activity through L6-Drd1a neurons in the presence of glutamatergic and GABAergic agonists and antagonists. Overall, this chapter provides valuable insight into the functional role of orexin-sensitive L6-Drd1a neurons in differentially modulating the arousal of local mPFC networks through D1 and D2 receptors.

IV. Dopaminergic modulation of L6-Drd1a and L6-non-Drd1a neurons in the mPFC

4.1 Introduction

This chapter addresses the second aim of this thesis: characterizing D1 and D2 receptor modulation of L6-Drd1a and L6-non-Drd1a intrinsic neuronal excitability and spontaneous synaptic potentials in the mPFC using *in-vitro* whole-cell patch clamp recordings. While D1 receptor-expressing cortical neurons are not restricted to L6 corticothalamic projections (Anastasiades et al., 2019), D1 receptor expression in adult L6-Drd1a neurons likely plays an important role in regulating network excitability according to our findings in Chapter 3. Given L6-Drd1a neurons' enhanced expression for D1 receptors and their orexin sensitivity compared to other L6 neurons in the mPFC, we hypothesize that dopamine and orexin play a synergistic role in regulating cortical arousal through activation of L6-Drd1a neurons. Specifically, we expect that D1 receptor agonist selectively excites L6-Drd1a neurons compared to other L6 neurons in the mPFC, with a non-selective effect of D2 receptor agonist.

4.1.1 L6b neuronal cell types and electrophysiological properties

L6b is a highly heterogenous layer with morphological and physiological diversity in excitatory and inhibitory cell types. In the rat S1 barrel cortex, five types of excitatory neurons have been identified based on their structural and electrophysiological properties: pyramidal neurons with apical dendrites projecting toward the pial surface, inverted pyramidal neurons with dendrites projecting toward the white mater, tangentially-oriented pyramidal neurons with oblique dendrites, horizontally-oriented pyramidal neurons with anterior-posterior or medial-

lateral dendritic projections, and non-pyramidal multipolar neurons without preferential dendritic orientations (Figure 4.1) (Marx & Feldmeyer, 2013). L6b upright and tangential pyramidal neurons can extend their dendrites to superficial L5, whereas inverted and horizonal pyramidal neuronal dendrites generally reside in L6 and the white matter (Marx & Feldmeyer, 2013). L6b multipolar neurons display broad dendritic domains within L5, L6, and the white matter. The axonal projections of L6b inverted and horizontal pyramidal neurons are generally horizontal and long-distance but remain within L6 and the white matter, whereas tangential pyramidal neurons and multipolar neurons exhibit more superficial axonal projections (Feldmeyer, 2023). Generally, L6b non-pyramidal neurons establish corticocortical connections, while pyramidal neurons send cortical and subcortical axonal projections, particularly to higher-order thalamic nuclei (Marx & Feldmeyer, 2013; Zolnik et al., 2023).

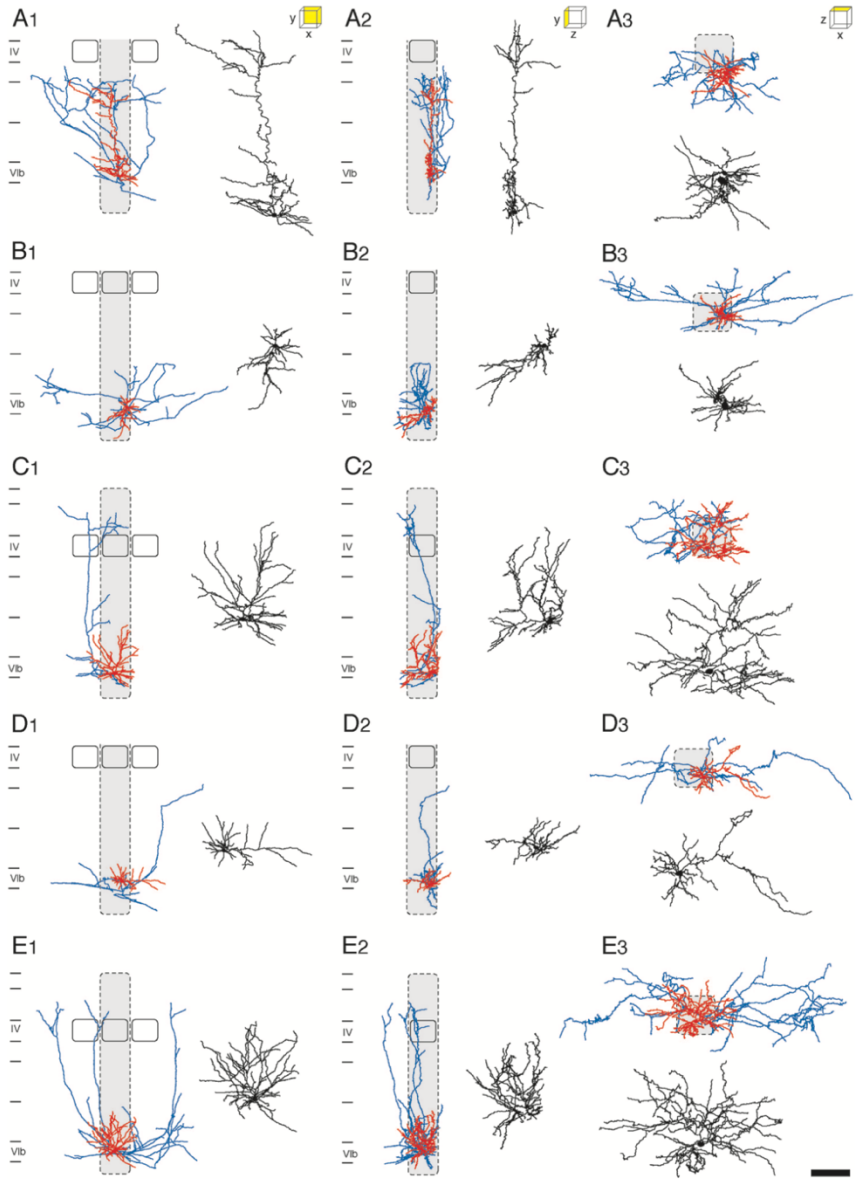


Figure 4.1. Morphological diversity among L6b excitatory neurons.
(Adapted from Marx & Feldmeyer, 2013).
Reconstruction of each of the five L6b excitatory neuron groups in the S1 barrel cortex shown from three angles: (**A1-E1**) xy-direction; (**A2-E2**) yz-direction; (**A3-E3**) xz-direction.
(**A1-A3**) Pyramidal neuron with apical dendrites projecting toward the pial surface.
(**B1-B3**) Inverted pyramidal neuron with dendrite pointing toward the white matter.
(**C1-C3**) Tangentially-oriented pyramidal neuron with oblique dendrites.
(**D1-D3**) Horizontally-oriented pyramidal neuron with anterior-posterior or medial-lateral dendritic projections.
(**E1-E3**) Multipolar neuron without preferential dendritic orientations.
Axons are shown in blue, dendrites are shown in red, and a two-fold magnification of each somatodendritic structure is shown in black. Scale bar for A1-E2: 300 µm (150 µm for somatodendritic magnification); scale bar for A3-E3: 200 µm (100 µm for somatodendritic magnification).

L6b excitatory neurons also exhibit diverse physiological properties. They mostly have a regular spiking pattern with no significant differences in resting membrane potential, action potential half-width, or afterhyperpolarization. Inverted pyramidal neurons particularly display a higher spiking frequency with a lower adaptation ratio, and multipolar neurons tend to have the longest interspike intervals (Marx & Feldmeyer, 2013). There is also a set of spiny multipolar L6b neurons in S1 that fire spontaneously in slow rhythmic bursts and are directly excited by orexin, noradrenaline, histamine, dopamine, and neurotensin through a postsynaptic mechanism (Combremont et al., 2016b). These neurons display delayed action potential firing during small depolarizing current steps, and they rapidly inactivate at larger current steps followed by a depolarizing afterpotential. During hyperpolarizing current steps, these neurons also display a hyperpolarization-induced sag with a depolarizing rebound. Interestingly, the rhythmic bursting of these neurons represents a mix of intrinsic and network-dependent activity, suggesting that these L6b neurons may functionally contribute to slow oscillation networks that drive cortical arousal through orexin and dopamine (Combremont et al., 2016b).

As described in Chapter 1, Drd1a neurons and Ctgf neurons have been characterized as two prominent L6b excitatory neuron subpopulations in S1. Drd1a neurons (which can be pyramidal or non-pyramidal) and Ctgf neurons (which are mostly non-pyramidal) represent 25-40% and 25% of S1 L6b neurons, respectively (Hoerder-Suabedissen et al., 2018; Zolnik et al., 2020). In S1, Drd1a neurons elicit spikes at higher frequencies and exhibit a more potent hyperpolarization-induced sag compared to Ctgf neurons (Zolnik et al., 2020). L6-Drd1a pyramidal neurons almost exclusively target higher-order nuclei such as the POm and are highly sensitive to orexin, suggesting an important role for these neurons in driving cortical arousal via the higher-order thalamocortical system (refer to Chapter 3 for a detailed description of L6-

Drd1a functional connectivity). In S1, *in-vitro* orexin administration leads to sustained spiking activity in L6-Drd1a neurons (Zolnik et al., 2023). In the mPFC, *in-vitro* orexin administration increases L6-Drd1a intrinsic excitability by decreasing rheobase current and increasing membrane resistance and resting membrane potential without changing threshold potential (Messore et al., 2024).

While the proportion of GABAergic interneurons in L6b is low, they likely exert a strong functional effect on local network activity. The majority of L6 interneurons are fast-spiking PV and non-fast-spiking SST interneurons, with the presence of VIP and neuropeptide Y (NPY) interneurons as well (Perrenoud et al., 2013). L6b interneurons display dense local dendritic and axonal arborizations within L6, likely exerting a strong functional effect on local neuronal networks (Feldmeyer, 2023). L6b fast-spiking GABAergic basket interneurons in S1 (which exhibit high-frequency spiking with deep afterhyperpolarizations, along with a high level of spontaneous synaptic activity) are indirectly excited by orexin, which is mediated by neighboring orexin-sensitive neurons rather than presynaptic glutamatergic terminals (Combremont et al., 2016a). A similar indirect effect is observed with neurotensin, which is known to colocalize in orexinergic neurons (Furutani et al., 2013), whereas noradrenaline and acetylcholine excite these fast-spiking GABAergic interneurons through a direct postsynaptic mechanism. L6-Drd1a neurons are likely the orexin-sensitive neurons that excite these fast-spiking interneurons in L6b, which may help drive cortical arousal and facilitate high-frequency oscillations that are a characteristic result of fast-spiking PV interneurons (Freund, 2003; Cardin et al., 2009; Sohal et al., 2009).

4.1.2 Dopaminergic modulation of PFC neurons in-vitro

As a neuromodulator, dopamine generally functions to potentiate or attenuate responses by other neurotransmitters. The mechanism of dopamine action involves modulating intrinsic neuronal excitability, synaptic transmission, plasticity, and local glutamatergic and GABAergic networks. D1 receptor agonists increase PFC neuronal excitability by lowering the threshold for tetrodotoxin (TTX)-sensitive voltage-gated sodium channel activation and reducing its inactivation time constant (Gorelova & Yang, 2000), while simultaneously reducing leak currents and 4-AP-sensitive voltage-gated potassium delayed rectifier currents (Yang & Seamans, 1996). In the PFC, D1 receptors seem to exert little effect on calcium influx in distal apical dendrites compared to back-propagating sodium-dependent action potentials (Gulledge & Stuart, 2003). This is likely due to the smaller dendritic-somatic distance of pyramidal neurons in the PFC, which lacks a clear L4. However, D1 receptor stimulation can strongly modulate longer duration L-type calcium currents near basal dendrites. Interestingly, this state-dependent bidirectional modulation occurs through different intracellular signaling pathways. D1 receptor stimulation potentiates subthreshold L-type calcium 'hump' potentials via PKA activation, followed by a suppression of L-type calcium channel activity over time via PKC activation (Young & Yang, 2004). This bidirectional modulation of dendritic calcium spikes near the soma likely allows dopamine to augment or attenuate different synaptic responses to 'fine-tune' their integration by the soma (Seamans & Yang, 2004).

There is also a biphasic effect of dopamine dependent on time after bath application. D2 receptor activation initially reduces spike firing likely through increased leak currents, followed by a prolonged increase in evoked spiking after 10-15 minutes that is mediated by D1 receptor activation (Gulledge & Jaffe, 1998; Gorelova & Yang, 2000; Seamans et al., 2001b). The initial

decrease in activity is likely due to dopamine-mediated increases in GABA release onto PFC pyramidal neurons, since GABA-A antagonists and TTX separately block this inhibitory effect while focal GABA application mimics the inhibitory effect (Gulledge & Jaffe, 2001; Seamans et al., 2001b). The prolonged increase in activity is likely due to NMDA-mediated responses to D1 receptor activation and DARPP-32 signaling (Zheng et al., 1999; Seamans et al., 2001a; Wang & O'Donnell, 2001). Furthermore, long-lasting NMDA receptor-mediated responses activate intracellular calcium-dependent pathways that lead to protein synthesis and structural changes in dendritic spines (Huang & Kandel, 1995). D1 receptor agonists can also decrease evoked NMDA and AMPA responses by reducing presynaptic glutamate release since D1 receptors localize near NMDA and AMPA receptors at asymmetric synapses (Law-Tho et al., 1994; Momiyama et al., 1996; Seamans & Yang, 2004).

Since dopamine modulates both inhibitory GABAergic responses and excitatory NMDA responses, the level of local PFC network activity can drive opposite effects of dopamine. At low levels of activity, NMDA currents are relatively low compared to GABA currents, thus D1 responses mediated by GABA receptors would outweigh those that are mediated by NMDA receptors, and vice versa at high network activity levels (Seamans & Yang, 2004). This state-dependent effect is also observed when D1 receptors increase neuronal excitability during depolarized 'up' states but decrease excitability during hyperpolarized 'down' states (Lavin & Grace, 2001). Dopamine also exerts a dose-dependent effect in the PFC, where low concentrations of dopamine (< 50 μM) act preferentially on D1-like receptors to potentiate NMDA currents while high concentrations of dopamine (> 50 μM) also activate D2-like receptors to attenuate NMDA currents (Zheng et al., 1999).

Dopamine also modulates inhibitory synaptic responses in PFC deep-layer pyramidal neurons. D1 receptor agonists increase evoked inhibitory postsynaptic current (IPSC) amplitude gradually over a prolonged period while D2 receptor agonists decrease evoked IPSC amplitude more rapidly (Seamans et al., 2001b). D1 receptor agonists, but not D2 receptor agonists, depolarize and increase the excitability of fast-spiking interneurons, which synaptically inhibit PFC pyramidal neurons near the spike initiation zone (Gorelova et al., 2002). Postsynaptically, PKA signaling enhances while PKC signaling reduces GABA-mediated currents, and both PKA and PKC signaling pathways are involved in D1-like and D2-like receptor activity.

In summary, not only do D1-like and D2-like receptors differentially regulate the intrinsic excitability of PFC pyramidal neurons, but they also modulate excitatory and inhibitory synaptic responses, both presynaptically through local glutamatergic and GABAergic networks and postsynaptically through NMDA, AMPA, and GABA receptors (Figure 4.2). The effects of dopamine are also dependent on local network activity levels, application dose, intracellular signaling pathways, and the temporal profile of D1 and D2 receptor activation.

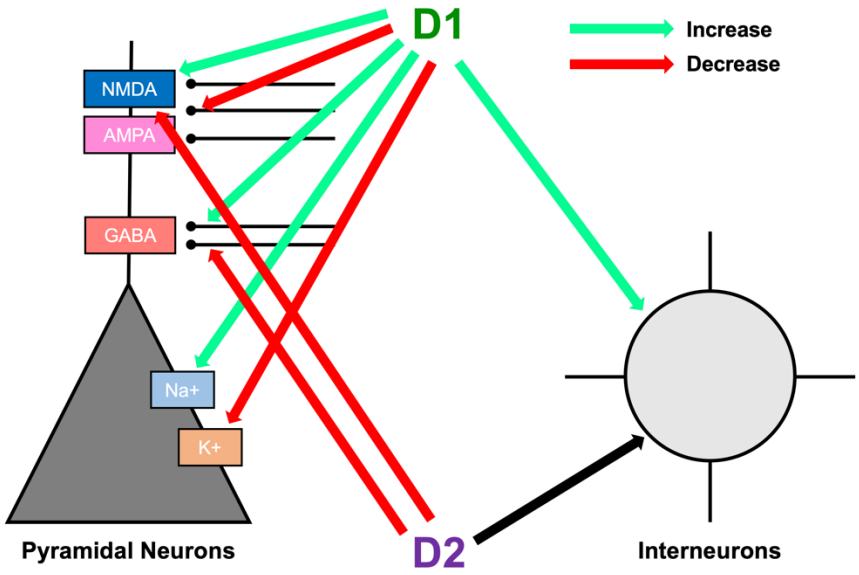


Figure 4.2. Summary of D1 and D2 receptor modulation in PFC circuits.
(Modified from Seamans & Yang, 2004).
Schematic summarizing the diverse actions of D1 and D2 receptor agonists in modulating PFC pyramidal neurons and interneurons. D1 receptor agonists increase NMDA currents, decrease presynaptic glutamate release, increase persistent sodium current (I_{NaP}), reduce outward rectification of slowly inactivated potassium currents (I_D), and increase interneuron excitability and IPSC amplitude in pyramidal neurons. D2 receptor agonists reduce NMDA currents and IPSCs onto pyramidal neurons.

In this chapter, we investigated the functional role of *in-vitro* D1 and D2 receptor activation on modulating L6-Drd1a and L6-non-Drd1a neuronal activity in the mPFC in an effort to explain the D1 and D2 receptor-mediated network activity pattern differences reported in Chapter 3.

4.2 Materials and Methods

4.2.1 Electrophysiology recordings and signal processing

For patch clamp recordings, slices were transferred to a submerged chamber and superfused at 5-8 ml/min with carbogenated aCSF at room temperature. Whole-cell current-clamp recordings of mPFC neurons were obtained with standard borosilicate glass micropipettes (5-12 MΩ) pulled on a Narishige PC-10 puller and filled with potassium-gluconate internal solution (in mM: 110 potassium-gluconate, 40 HEPES, 2 ATP-Mg, 0.3 GTP-NaCl, 4 NaCl, and

4 mg/ml biocytin (Sigma-Aldrich B4261); pH adjusted to ~7.2 with KOH; osmolality 270-290 mOsmol/kg). Oblique illumination (Olympus, BX51WI, 40x/0.8 NA water-immersion objective) was used to visualize cell morphology and guide patch clamp recordings. Epifluorescence imaging using a Cairn OptoLED system was used to identify L6-Drd1a neurons based on their tdTomato expression. L6-non-Drd1a neurons were visually identified as non-fluorescing neurons within ~100 μm of the white matter (Zolnik et al., 2023). Both transmitted light and epifluorescence were captured using an optiMOS Scientific CMOS camera (QImaging). An average of 3-4 neurons were used from each animal. Whole-cell current-clamp recordings were carried out using an Axon Multiclamp 700B amplifier (Molecular Devices) and low-pass filtered and digitized at 10 kHz using an ITC-18 A/D board (Instrutech), with data acquisition and stimulation protocols controlled using custom-written procedures in IgorPro (WaveMetrics). Input resistance was determined by hyperpolarizing current steps that elicited -5 mV to -15 mV voltage responses, and neurons were excluded if their input resistance changed by more than 30% throughout the recording session.

For the current step protocol, 20 depolarizing and 20 hyperpolarizing square current pulses (800 ms each) with 10 pA intervals were applied in an alternating order (Figure 4.3C). For spontaneous EPSP (sEPSP) recordings, 5-second sweeps were carried out for two minutes while the neuron was hyperpolarized to around -75 mV (Figure 4.3D). For each neuron, two current step protocols and two sEPSP recordings were carried out at baseline and repeated for either 2 μM SKF-81297 (Tocris) or 2 μM quinpirole (Tocris), with a 15-minute wait period after first administering the agonist (Figure 4.3A).

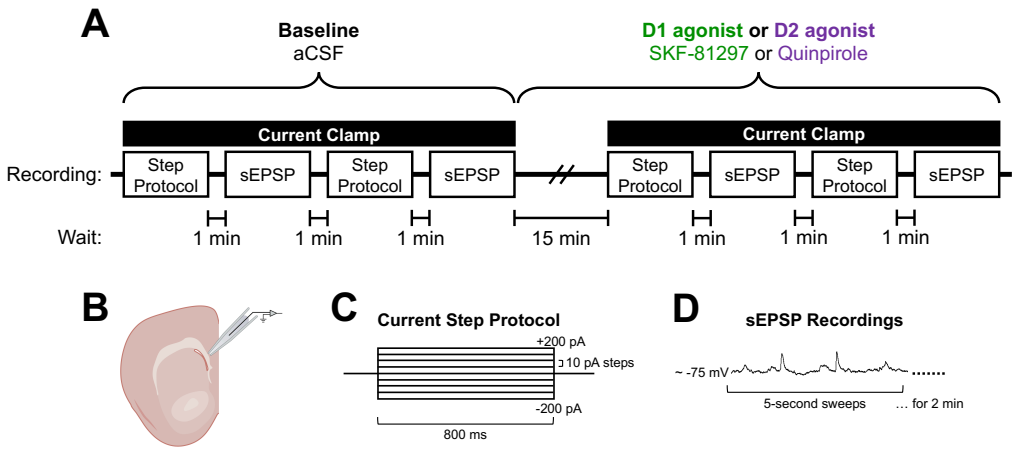


Figure 4.3. *In-vitro* whole-cell patch clamp experimental protocol.
(**A**) Experimental timeline for whole-cell current clamp recordings included two baseline step protocols and spontaneous excitatory postsynaptic potential (sEPSP) recordings with aCSF, followed by two step protocols and sEPSP recordings with D1 receptor agonist SKF-81297 or D2 receptor agonist quinpirole (with a 15-minute waiting period after initial drug administration).
(**B**) Schematic of one hemisphere of a coronal mPFC slice with a patch clamp electrode in the mPFC.
(**C**) Current step protocol included alternating 20 depolarizing and 20 hyperpolarizing square current pulses (800 ms each) with 10 pA step intervals.
(**D**) sEPSP recording protocol included 5-second sweeps for two minutes while the neuron was hyperpolarized to around -75 mV.

4.2.2 Data analysis

Data analysis was performed using custom-written procedures in IgorPro (WaveMetrics) and Python. We analyzed input-output curves (rheobase current, input-output coefficient, and spike frequency at maximum average input-output slope), intrinsic membrane properties (resting membrane potential, spike threshold potential, spike latency, membrane resistance, membrane capacitance, and hyperpolarization-induced sag ratio), action potential properties (spike amplitude and adaptation, spike half-width, interspike interval and adaptation, and afterhyperpolarization amplitude), and synaptic potentials (sEPSP amplitude, rise time, interevent interval, and frequency). The action potential spike detection threshold was 100 dV/dt or -10 mV to 0 mV, based on the properties of the smallest visually-identified spike during the current step protocol. We estimated rheobase current and input-output coefficient by fitting a square-root function to the input-output curves: $f = \beta\sqrt{I - I_T}$, where f is the spike frequency

output, I is the current step input, β is the input-output coefficient, and I_T is the rheobase current (Fourcaud-Trocmé et al., 2003).

Resting membrane potential was calculated as the median voltage before the onset of the current step pulse. Spike onset was detected as the peak in the voltage differential preceding spike detection. Spike threshold potential was calculated as the voltage immediately before the spike onset, and spike latency was calculated as the time between the onset of the current step pulse and the spike onset. Membrane resistance and membrane capacitance were determined by exponential curve-fitting of 5-15 mV voltage deflections elicited by hyperpolarizing current steps. Sag ratio was calculated as the ratio of the steady state voltage to the peak voltage deflection during hyperpolarizing current steps that elicited -5 mV to -15 mV voltage responses (lower ratio indicates larger sag current). Adaptation ratios were calculated as the ratio of the action potential properties at the end of the current step pulse to those at the beginning of the current step pulse (lower ratio indicates higher adaptation).

Spontaneous synaptic events in the form of sEPSPs were detected by fitting a waveform with the time course of a typical synaptic event along the voltage traces (Clements & Bekkers, 1997). The signal was lowpass filtered at 1 kHz with a bandstop filter at 50 Hz using regression, and we used a signal-to-noise ratio of 6 for synaptic event detection.

4.3 Results

Because dopamine's mechanism of action on PFC pyramidal neurons involves both direct and indirect modulation of intrinsic neuronal excitability and synaptic potentials, we sought to characterize the mechanism by which D1 and D2 receptors activate L6-Drd1a neurons compared to other L6 neurons in the mPFC.

4.3.1 D1 receptor activation selectively increases L6-Drd1a intrinsic neuronal excitability in the mPFC

We first examined how D1 receptor activation modulates intrinsic neuronal excitability of L6-Drd1a neurons compared to other L6 neurons in the mPFC. We applied a series of depolarizing and hyperpolarizing current step pulses and recorded voltage responses in L6 mPFC neurons. We found that only in L6-Drd1a neurons, D1 receptor agonist SKF-81297 increased spike frequency in response to low current step pulses and facilitated depolarization block leading to a significant reduction in spike frequency at high current step pulses, as shown in the input-output curves in Figure 4.4B,D. To further examine the intrinsic properties that are likely driving this D1 receptor-mediated increase in L6-Drd1a neuronal excitability, we analyzed input-output properties (rheobase current, input-output coefficient, and spike frequency at maximum average input-output slope), membrane properties (resting membrane potential, spike threshold potential, spike latency, membrane resistance, membrane capacitance, and hyperpolarization-induced sag ratio), and action potential properties (spike amplitude and adaptation, spike half-width, interspike interval and adaptation, and afterhyperpolarization amplitude). We found that D1 receptor agonist significantly increased resting membrane potential with no change in spike threshold potential only in L6-Drd1a neurons, while significantly increasing spike latency and hyperpolarization-induced sag (lower sag ratio) only in L6-non-Drd1a neurons (Figure 4.4E1-E2,G,J). In both L6 cell types, D1 receptor agonist significantly increased membrane resistance, despite L6-Drd1a neurons generally having a significantly higher membrane resistance than L6-non-Drd1a neurons (Figure 4.4F1). Independent of the effect of D1 receptor agonist, L6-Drd1a neurons displayed a significantly higher spike amplitude adaptation (lower adaptation ratio)

compared to L6-non-Drd1a neurons (Figure4.4I2). Taken together, these results suggest that L6-Drd1a neurons are generally more excitable than other L6 neurons in the mPFC, and D1 receptor activation further increases their intrinsic excitability.

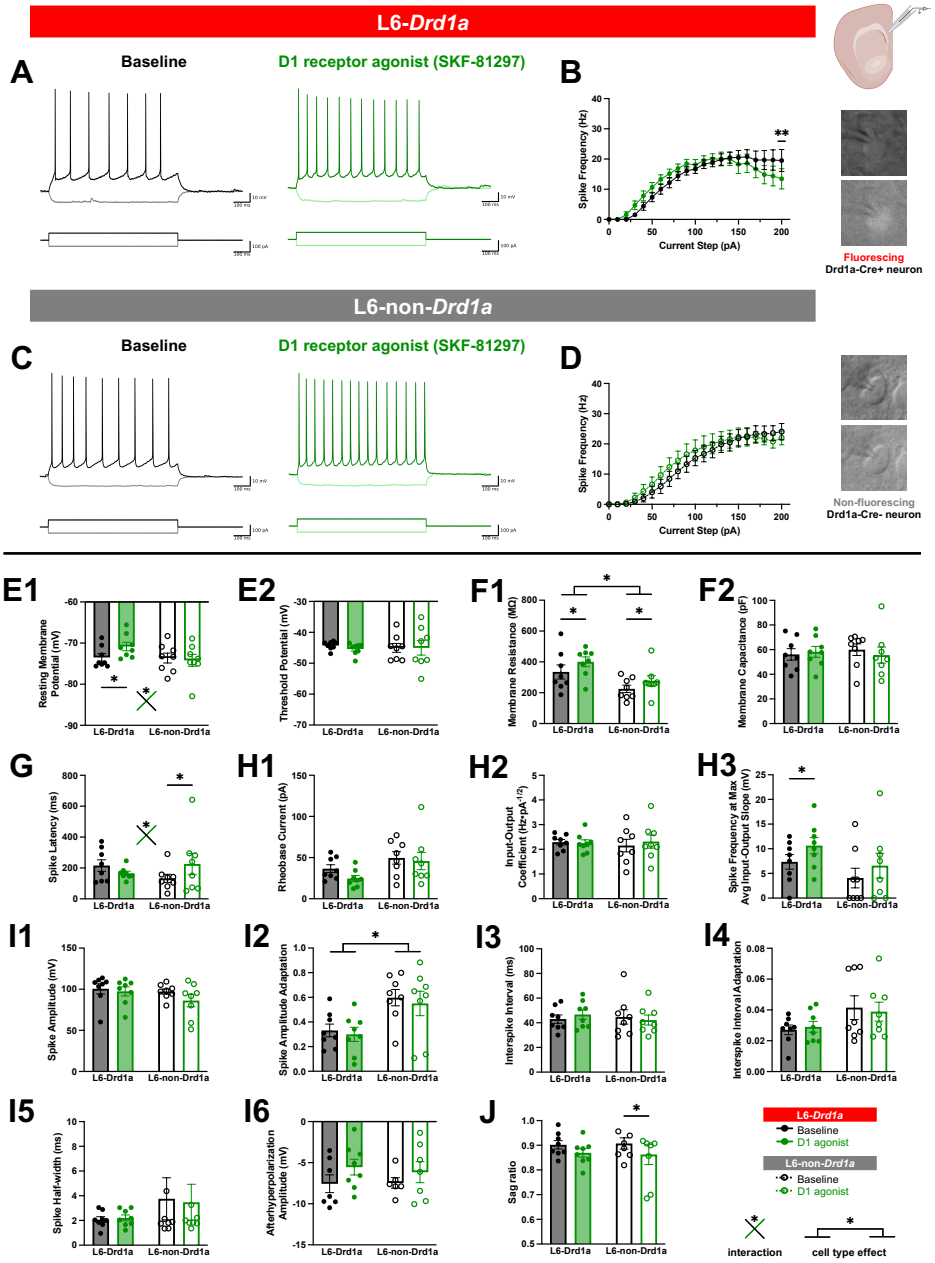


Figure 4.4. D1 receptor activation selectively increases L6-Drd1a intrinsic neuronal excitability in the mPFC. (**A, C**) Current-clamp recordings of a L6-Drd1a neuron and a L6-non-Drd1a neuron in the mPFC, showing responses to depolarizing and hyperpolarizing current steps at baseline (black) and following SKF-81297 administration (green).

(**B, D**) Input-output curves reveal that SKF-81297 (green) significantly facilitates depolarization block compared to baseline (black) in L6-Drd1a neurons (solid circles and lines), unlike L6-non-*Drd1a* neurons (open circles and dashed lines), with a significant current step effect, interaction between current step and cell type, and interaction between current step and drug (three-way ANOVA; current step: $F(41,574) = 97.95$, $p < 0.0001$; current step * cell type interaction: $F(41,574) = 1.539$, $p = 0.0192$; current step * drug interaction: $F(41,574) = 5.051$, $p = < 0.0001$) (Bonferroni multiple comparisons post-hoc test; $p = 0.0027$).
(**E1**) Resting membrane potential is significantly higher in L6-Drd1a neurons (solid circles) after SKF-81297 administration (green) compared to baseline (black), with a significant drug effect and interaction between drug and cell type (two-way ANOVA; drug: $F(1,7) = 10.54$, $p = 0.0141$; drug * cell type interaction: $F(1,7) = 5.878$, $p = 0.0458$) (Bonferroni multiple comparisons post-hoc test; $p = 0.0252$).
(**E2**) No significant difference in spike threshold potential between SKF-81297 (green) and baseline (black) in L6-Drd1a (solid circles) and L6-non-Drd1a neurons (open circles).
(**F1**) Membrane resistance is significantly higher in L6-Drd1a neurons (solid circles) compared to L6-non-Drd1a neurons (open circles), and SKF-81297 (green) significantly increases membrane resistance in both cell types, with a significant drug effect and cell type effect (two-way ANOVA; drug: $F(1,7) = 6.423$, $p = 0.0390$; cell type: $F(1,7) = 8.666$, $p = 0.0216$) (Bonferroni multiple comparisons post-hoc test; $p = 0.0174$ and $p = 0.0445$).
(**F2**) No significant difference in membrane capacitance between SKF-81297 (green) and baseline (black) in L6-Drd1a (solid circles) and L6-non-Drd1a neurons (open circles).
(**G**) Spike latency is significantly higher in L6-non-Drd1a neurons (open circles) after SKF-81297 administration (green) compared to baseline (black), with a significant interaction between drug and cell type (two-way ANOVA; drug * cell type interaction: $F(1,7) = 8.600$, $p = 0.0219$) (Bonferroni multiple comparisons post-hoc test; $p = 0.0314$).
(**H1**) No significant difference in rheobase current between SKF-81297 (green) and baseline (black) in L6-Drd1a (solid circles) and L6-non-Drd1a neurons (open circles).
(**H2**) No significant difference in input-output coefficient between SKF-81297 (green) and baseline (black) in L6-Drd1a (solid circles) and L6-non-Drd1a neurons (open circles).
(**H3**) Spike frequency at the maximum average input-output slope is significantly higher in L6-Drd1a neurons (solid circles) after SKF-81297 administration (green) compared to baseline (black), with a significant drug effect (two-way ANOVA; drug: $F(1,7) = 10.34$, $p = 0.0148$) (Bonferroni multiple comparisons post-hoc test; $p = 0.0486$).
(**I1**) No significant difference in spike amplitude between SKF-81297 (green) and baseline (black) in L6-Drd1a (solid circles) and L6-non-Drd1a neurons (open circles).
(**I2**) Spike amplitude adaptation ratio is significantly higher in L6-Drd1a neurons (solid circles) compared to L6-non-Drd1a neurons (open circles), with a significant cell type effect (two-way ANOVA; cell type: $F(1,7) = 8.773$, $p = 0.0210$).
(**I3**) No significant difference in interspike interval between SKF-81297 (green) and baseline (black) in L6-Drd1a (solid circles) and L6-non-Drd1a neurons (open circles).
(**I4**) No significant difference in interspike interval adaptation ratio between SKF-81297 (green) and baseline (black) in L6-Drd1a (solid circles) and L6-non-Drd1a neurons (open circles).
(**I5**) No significant difference in spike half-width between SKF-81297 (green) and baseline (black) in L6-Drd1a (solid circles) and L6-non-Drd1a neurons (open circles).
(**I6**) No significant difference in afterhyperpolarization amplitude between SKF-81297 (green) and baseline (black) in L6-Drd1a (solid circles) and L6-non-Drd1a neurons (open circles).
(**J**) Sag ratio is significantly lower in L6-non-Drd1a neurons (solid circles) after SKF-81297 administration (green) compared to baseline (black), with a significant drug effect (two-way ANOVA; drug: $F(1,7) = 9.797$, $p = 0.0166$) (Bonferroni multiple comparisons post-hoc test; $p = 0.0436$).
For all plots, data are presented as mean +/- s.e.m. ($n = 8$ L6-Drd1a neurons and $n = 8$ L6-non-Drd1a neurons. Baseline is shown in black, SKF-81297 is shown in green, L6-Drd1a neuron results are shown in solid circles and lines, and L6-non-Drd1a neuron results are shown in open circles and dashed lines. Significance is denoted as follows: $*p < 0.05$, $**p < 0.01$, and $***p < 0.001$ (three-way and two-way ANOVA with Bonferroni multiple comparisons tests).

4.3.2 D2 receptor activation exerts non-selective effects on L6 intrinsic neuronal excitability in the mPFC

To examine if the L6-Drd1a response to dopamine is selectively driven by D1 receptors, we also tested the effects of D2 receptor activation on L6-Drd1a and L6-non-Drd1a intrinsic neuronal excitability. We found that in L6-Drd1a neurons, D2 receptor agonist quinpirole did not alter spike frequency at low current step pulses but facilitated depolarization block leading to a significant reduction in spike frequency at high current step pulses, as shown in the input-output curves in Figure 4.5B,D. This depolarization block was strikingly similar to the D1 receptor agonist response, suggesting that it is a general electrophysiological property of L6-Drd1a response to dopamine. Upon further examination of intrinsic properties, we found that D2 receptor agonist significantly lowered spike threshold potential in both L6-Drd1a and L6-non-Drd1a neurons (Figure 4.5E2). However, D2 receptor agonist decreased the rate of spike frequency increase in response to increasing depolarizing current step pulses (input-output coefficient) independent of L6 cell type (Figure 4.5H2). Independent of the effect of D2 receptor agonist, L6-Drd1a neurons displayed a higher resting membrane potential and spike amplitude adaptation (lower adaptation ratio) than L6-non-Drd1a neurons, further supporting our claim that L6-Drd1a are generally more excitable than other L6 neurons in the mPFC (Figure 4.5E1,I2). Overall, these results suggest that D2 receptor activation generally increased L6 intrinsic neuronal excitability in a perithreshold, non-cell type-specific manner to increase the likelihood of action potential firing.

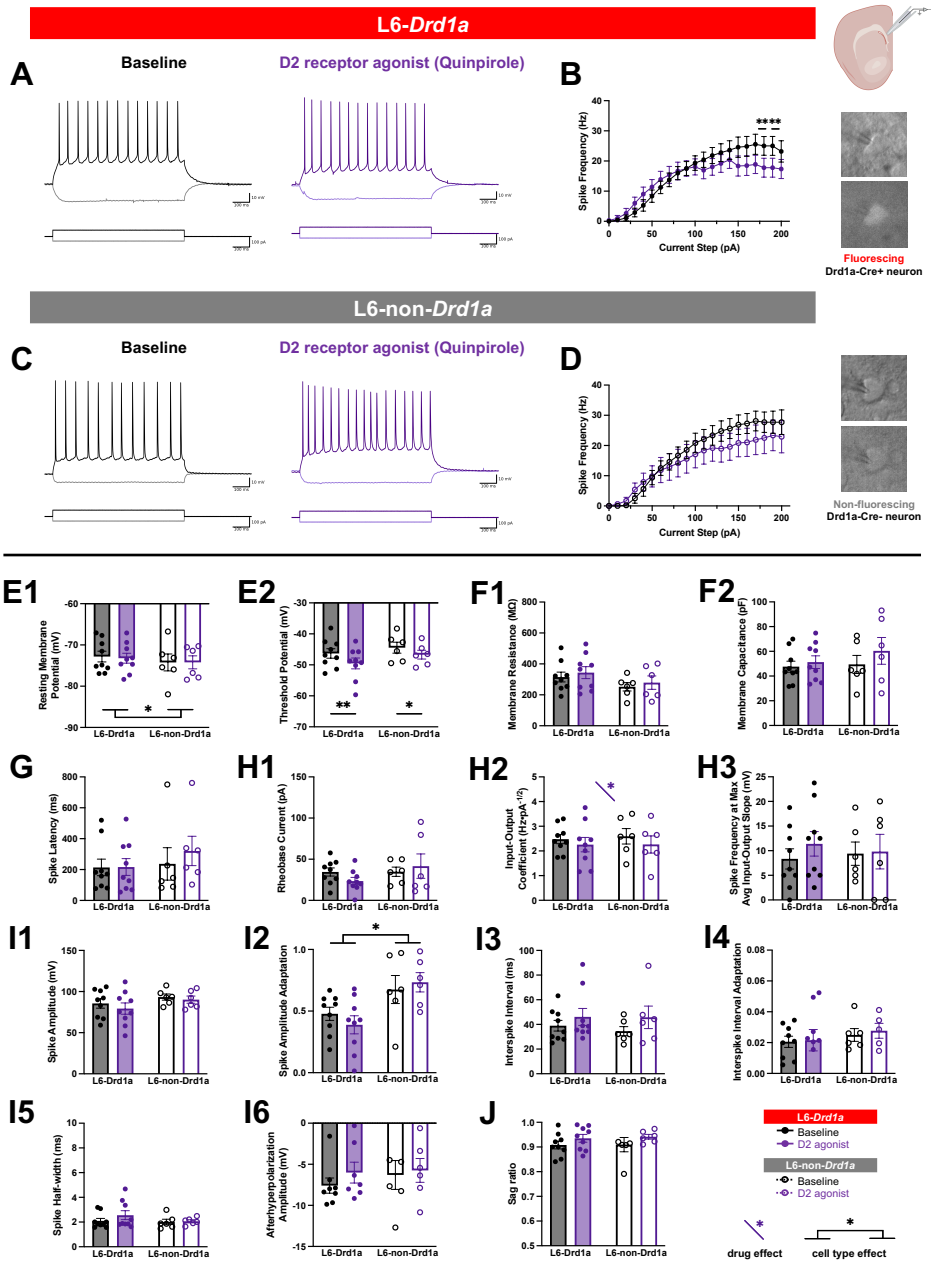


Figure 4.5. D2 receptor activation exerts non-selective effects on L6 intrinsic neuronal excitability in the mPFC.

(**A, C**) Current-clamp recordings of a L6-Drd1a neuron and a L6-non-Drd1a neuron in the mPFC, showing responses to depolarizing and hyperpolarizing current steps at baseline (black) and following quinpirole administration (purple).

(**B, D**) Input-output curves reveal that quinpirole (purple) significantly facilitates depolarization block compared to baseline (black) in L6-Drd1a neurons (solid circles and lines), unlike L6-non-*Drd1a* neurons (open circles and dashed lines), with a significant drug effect, current step effect, and interaction between current step and drug (three-way ANOVA; current step: $F(41,546) = 47.66$, $p < 0.0001$; drug: $F(1,546) = 41.27$, $p < 0.0001$; current step * drug interaction: $F(41,546) = 5.258$, $p = < 0.0001$) (Bonferroni multiple comparisons post-hoc test; $p = 0.0078$ and $p = 0.0078$).

(**E1**) Resting membrane potential is significantly higher in L6-Drd1a neurons (solid circles) compared to L6-non-Drd1a neurons (open circles), with a significant cell type effect (mixed-effects analysis; cell type: $F(1,8) = 5.981$, $p = 0.0402$).

(**E2**) Quinpirole (purple) significantly increases spike threshold potential in L6-Drd1a (solid circles) and L6-non-Drd1a neurons (open circles), with a significant drug effect (mixed-effects analysis; drug: $F(1,8) = 19.14$, $p = 0.0024$) (Bonferroni multiple comparisons post-hoc test; $p = 0.0022$ and $p = 0.0426$).
(**F1**) No significant difference in membrane resistance between quinpirole (purple) and baseline (black) in L6-Drd1a (solid circles) and L6-non-Drd1a neurons (open circles).
(**F2**) No significant difference in membrane capacitance between quinpirole (purple) and baseline (black) in L6-Drd1a (solid circles) and L6-non-Drd1a neurons (open circles).
(**G**) No significant difference in spike latency between quinpirole (purple) and baseline (black) in L6-Drd1a (solid circles) and L6-non-Drd1a neurons (open circles).
(**H1**) No significant difference in rheobase current between quinpirole (purple) and baseline (black) in L6-Drd1a (solid circles) and L6-non-Drd1a neurons (open circles).
(**H2**) There is a significant drug effect of quinpirole (purple) on input-output coefficient in L6-Drd1a (solid circles) and L6-non-Drd1a neurons (open circles) (mixed-effects analysis; drug: $F(1,8) = 7.470$, $p = 0.0257$).
(**H3**) No significant difference in spike frequency at the maximum average input-output slope between quinpirole (purple) and baseline (black) in L6-Drd1a (solid circles) and L6-non-Drd1a neurons (open circles).
(**I1**) No significant difference in spike amplitude between quinpirole (purple) and baseline (black) in L6-Drd1a (solid circles) and L6-non-Drd1a neurons (open circles).
(**I2**) Spike amplitude adaptation ratio is significantly higher in L6-Drd1a neurons (solid circles) compared to L6-non-Drd1a neurons (open circles), with a significant cell type effect (mixed-effects analysis; cell type: $F(1,7) = 6.794$, $p = 0.0313$).
(**I3**) No significant difference in interspike interval between quinpirole (purple) and baseline (black) in L6-Drd1a (solid circles) and L6-non-Drd1a neurons (open circles).
(**I4**) No significant difference in interspike interval adaptation ratio between quinpirole (purple) and baseline (black) in L6-Drd1a (solid circles) and L6-non-Drd1a neurons (open circles).
(**I5**) No significant difference in spike half-width between quinpirole (purple) and baseline (black) in L6-Drd1a (solid circles) and L6-non-Drd1a neurons (open circles).
(**I6**) No significant difference in afterhyperpolarization amplitude between quinpirole (purple) and baseline (black) in L6-Drd1a (solid circles) and L6-non-Drd1a neurons (open circles).
(**J**) No significant difference in sag ratio between quinpirole (purple) and baseline (black) in L6-Drd1a (solid circles) and L6-non-Drd1a neurons (open circles).
For all plots, data are presented as mean +/- s.e.m. ($n = 9$ L6-Drd1a neurons and $n = 6$ L6-non-Drd1a neurons. Baseline is shown in black, quinpirole is shown in purple, L6-Drd1a neuron results are shown in solid circles and lines, and L6-non-Drd1a neuron results are shown in open circles and dashed lines. Significance is denoted as follows: $*p < 0.05$, $**p < 0.01$, and $***p < 0.001$ (three-way ANOVA and mixed-effects analysis with Bonferroni multiple comparisons tests).

4.3.3 D1 receptor activation selectively increases amplitude of spontaneous excitatory synaptic potentials in mPFC L6-Drd1a neurons

After observing a selective D1 receptor-mediated increase in L6-Drd1a intrinsic neuronal excitability, we sought to characterize the synaptic potential properties that may drive this activity. As such, we recorded sEPSPs in L6 mPFC neurons hyperpolarized to around -75 mV and measured synaptic potential properties such as sEPSP amplitude, rise time, interevent interval, and frequency. We found that D1 receptor agonist SKF-81297 significantly increased sEPSP amplitude only in L6-Drd1a neurons, with no significant change in frequency in either

L6-Drd1a or L6-non-Drd1a neurons (Figure 4.6B1,E1). Given the nonparametric distribution of sEPSP events, we also analyzed the cumulative distributions of their properties and found that L6-Drd1a neurons generally displayed larger sEPSP amplitudes compared to other L6 neurons (Figure 4.6B2). These results suggest that the differences in spontaneous synaptic events in L6-Drd1a neurons are largely postsynaptically driven, and the D1 receptor-mediated increase in L6-Drd1a excitability is also likely driven by a postsynaptic mechanism of D1 receptor activation.

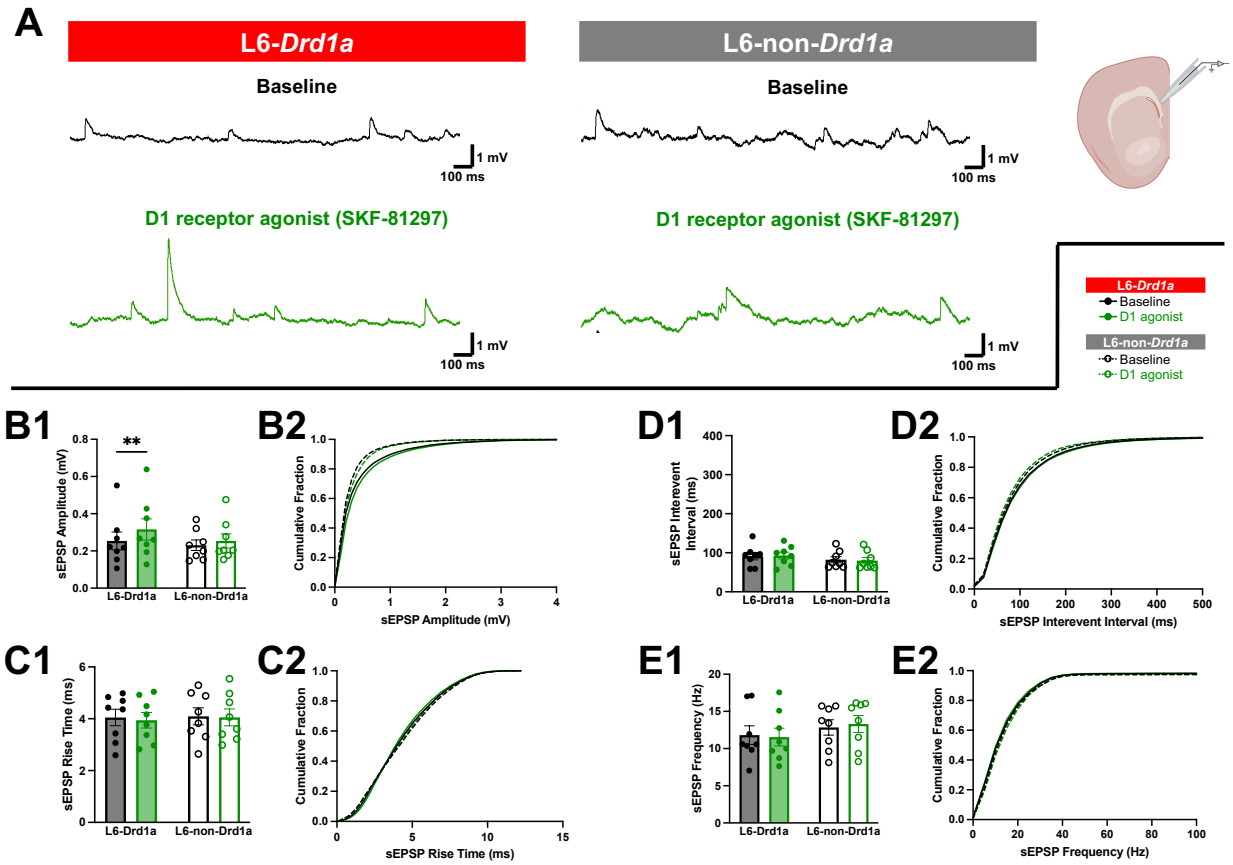


Figure 4.6. D1 receptor selectively increases sEPSP amplitude in mPFC L6-Drd1a neurons.
(**A**) Current-clamp recordings of a L6-Drd1a neuron and a L6-non-Drd1a neuron in the mPFC, showing spontaneous excitatory postsynaptic potentials (sEPSPs) at baseline (black) and following SKF-81297 administration (green).
(**B1**) Median sEPSP amplitude is significantly higher in L6-Drd1a neurons (solid circles) after SKF-81297 administration (green) compared to baseline (black), with a significant drug effect (two-way ANOVA; drug: $F(1,14) = 9.350$, $p = 0.0085$) (Bonferroni multiple comparisons post-hoc test; $p = 0.0072$).
(**B2**) Cumulative distribution of sEPSP amplitude increases in L6-Drd1a neurons (solid lines) after SKF-81297 administration (green) compared to baseline (black).
(**C1**) No significant difference in median sEPSP rise time between SKF-81297 (green) and baseline (black) in L6-Drd1a (solid circles) and L6-non-Drd1a neurons (open circles).

(**C2**) Cumulative distribution of sEPSP rise time does not significantly change between SKF-81297 (green) and baseline (black) in L6-Drd1a (solid lines) and L6-non-Drd1a neurons (dashed lines).
(**D1**) No significant difference in median sEPSP interevent interval between SKF-81297 (green) and baseline (black) in L6-Drd1a (solid circles) and L6-non-Drd1a neurons (open circles).
(**D2**) Cumulative distribution of sEPSP interevent interval does not significantly change between SKF-81297 (green) and baseline (black) in L6-Drd1a (solid lines) and L6-non-Drd1a neurons (dashed lines).
(**E1**) No significant difference in median sEPSP frequency between SKF-81297 (green) and baseline (black) in L6-Drd1a (solid circles) and L6-non-Drd1a neurons (open circles).
(**E2**) Cumulative distribution of sEPSP frequency does not significantly change between SKF-81297 (green) and baseline (black) in L6-Drd1a (solid lines) and L6-non-Drd1a neurons (dashed lines).
For all plots, data are presented as mean +/- s.e.m. (n = 8 L6-Drd1a neurons and n = 8 L6-non-Drd1a neurons. Baseline is shown in black, SKF-81297 is shown in green, L6-Drd1a neuron results are shown in solid circles and lines, and L6-non-Drd1a neuron results are shown in open circles and dashed lines. Significance is denoted as follows: *$p < 0.05$, **$p < 0.01$, and ***$p < 0.001$ (two-way ANOVA with Bonferroni multiple comparisons tests).

4.3.4 D2 receptor activation does not significantly alter spontaneous synaptic potentials in mPFC L6 neurons

Upon observing a generalized increase in L6 intrinsic neuronal excitability mediated by D2 receptor activation, we sought to characterize any differences in spontaneous synaptic potentials modulated by D2 receptors. We found that D2 receptor agonist did not significantly alter sEPSP amplitude, rise time, interevent interval, or frequency in L6-Drd1a and L6-non-Drd1a neurons (Figure 4.7B1-E1). We then analyzed the cumulative distributions of these synaptic properties and found no significant differences driven by D2 receptor activation (Figure 4.7B2-E2). These results confirm that D2 receptor activation exerts non-selective effects on L6 neuronal activity in the mPFC.

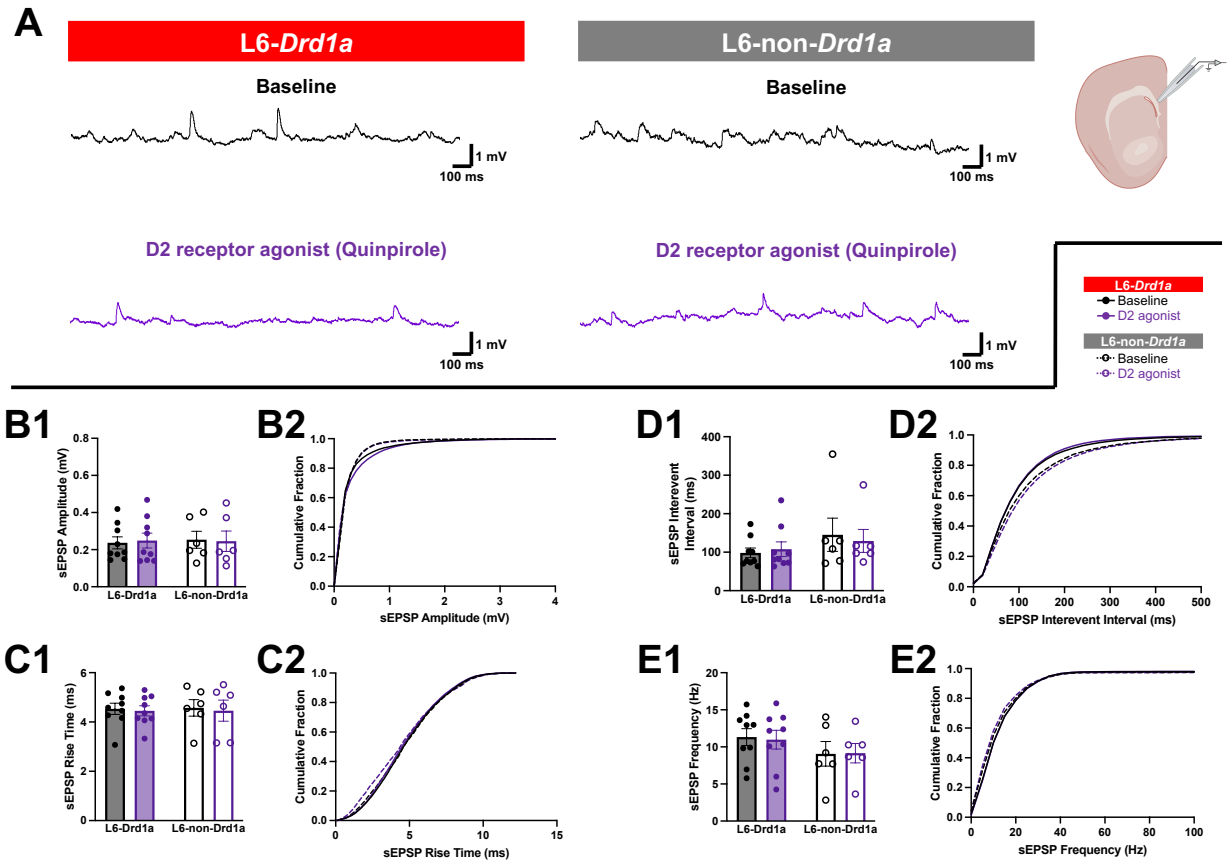


Figure 4.7. D2 receptor activation does not significantly alter sEPSPs in mPFC L6 neurons.
(**A**) Current-clamp recordings of a L6-Drd1a neuron and a L6-non-Drd1a neuron in the mPFC, showing spontaneous excitatory postsynaptic potentials (sEPSPs) at baseline (black) and following quinpirole administration (purple).
(**B1**) No significant difference in median sEPSP amplitude between quinpirole (purple) and baseline (black) in L6-Drd1a (solid circles) and L6-non-Drd1a neurons (open circles).
(**B2**) Cumulative distribution of sEPSP amplitude does not significantly change between quinpirole (purple) and baseline (black) in L6-Drd1a (solid lines) and L6-non-Drd1a neurons (dashed lines).
(**C1**) No significant difference in median sEPSP rise time between quinpirole (purple) and baseline (black) in L6-Drd1a (solid circles) and L6-non-Drd1a neurons (open circles).
(**C2**) Cumulative distribution of sEPSP rise time does not significantly change between quinpirole (purple) and baseline (black) in L6-Drd1a (solid lines) and L6-non-Drd1a neurons (dashed lines).
(**D1**) No significant difference in median sEPSP interevent interval between quinpirole (purple) and baseline (black) in L6-Drd1a (solid circles) and L6-non-Drd1a neurons (open circles).
(**D2**) Cumulative distribution of sEPSP interevent interval slightly increases in L6-non-Drd1a neurons (dashed lines) compared to L6-Drd1a neurons (solid lines).
(**E1**) No significant difference in median sEPSP frequency between quinpirole (purple) and baseline (black) in L6-Drd1a (solid circles) and L6-non-Drd1a neurons (open circles).
(**E2**) Cumulative distribution of sEPSP frequency slightly decreases in L6-non-Drd1a neurons (dashed lines) compared to L6-Drd1a neurons (solid lines).
For all plots, data are presented as mean +/- s.e.m. (n = 9 L6-Drd1a neurons and n = 6 L6-non-Drd1a neurons. Baseline is shown in black, quinpirole is shown in purple, L6-Drd1a neuron results are shown in solid circles and lines, and L6-non-Drd1a neuron results are shown in open circles and dashed lines. Significance is denoted as follows: *$p < 0.05$, **$p < 0.01$, and ***$p < 0.001$ (two-way ANOVA with Bonferroni multiple comparisons tests).

4.4 Discussion

L6 in the PFC contains a highly heterogenous population of excitatory and inhibitory neurons sharing diverse developmental origins, particularly considering the PFC's protracted developmental timeline compared to posterior primary sensory regions (Kolk & Rakic, 2022). This heterogeneity is exhibited by their diverse morphological and electrophysiological properties, especially in L6b (Marx & Feldmeyer, 2013; Combremont et al., 2016a, 2016b). In this chapter, we directed our attention to the excitatory L6-Drd1a neuronal subpopulation that selectively projects to higher-order thalamic nuclei and likely functions to gate cortical arousal through orexin (Hoerder-Suabedissen et al., 2018; Zolnik et al., 2020, 2023; Messore et al., 2024). Given the enhanced D1 receptor expression in L6 (Berger et al., 1991; Santana et al., 2009; Allen Brain Map Single-cell Transcriptomics, 2020), we sought to characterize their electrophysiological response to D1 and D2 receptor modulation in the mPFC compared to other L6 neurons, namely by examining their intrinsic neuronal excitability and synaptic potential properties. We speculate that D1 receptor modulation plays an analogous role to the orexinergic activation of L6-Drd1a neurons and functions alongside a more generalized D2 receptor modulation of L6 neurons to potentiate cross-network activity in the mPFC.

4.4.1 Dopaminergic modulation of L6 intrinsic neuronal excitability in the mPFC

To test the above hypothesis, we bath-applied D1 and D2 receptor agonists to acute mPFC slices *in-vitro* and carried out whole-cell current clamp recordings in L6-Drd1a and L6-non-Drd1a neurons. We began by first examining the general excitability of both cell types independent of D1 or D2 receptor activation. We found that L6-Drd1a neurons displayed higher intrinsic excitability compared to other L6 neurons in the mPFC, as evidenced by their

significantly higher resting membrane potential, membrane resistance, and spike amplitude adaptation (Figure 4.4F1,I2, 4.5E1,I2). We then tested the effects of D1 receptor activation and found that the D1 receptor agonist SKF-81297 significantly increased spike frequency and facilitated depolarization block only in L6-Drd1a neurons (Figure 4.4B,D). This increase in spike frequency can be explained by the significantly higher resting membrane potential and membrane resistance in L6-Drd1a neurons upon D1 receptor activation (Figure 4.4E1,F1), which is known to reduce leak currents and 4-AP sensitive voltage-gated potassium delayed rectifier currents (Yang & Seamans, 1996). Interestingly, *in-vitro* orexin-B administration also depolarizes L6-Drd1a neurons in S1 to induce tonic firing (Zolnik et al., 2023), and other neuromodulators such as acetylcholine, neurotensin, and noradrenaline also depolarize L6b neurons to elicit spontaneous action potential firing (Bayer et al., 2004; Hay et al., 2015; Combremont et al., 2016a, 2016b). Furthermore, D1 receptor agonists alter the activation/inactivation dynamics of TTX-sensitive voltage-gated sodium channels, which likely explains the depolarization block observed in L6-Drd1a neurons upon D1 receptor activation (Gorelova & Yang, 2000). The general increased excitability of L6-Drd1a neurons compared to other L6 neurons in the mPFC may serve an important function in driving cortical arousal, as they need to integrate long-range intracortical inputs to functionally excite higher-order thalamic nuclei directly and indirectly through L5 corticothalamic projections (Zolnik et al., 2020, 2023). The increased intrinsic excitability of L6-Drd1a neurons appropriately serves their functional demand in modulating higher-order cortico-thalamo-cortical loops.

After observing selective D1 receptor effects on L6-Drd1a intrinsic excitability, we tested the effects of D2 receptor activation to determine if L6-Drd1a neurons selectively respond to D1 receptor agonists or are generally excitable by dopamine. We found that the L6-Drd1a

depolarization block was not dependent on dopamine receptor subtype, and D2 receptor agonist quinpirole exerted perithreshold, non-cell type-specific effects across L6 in the mPFC by significantly lowering spike threshold potential in both L6-Drd1a and L6-non-Drd1a neurons (Figure 4.5B,D,E2). This non-selective effect of D2 receptor activation likely activates the extensive local GABAergic networks in L6 to broadly lower network activity in the mPFC (Zolnik et al., 2020). Furthermore, D2 receptor activation in PFC pyramidal neurons exerts a more rapid reduction of spike firing following bath application, whereas D1 receptor activation exerts a prolonged increase in evoked firing 10-15 minutes after bath application (Gulledge & Jaffe, 1998; Gorelova & Yang, 2000; Seamans et al., 2001b). In our experimental design, we recorded neuronal responses 15 minutes after bath application of either D1 or D2 receptor agonist, thus likely explaining the non-selective effects of D2 compared to D1 receptor activation.

4.4.2 Dopaminergic modulation of L6 spontaneous synaptic potentials in the mPFC

Not only do D1 and D2 receptors regulate the intrinsic excitability of PFC pyramidal neurons, but they also modulate their excitatory and inhibitory synaptic responses (Seamans & Yang, 2004), and L6-Drd1a neurons exhibit strong functional connectivity with both intracortical and corticothalamic networks (Zolnik et al., 2020, 2023). As such, we hypothesized that L6-Drd1a neurons receive stronger synaptic input in response to D1 receptor activation, which could contribute to their selective D1 receptor-mediated increase in excitability. To test this hypothesis, we measured spontaneous synaptic potentials in response to D1 receptor agonist SKF-81297 and found that sEPSP amplitude significantly increased in L6-Drd1a neurons upon D1 receptor activation, with no change in sEPSP frequency (Figure 4.6B1,E1). This difference suggests that a

postsynaptic mechanism of D1 receptor activation drives L6-Drd1a excitability in the mPFC. D1 receptors are known to selectively increase NMDA currents in PFC pyramidal neurons through a postsynaptic mechanism (Seamans et al., 2001a), but they can also reduce evoked NMDA and AMPA responses by localizing near asymmetric synapses and inhibiting presynaptic glutamate release (Law-Tho et al., 1994; Momiyama et al., 1996; Seamans & Yang, 2004). Further experimentation with D-AP5 (to selectively block NMDA receptors) or TTX (to silence presynaptic input) is needed to explore the postsynaptic and presynaptic glutamatergic contribution to the D1 receptor-mediated synaptic response. We then examined the effects of D2 receptor activation on spontaneous synaptic potentials and found no significant differences between L6-Drd1a neurons and L6-non-Drd1a neurons (Figure 4.7). This result confirms the non-selective D2 receptor effects on L6 neuronal excitability, and it is also likely explained by the difference in temporal activation patterns of D1 and D2 receptors, with D2 receptor activation displaying a more rapid onset after bath application (Seamans et al., 2001b).

4.4.3 Limitations and future directions

Although we observed a significant D1 receptor-mediated increase in L6-Drd1a neuronal excitability, this subpopulation includes both pyramidal and nonpyramidal neurons, and the non-Drd1a excitatory neurons in L6 display even higher morphological and electrophysiological diversity (Marx & Feldmeyer, 2013; Zolnik et al., 2020). In our present study, we only classified L6 neurons based on their Cre expression in our specific Drd1a-Cre mouse line. Thus, morphological differences in each cell type could mask differences in the response to D1 and D2 receptor activation.

As a follow-up to this study, we would like to reconstruct the morphologies of the L6 neurons that we recorded from and cluster their intrinsic properties and synaptic potential properties based on their morphological classification. Given the strong link between NMDA receptor and D1 receptor activation through DARPP-32 signaling in PFC pyramidal neurons (Zheng et al., 1999; Seamans et al., 2001a; Wang & O'Donnell, 2001), we would also like to test the NMDA receptor-dependency of D1 and D2 receptor activation on exciting L6-Drd1a neurons in the mPFC by isolating NMDA and AMPA receptor synaptic currents and blocking their conductance. Furthermore, it would be interesting to investigate the inhibitory and excitatory presynaptic mechanisms that are likely involved in modulating L6-Drd1a neuronal activity since D1 receptors can increase the excitability of fast-spiking GABAergic interneurons in the PFC (Gorelova et al., 2002) and can also modulate glutamatergic release at symmetric synapses (Law-Tho et al., 1994; Momiyama et al., 1996; Seamans & Yang, 2004). Overall, this chapter provides novel insight into the dopaminergic modulation of intrinsic excitability and spontaneous synaptic activity in a subpopulation of L6 neurons in the mPFC that drive higher-order thalamocortical arousal.

V. General Discussion

D1 receptor is highly expressed in L6 across the cortical mantle (Berger et al., 1991; Santana et al., 2009; Allen Brain Map Single-cell Transcriptomics, 2020), and the excitatory L6-Drd1a neuronal subpopulation selectively projects to higher-order thalamic nuclei and is highly sensitive to the arousal neuropeptide orexin (Hoerder-Suabedissen et al., 2018; Zolnik et al., 2020, 2023; Messore et al., 2024). Activation of the higher-order thalamocortical system by L6-Drd1a neurons is highly relevant in the PFC, which is involved in executive and cognitive functions such as flexible decision making, stimulus selection, goal-directed behavior, and working memory (Miller & Wallis, 2009; Miller & Cohen, 2001). The PFC is also often implicated in schizophrenia, autism, and attention-deficit disorders, and its orexinergic activation is implicated in anxiety behaviors (Cole et al., 2020; Karimi et al., 2019). Modulating arousal sustains an appropriate level of attention and stress for healthy functioning. However, functional alterations in higher-order cortico-thalamo-cortical loops that modulate arousal, namely those driven by orexin-sensitive L6-Drd1a neurons, yield anxiety phenotypes (Messore et al., 2024). The structural and functional connectivity of L6-Drd1a neurons, along with their neuromodulation, has been extensively characterized in primary sensory areas, but relatively little is known about their role in the mPFC. Moreover, their dopaminergic modulation in the mPFC remains elusive, despite dopamine likely playing an important role in potentiating the orexinergic activation that drives cortical arousal. Thus, we investigated the dopaminergic modulation of L6-Drd1a neuronal network activity in the mPFC by examining network activity responses to D1 and D2 receptor activation, along with individual neuronal responses in L6-Drd1a and L6-non-Drd1a neurons.

5.1 L6-Drd1a neurons mediate dopaminergic modulation of local mPFC network activity

We began by measuring LFP network activity using a high-density planar MEA as a general measure of cortical arousal. We manipulated the functional activity of L6-Drd1a neurons (i.e., chronic 'silencing') through a conditional knockout of the presynaptic SNARE protein SNAP25, which abolishes action potential-evoked neurotransmission while displaying normal initial axon development and synapse formation (Hoerder-Suabedissen et al., 2019; Hayashi et al., 2021; Washbourne et al., 2002; Bronk et al., 2007). Using this model, we tested D1 and D2 receptor-mediated mPFC network activity differences in control slices and chronically 'silenced' L6-Drd1a slices. We found that D1 receptor activation significantly increased broadband LFP activity in the infralimbic mPFC, which was eliminated upon chronic 'silencing' of L6-Drd1a neurons (Figure 3.3, 3.4). On the other hand, we found that D2 receptor activation only increased infralimbic broadband LFP activity after chronically 'silencing' L6-Drd1a neurons (Figure 3.5, 3.6). These results suggest that L6-Drd1a neurons fine-tune local network activity in the mPFC by balancing D1 and D2 receptor modulation to gate cortical arousal alongside OX2R, which has been shown to activate slow-bursting infralimbic activity in the mPFC through L6-Drd1a neurons as well (Messore et al., 2024). Interestingly, the nuanced difference between orexin-induced slow-bursting activity and D1-induced broadband LFP activity may reflect their unique roles in cortical arousal. OX2R and D1 receptor activation likely play a synergistic role in activating the higher-order corticothalamic system through L6-Drd1a neurons, which can be further modulated by D1 receptors.

As discussed in Chapter 3, the paradoxical increase in infralimbic network activity by D2 receptor activation upon chronic 'silencing' of L6-Drd1a neurons can be explained from the lens

of a disinhibition mechanism mediated by GABAergic interneurons, or from the lens of a compensatory shift in the activation of D2-expressing excitatory neurons. The first scenario is based on the assumption that L6-Drd1a neurons indirectly modulate D2-expressing neurons through a biphasic disynaptic mechanism involving GABAergic interneurons. There is evidence for extensive excitatory-inhibitory loops within L6 involving L6-Drd1a neurons (Zolnik et al., 2020, 2023), along with prominent D2 receptor expression in PFC L5 and L6 (Santana et al., 2009). It is also known that the rapid inhibitory effects of dopamine are mediated by D2 receptors, while the prolonged stimulatory effects are mediated by D1 receptors (Gulledge & Jaffe, 1998; Gorelova & Yang, 2000; Seamans et al., 2001b). Hence, the late onset of D1 receptor activation likely exerts its stimulatory effects through indirect inhibition of D2-expressing neurons, which corroborates our observation that the increase in infralimbic network activity induced by D2 receptor activation in L6-Drd1a 'silenced' slices was only evident 15 minutes after D2 receptor agonist administration.

The second scenario is based on the assumption of D1/D2 receptor coactivation in L6-Drd1a neurons, which may in fact be true given our finding in Chapter 4 that D2 receptor activation lowers spike threshold potential in both L6-Drd1a neurons and L6-non-Drd1a neurons (Figure 4.5E2). There is evidence for coactivation of D1 and D2 receptors in the lateral orbitofrontal cortex that potentiates NMDA-dependent synaptic transmission and cognitive flexibility behavior (Thompson et al., 2016), and perhaps coactivation of D1 and D2 receptors in L6-Drd1a neurons is needed to modulate arousal depending on the salience of the sensory input. A compensatory shift in the activation of D2-expressing neurons may underlie the anxiolytic effect of chronically 'silencing' L6-Drd1a neurons (Messore et al., 2024).

5.2 D1 receptor activation selectively excites L6-Drd1a neurons while D2 receptor generally excites L6 neurons in the mPFC

To explain these network activity differences in response to D1 and D2 receptor activation, we examined D1 and D2 receptor modulation of L6-Drd1a and L6-non-Drd1a intrinsic neuronal excitability and spontaneous synaptic potentials in the mPFC. We first found that L6-Drd1a neurons displayed higher intrinsic excitability compared to other L6 neurons in the mPFC, most notably due to significantly higher resting membrane potential and membrane resistance (Figure 4.4F1, 4.5E1). Interestingly, both D1 and D2 receptor agonists selectively induced depolarization block in L6-Drd1a neurons (Figure 4.4B,D, 4.5B,D), perhaps due to their increased excitability and functional demand in driving higher-order cortico-thalamo-cortical loops (Zolnik et al., 2023). We then found that D1 receptor activation selectively excited L6-Drd1a neurons by increasing their resting membrane potential and membrane resistance (Figure 4.4E1,F1), while D2 receptor activation non-selectively excited L6 neurons by lowering their spike threshold potential (Figure 4.5E2). This non-selective L6 neuronal excitation by D2 receptor activation could explain a compensatory shift in the activity of L6-non-Drd1a neurons once L6-Drd1a neurons are 'silenced,' resulting in the D2 receptor-mediated increase in mPFC network activity that was observed in Chapter 3 (Figure 3.6).

After examining intrinsic neuronal excitability, we explored synaptic potentials that may mediate these D1 and D2 receptor responses. We found that D1 receptor activation also selectively increased the amplitude of spontaneous excitatory synaptic potentials in L6-Drd1a neurons (Figure 4.6B1), while D2 receptor activation yielded no significant changes in synaptic potentials in L6 (Figure 4.7). Notably, D1 receptor activation did not increase sEPSP frequency, which supports a postsynaptic mechanism of D1 receptor activation that drives L6-Drd1a

excitability and local network activity in the mPFC. This mechanism may be NMDA receptor-dependent given that D1 receptors selectively increase NMDA receptor-mediated currents in PFC pyramidal neurons (Seamans et al., 2001a). A follow-up study is needed to investigate the contribution of NMDA receptor- and AMPA receptor-mediated currents to our observed D1 receptor-mediated increase sEPSP amplitude.

5.3 Limitations and future directions

As discussed in Chapters 3 and 4, there is a biphasic time-dependent effect of *in-vitro* dopamine application in the PFC (Gulledge & Jaffe, 1998; Gorelova & Yang, 2000; Seamans et al., 2001b). In our present study, we only measured these effects 15 minutes after dopamine administration. Future studies should measure network responses and L6-Drd1a neuronal responses to D1 and D2 receptor agonists as a function of time, which may uncover interesting temporal dynamics of dopaminergic modulation of L6 networks. Dopamine also exerts dose-dependent effects in the PFC (Zheng et al., 1999), and thus future studies should also compare different concentrations of D1 and D2 receptor agonists. It should also be noted that we used a sucrose-based aCSF cutting solution for the MEA experiments and an NMDG-based aCSF cutting solution for the patch clamp experiments. While there may be differences in slice quality, we carried out each set of experiments using the same cutting solution and detected neuronal activity from slices cut in both solutions.

There are a series of experiments that we would like to conduct as a follow-up to this study. First, we would like to investigate if L6-Drd1a neurons co-express D2 receptors. This would support our electrophysiological findings that D2 receptors non-selectively excite L6-Drd1a neurons (Figure 4.5) and mediate an increase in mPFC network activity upon chronic

'silencing' of L6-Drd1a neurons (Figure 3.6). We would also like to probe the modulatory interactions between orexin and dopamine on L6-Drd1a neuronal excitability and local network activity in the mPFC, given their independent activation of L6-Drd1a neurons and infralimbic network activity (Messore et al., 2024). Because dopamine is fundamentally a neuromodulator, its mechanism of action potentiates or attenuates responses by other neurotransmitters, such as glutamate and GABA. Dopamine can modulate GABA release onto PFC pyramidal neurons (Gulledge & Jaffe, 2001; Seamans et al., 2001b), and D1 receptors have been shown to localize near asymmetric synapses and reduce presynaptic glutamate release (Law-Tho et al., 1994; Momiyama et al., 1996; Seamans & Yang, 2004). Thus, we are interested in elucidating the presynaptic mechanisms by which D1 and D2 receptors modulate L6 neuronal activity through glutamatergic or GABAergic terminals.

Finally, we would like to investigate social and anxiety behavior in response to *in-vivo* D1 or D2 receptor agonist application in control and L6-Drd1a 'silenced' animals, which have been shown to display anxiolytic behavior (Messore et al. 2024). Our findings suggest that D1 receptor activation is involved in driving cortical arousal through L6-Drd1a neurons, and D2 receptor activation compensates for the 'silencing' of L6-Drd1a neurons in driving cortical arousal. Thus, D1 or D2 receptor agonist administration in the mPFC may rescue behavioral deficits associated with 'silencing' L6-Drd1a neurons.

5.4 Conclusion

In this thesis, we investigated the dopaminergic modulation of a subpopulation of L6 neurons in the mPFC that project to higher-order thalamic nuclei and drive cortical arousal. Our findings provide novel insight into the mechanisms by which D1 and D2 receptors differentially

modulate local mPFC networks through selective excitation of these L6-Drd1a neurons. Most of these L6-Drd1a neurons derive from the transient developmental subplate, which is involved in establishing some of the earliest intracortical and corticothalamic connections (Hoerder-Suabedissen & Molnár, 2015). Interestingly, altered subplate cell density, distribution, and transcriptomics in the PFC are implicated in schizophrenia and autism (Akbarian et al. 1993a, 1993b; Bailey et al., 1998; Wegiel et al., 2010; Avino & Hutsler, 2010; McFadden & Minshew, 2013; Willsey et al., 2013), both of which likely involve dopamine signaling dysfunctions (Bogerts et al., 1983; Pavăl, 2017). As such, our findings carry significant implications for dopamine- and subplate-related disorders such as schizophrenia and autism, along with anxiety and stress-related disorders driven by altered salience processing and arousal.

References

Abe, K. Kambe, Y., Majima, K., Hu, Z., Ohtake, M., Momennezhad, A., … Sato, T. (2024). Functional diversity of dopamine axons in prefrontal cortex during classical conditioning. *eLife, 12*, https://doi.org/10.7554/eLife.91136.3

Adamantidis, A. R., Zhang, F., Aravanis, A. M., Deisseroth, K., & de Lecea, L. (2007). Neural substrates of awakening probed with optogenetic control of hypocretin neurons. *Nature, 450*, 420-424. https://doi.org/10.1038/nature06310

Akbarian, S., Bunney, W. E., Potkin, S. G., Wigal, S. B., Hagman, J. O., Sandman, C. A., & Jones, E. G. (1993a). Distorted distribution of nicotinamide-adenine dinucleotide phosphate-diaphorase neurons in frontal lobe of schizophrenics implies disturbances of cortical development. *Archives of General Psychiatry, 50*(3), 169-177. doi:10.1001/archpsyc.1993.01820150007001

Akbarian, S., Viñuela, A., Kim, J. J., Potkin, S. G., Benney, W. E., & Jones, E. G. (1993b). Distorted distribution of nicotinamide-adenine dinucleotide phosphate-diaphorase neurons in temporal lobe of schizophrenics implies anomalous cortical development. *Archives of General Psychiatry, 50*(3), 178-187. doi:10.1001/archpsyc.1993.01820150016002

Allen Brain Map Single-cell Transcriptomics. (2020). Mouse – Whole Cortex and Hippocampus – 10x Genomics. https://celltypes.brain-map.org/rnaseq/mouse_ctx-hpf_10x

Allendoerfer K. L. & Shatz, C. J. (1994). The subplate, a transient neocortical structure: its role in the development of connections between thalamus and cortex. *Annual Review of Neuroscience, 17*, 185-218. https://doi.org/10.1146/annurev.ne.17.030194.001153

Anastasiades, P. G., Boada, C., & Carter, A. G. (2019). Cell-type-specific D1 dopamine receptor modulation of projection neurons and interneurons in the prefrontal cortex. *Cerebral Cortex, 29*(7), 3224-3242. https://doi.org/10.1093/cercor/bhy299

Anderson, S. A., Eisenstat, D. D., Shi, L., & Rubenstein, J. L. R. (1997). Interneuron migration from basal forebrain to neocortex: dependence on Dlx genes. *Science, 278*(5337), 474-476. doi:10.1126/science.278.5337.474

Arimatsu, Y., Ishida, M., Kaneko, T., Ichinose, S., & Omori, A. (2003). Organization and development of corticocortical associative neurons expressing the orphan nuclear receptor Nurr1. *The Journal of Comparative Neurology, 466*(2), 180-196. https://doi.org/10.1002/cne.10875

Avino, T. A. & Hutsler, J. J. (2010). Abnormal cell patterning at the cortical gray-white matter boundary in autism spectrum disorders. *Brain Research, 1360*, 138-146. https://doi.org/10.1016/j.brainres.2010.08.091

Ayano, G. (2016). Dopamine: receptors, functions, synthesis, pathways, locations and mental disorders: review of literatures. *Journal of Mental Disorders and Treatment, 2*(2), doi:10.4172/2471-271X.1000120

Bailey, A., Luthert, P., Dean, A., Harding, B., Janota, I., Montgomery, M., … Lantos, P. (1998). A clinicopathological study of autism. *Brain, 121*(5), 889-905. https://doi.org/10.1093/brain/121.5.889

Bayer, L., Serafin, M., Eggermann, E., Saint-Mleux, B., Machard, D., Jones, B. E., & Mühlethaler, M. (2004). Exclusive postsynaptic action of hypocretin-orexin on sublayer 6b cortical neurons. *The Journal of Neuroscience, 24*(30), 6760-6764. https://doi.org/10.1523/JNEUROSCI.1783-04.2004

Bentivoglio, M. & Morelli, M. (2005). Chapter 1: The organization and circuits of mesencephalic dopaminergic neurons and the distribution of dopamine receptors in the brain. In S. B. Dunnett, M. Bentivoglio, A. Björklund, & T. Hökfelt (Eds.), *Handbook of Chemical Neuroanatomy, Vol. 21: Dopamine* (pp. 1-107). Elsevier. https://doi.org/10.1016/S0924-8196(05)80005-3

Berger, B., Gaspar, P., & Verney, C. (1991). Dopaminergic innervation of the cerebral cortex: unexpected differences between rodents and primates. *Trends in Neurosciences, 14*(1), 21-27. https://doi.org/10.1016/0166-2236(91)90179-X

Björklund, A. & Dunnett, S. B. (2007). Dopamine neuron systems in the brain: an update. *Trends in Neurosciences, 30*(5), 194-202. https://doi.org/10.1016/j.tins.2007.03.006

Bogerts, B., Häntsch, J., & Herzer, M. (1983). A morphometric study of the dopamine-containing cell groups in the mesencephalon of normals, Parkinson patients, and schizophrenics. *Biological Psychiatry, 18*(9), 951-969. PMID:6640008

Bronk, P., Deák, F., Wilson, M. C., Liu, X., Südhof, T. C., & Kavalali, E. T. (2007). Differential effects of SNAP-25 deletion on Ca2+-dependent and Ca2+-independent neurotransmission. *Journal of Neurophysiology, 98*(2), 794-806. https://doi.org/10.1152/jn.00226.2007

Cardin, J. A., Carlén, M., Meletis, K., Knoblich, U., Zhang, F., Deisseroth, K., … Moore, C. I. (2009). Driving fast-spiking cells induces gamma rhythm and controls sensory responses. *Nature, 459*, 663-667. https://doi.org/10.1038/nature08002

Case, L., Lyons, D. J., & Broberger, C. (2017). Desynchronization of the rat cortical network and excitation of white matter neurons by neurotensin. *Cerebral Cortex, 27*(4), 2671-2685. https://doi.org/10.1093/cercor/bhw100

Caviness, V. S. & Sidman, R. L. (1973). Time of origin or corresponding cell classes in the cerebral cortex of normal and reeler mutant mice: an autoradiographic analysis. *Journal of Comparative Neurology, 148*(2), 141-151. https://doi.org/10.1002/cne.901480202

Clark, M. & Bracci, E. (2018). Dichotomous dopaminergic control of ventral pallidum neurons. *Frontiers in Cellular Neuroscience, 12*(260), https://doi.org/10.3389/fncel.2018.00260

Clements, J. D. & Bekkers, J. M. (1997). Detection of spontaneous synaptic events with an optimally scaled template. *Biophysical Journal, 73*(1), 220-229. doi:10.1016/S0006-3495(97)78062-7

Cole, S., Keefer, S. E., Anderson, L. C., & Petrovich, G. D. (2020). Medial prefrontal cortex neural plasticity, orexin receptor 1 signaling, and connectivity with the lateral hypothalamus are necessary in cue-potentiated feeding. *The Journal of Neuroscience, 40*(8), 1744-1755. https://doi.org/10.1523/JNEUROSCI.1803-19.2020

Combremont, A. L. W., Bayer, L., Dupré, A., Mühlethaler, M., & Serafin, M. (2016a). Effects of hypocretin/orexin and major transmitters of arousal on fast spiking neurons in mouse cortical layer 6B. *Cerebral Cortex, 26*(8), 3533-3562. https://doi.org/10.1093/cercor/bhw158

Combremont, A. L. W., Bayer, L., Dupré, A., Mühlethaler, M., & Serafin, M. (2016b). Slow bursting neurons of mouse cortical layer 6b are depolarized by hypocretin/orexin and major transmitters of arousal. *Frontiers in Neurology, 7*(88), https://doi.org/10.3389/fneur.2016.00088

De Carlos, J. A. & O'Leary, D. D. M. (1992). Growth and targeting of subplate axons and establishment of major cortical pathways. *The Journal of Neuroscience, 12*(4), 1194-1211. https://doi.org/10.1523/JNEUROSCI.12-04-01194.1992

De Lecea, L., Kilduff, T. S., Peyron, C., Gao, X. B., Foye, P. E., Danielson, P. E., …Sutcliffe, J. G. (1998). The hypocretins: hypothalamus-specific peptides with neuroexcitatory activity. *PNAS, 95*(1), 322-327. https://doi.org/10.1073/pnas.95.1.322

Di Domenico, D. & Mapelli, L. (2023). Dopaminergic Modulation of Prefrontal Cortex Inhibition. *Biomedicines, 11*(5), https://doi.org/10.3390/biomedicines11051276

Doyle, D. Z., Lam, M. M., Qalieh, A., Qalieh, Y., Sorel, A., Funk, O. H., & Kwan, K. Y. (2021). Chromatin remodeler Arid1a regulates subplate neuron identity and wiring of cortical connectivity. *PNAS, 118*(21). https://doi.org/10.1073/pnas.2100686118

Feldmeyer, D. (2023). Structure and function of neocortical layer 6b. *Frontiers in Cellular Neuroscience, 17*, https://doi.org/10.3389/fncel.2023.1257803

Fourcaud-Trocmé, N., Hansel, D., van Vreeswijk, C., & Brunel, N. (2003). How spike generation mechanisms determine the neuronal response to fluctuating inputs. *The Journal of Neuroscience, 23*(37), 11628-11640. https://doi.org/10.1523/JNEUROSCI.23-37-11628.2003

Freund, T. F. (2003). Interneuron diversity series: rhythm and mood in perisomatic inhibition. *Trends in Neuroscience, 26*(9). 489-495. https://doi.org/10.1016/S0166-2236(03)00227-3

Furutani, N., Hondo, M., Kageyama, H., Tsujino, N., Mieda, M., Yanagisawa, M., … Sakurai, T. (2013). Neurotensin co-expressed in orexin-producing neurons in the lateral hypothalamus plays an important role in regulation of sleep/wakefulness states. *PLOS, 8*(4), https://doi.org/10.1371/journal.pone.0062391

Gerfen, C. R., Herkenham, M., & Thibault, J. (1987). The neostriatal mosaic: II. Patch- and matrix-directed mesostriatal dopaminergic and non-dopaminergic systems. *The Journal of Neuroscience, 7*(12), 3915-3934. https://doi.org/10.1523/JNEUROSCI.07-12-03915.1987

Ghosh, A., Antonini, A., McConnell, S. K., & Shatz, C. J. (1990). Requirement for subplate neurons in the formation of thalamocortical connections. *Nature, 347*, 179-181. https://doi.org/10.1038/347179a0

Goldman-Rakic, P. S., Leranth, C., Williams, S. M., Mons, N., & Geffard, M. (1989). Dopamine synaptic complex with pyramidal neurons in primate cerebral cortex. *PNAS, 86*(22), 9015-9019. https://doi.org/10.1073/pnas.86.22.9015

Goldman-Rakic, P. S., Muly, E. C., & Williams, G. V. (2000). D1 receptors in prefrontal cells and circuits. *Brain Research Reviews, 31*(2-3), 295-301. https://doi.org/10.1016/S0165-0173(99)00045-4

Gorelova, N. A., Seamans, J. K., & Yang, C. R. (2002). Mechanisms of dopamine activation of fast-spiking interneurons that exert inhibition in rat prefrontal cortex. *Journal of Neurophysiology, 88*(6), 3150-3166. https://doi.org/10.1152/jn.00335.2002

Gorelova, N. A. & Yang, C. R. (2000). Dopamine D1/D5 receptor activation modulates a persistent sodium current in rat prefrontal cortical neurons in vitro. *Journal of Neurophysiology, 84*(1), 75-87. https://doi.org/10.1152/jn.2000.84.1.75

Gulledge, A. T. & Jaffe, D. B. (1998). Dopamine decreases the excitability of layer V pyramidal cells in the rat prefrontal cortex. *The Journal of Neuroscience, 18*(21), 9139-9151. https://doi.org/10.1523/JNEUROSCI.18-21-09139.1998

Gulledge, A. T. & Jaffe, D. B. (2001). Multiple effects of dopamine on layer V pyramidal cell excitability in rat prefrontal cortex. *Journal of Neurophysiology, 86*(2), 586-595. https://doi.org/10.1152/jn.2001.86.2.586

Gulledge, A. T. & Stuart, G. J. (2003). Action potential initiation and propagation in layer 5 pyramidal neurons of the rat prefrontal cortex: absence of dopamine modulation. *The Journal of Neuroscience, 23*(36), 11363-11372. https://doi.org/10.1523/JNEUROSCI.23-36-11363.2003

Hanson, P. I., Roth, R., Morisaki, H., Jahn, R., & Heuser, J. E. (1997). Structure and conformational changes in NSF and its membrane receptor complexes visualized by quick-freeze/deep-etch electron microscopy. *Cell, 90*(3), 523-535. doi:10.1016/s0092-8674(00)80512-7

Hay, Y. A., Andjelic, S., Badr, S., & Lambolez, B. (2015). Orexin-dependent activation of layer VIb enhances cortical network activity and integration of non-specific thalamocortical inputs. *Brain Structure and Function, 220*(6), 3497-3512. https://doi.org/10.1007/s00429-014-0869-7

Hayashi, S., Hoerder-Suabedissen, A., Kiyokage, E., Maclachlan, C., Toida, K., Knott, G., & Molnár, Z. (2021). Maturation of complex synaptic connections of layer 5 cortical axons in the posterior thalamic nucleus requires SNAP25. *Cerebral Cortex, 31*(5), 2625-2638. https://doi.org/10.1093/cercor/bhaa379

Heuer, H., Christ, S., Friedrichsen, S., Brauer, D., Winckler, M., Bauer, K., & Raivich, G. (2003). Connective tissue growth factor: a novel marker of layer VII neurons in the rat cerebral cortex. *Neuroscience, 119*(1), 43-52. doi:10.1016/s0306-4522(03)00100-3

Hevner, R. F., Shi, L., Justice, N., Hsueh, Y. P., Sheng, M., Smiga, S., … Rubenstein, J. L. R. (2001). Tbr1 regulates differentiation of the preplate and layer 6. *Neuron, 29*(2), 353-366. doi:10.1016/S0896-6273(01)00211-2

Hoerder-Suabedissen, A., Hayashi, S., Upton, L., Nolan, Z., Casas-Torremocha, D., Grant, E., ... Molnár, Z. (2018). Subset of cortical layer 6b neurons selectively innervates higher order thalamic nuclei in mice. *Cerebral Cortex, 28*(5), 1882-1897. https://doi.org/10.1093/cercor/bhy036

Hoerder-Suabedissen, A., Korrell, K. V., Hayashi, S., Jeans, A., ... Kavalali, E. T., Wilson, M. C., & Molnár, Z. (2019). Cell-specific loss of SNAP25 from cortical projection neurons allows normal development but causes subsequent neurodegeneration. *Cerebral Cortex, 29*(5), 2148-2159. https://doi.org/10.1093/cercor/bhy127

Hoerder-Suabedissen, A. & Molnár, Z. (2013). Molecular diversity of early-born subplate neurons. *Cerebral Cortex, 23*(6), 1473-1483. https://doi.org/10.1093/cercor/bhs137

Hoerder-Suabedissen, A. & Molnár, Z. (2015). Development, evolution and pathology of neocortical subplate neurons. *Nature Reviews Neuroscience, 16*, 133-146. https://doi.org/10.1038/nrn3915

Hoerder-Suabedissen, A., Wang, W. Z., Lee, S., Davies, K. E., Goffinet, A. M., Rakić, S., … Molnár, Z. (2009). Novel markers reveal subpopulations of subplate neurons in the murine cerebral cortex. *Cerebral Cortex, 19*(8), 1738-1750. https://doi.org/10.1093/cercor/bhn195

Huang, Y. Y. & Kandel, E. R. (1995). D1/D5 receptor agonists induce a protein synthesis-dependent late potentiation in the CA1 region of the hippocampus. *PNAS, 92*(7), 2446-2450. https://doi.org/10.1073/pnas.92.7.2446

Jones, B. E. (2008). Modulation of cortical activation and behavioral arousal by cholinergic and orexinergic systems. *Annals of the New York Academy of Sciences, 1129*(1), 26-34. https://doi.org/10.1196/annals.1417.026

Kanold, P. O. & Luhmann, H. J. (2010). The subplate and early cortical circuits. *Annual Review of Neuroscience, 33*, 23-48. https://doi.org/10.1146/annurev-neuro-060909-153244

Karimi, S., Hamidi, G., Fatahi, Z., & Haghparast, A. (2019). Orexin 1 receptors in the anterior cingulate and orbitofrontal cortex regulate cost and benefit decision-making. *Progress in Neuro-Psychopharmacology and Biological Psychiatry, 89*(8), 227-235. https://doi.org/10.1016/j.pnpbp.2018.09.006

Kolk, S. M. & Rakic, P. (2022). Development of prefrontal cortex. *Neuropsychopharmacology, 47*(1), 41-57. https://doi.org/10.1038/s41386-021-01137-9

Korrell, K. V., Disser, J., Parley, K., Vadisiute, A., Requena-Komuro, M. C., … Molnár, Z., & Hoerder-Suabedissen, A. (2019). Differential effect on myelination through abolition of activity-dependent synaptic vesicle release or reduction of overall electrical activity of selected cortical projections in the mouse. *Journal of Anatomy, 235*(3), 452-467. https://doi.org/10.1111/joa.12974

Kostovic, I. (2024). Development of the basic architecture of neocortical circuitry in the human fetus as revealed by the coupling spatiotemporal pattern of synaptogenesis along with microstructure and macroscale in vivo MR imaging. *Brain Structure and Function,* https://doi.org/10.1007/s00429-024-02838-9

Kostovic, I. & Rakic, P. (1980). Cytology and time of origin of interstitial neurons in the white matter in infant and adult human and monkey telencephalon. *Journal of Neurocytology, 9*(2), 219-242. https://doi.org/10.1007/BF01205159

Kostovic, I. & Rakic, P. (1990). Developmental history of the transient subplate zone in the visual and somatosensory cortex of the macaque monkey and human brain. *Journal of Comparative Neurology, 297*(3), 441-470. https://doi.org/10.1002/cne.902970309

Krone, L. B., Yamagata, T., Blanco-Duque, C., Guillaumin, M . C. C., Kahn, M. C., van der Vinne, V., … Vyazovskiy, V. V. (2021). A role for the cortex in sleep-wake regulation. *Nature Neuroscience, 24*(9), 1210-1215. https://doi.org/10.1038/s41593-021-00894-6

Lak, A., Okun, M., Moss, M. M., Gurnani, H., Farrell, K., Wells, M. J., …Carandini, M. (2020). Dopaminergic and prefrontal basis of learning from sensory confidence and reward value. *Neuron, 105*(4), 700-711. https://doi.org/10.1016/j.neuron.2019.11.018

Lançon, K., Qu, C., Navratilova, E., Porreca, F., & Séguéla, P. (2021). Decreased dopaminergic inhibition of pyramidal neurons in anterior cingulate cortex maintains chronic neuropathic pain. *Cell Reports, 37*(9), https://doi.org/10.1016/j.celrep.2021.109933

Lavin, A. & Grace, A. A. (2001). Stimulation of D1-type dopamine receptors enhances excitability in prefrontal cortical pyramidal neurons in a state-dependent manner. *Neuroscience, 104*(2), 335-346. https://doi.org/10.1016/S0306-4522(01)00096-3

Law-Tho, D., Hirsch, J. C., & Crepel, F. (1994). Dopamine modulation of synaptic transmission in rat prefrontal cortex: an in vitro electrophysiological study. *Neuroscience Research, 21*(2), 151-160. https://doi.org/10.1016/0168-0102(94)90157-0

Lee, S. P., So, C. H., Rashid, A. J., Varghese, G., Cheng, R., Lança, A. J., … George, S. R. (2004). Dopamine D1 and D2 receptor co-activation generates a novel phospholipase C-mediated calcium signal. *The Journal of Biological Chemistry, 279*(34), 35671-35678. doi:10.1074/jbc.M401923200

Li, Y., Li, S., Wei, C., Wang, H., Sui, N., & Kirouac, G. J. (2010). Orexins in the paraventricular nucleus of the thalamus mediate anxiety-like responses in rats. *Psychopharmacology, 212*(2), 251-265. https://doi.org/10.1007/s00213-010-1948-y

López-Bendito, G. & Molnár, Z. (2003). Thalamocortical development: how are we going to get there. *Nature Reviews, 4*(4), 276-289. https://doi.org/10.1038/nrn1075

Lynd-Balta, E. & Haber, S. N. (1994). The organization of midbrain projections to the striatum in the primate: sensorimotor-related striatum versus ventral striatum. *Neuroscience, 59*(3), 625-640. https://doi.org/10.1016/0306-4522(94)90182-1

Magnani, D., Hasenpusch-Theil, K., & Theil, T. (2013). Gli3 controls subplate formation and growth of cortical axons. *Cerebral Cortex, 23*(11), 2542-2551. https://doi.org/10.1093/cercor/bhs237

Marin-Padilla, M. (1971). Early prenatal ontogenesis of the cerebral cortex (neocortex) of the cat (Felis domestica). A Golgi study. *Zeitschrift für Anatomie und Entwicklungsgeschichte, 134*(2), 117-145. https://doi.org/10.1007/BF00519296

Marx, M. & Feldmeyer, D. (2013). Morphology and physiology of excitatory neurons in layer 6b of the somatosensory rat barrel cortex. *Cerebral Cortex, 23*(12), 2803-2817. https://doi.org/10.1093/cercor/bhs254

Marx, M., Qi, G., Hanganu-Opatz, I. L., Kilb, W., Luhmann, H. J., & Feldmeyer, D. (2017). Neocortical layer 6B as a remnant of the subplate – a morphological comparison. *Cerebral Cortex, 27*(2), 1011-1026. https://doi.org/10.1093/cercor/bhv279

McConnell, S. K., Ghosh, A., & Shatz, C. J. (1989). Subplate neurons pioneer the first axon pathway from the cerebral cortex. *Science, 245*(4921), 978-982. doi:10.1126/science.2475909

McFadden, K. & Minshew, N. J. (2013). Evidence for dysregulation of axonal growth and guidance in the etiology of ASD. *Frontiers in Human Neuroscience, 7*(671), https://doi.org/10.3389/fnhum.2013.00671

McKellar, C. E. & Shatz, C. J. (2009). Synaptogenesis in purified cortical subplate neurons. *Cerebral Cortex, 19*(8), 1723-1737. https://doi.org/10.1093/cercor/bhn194

Messore, F., Therpurakal, R. N., Dufour, J. P., Hoerder-Suabedissen, A., ... Lak, A., Bannerman, D., Mann, E., & Molnár, Z. (2024). An orexin-sensitive subpopulation of layer 6 neurons regulates cortical excitability and anxiety behaviour. *bioRxiv*, https://doi.org/10.1101/2024.07.25.605138

Miller, E. K. & Cohen, J. D. (2001). An integrative theory of prefrontal cortex function. *Annual Review of Neuroscience, 24*, 167-202. https://doi.org/10.1146/annurev.neuro.24.1.167

Miller, E. K. & Wallis, J. D. (2009). Executive function and higher-order cognition: definition and neural substrates. *Encyclopedia of Neuroscience, 4*, 99-104. https://doi.org/10.1016/B978-008045046-9.00418-6

Molnár, Z. & Blakemore, C. (1995). How do thalamic axons find their way to the cortex. *Trends in Neuroscience, 18*(9), 389-397. https://doi.org/10.1016/0166-2236(95)93935-Q

Molnár, Z., López-Bendito, G., Small, J., Partridge, L. D., Blakemore, C., & Wilson, M. C. (2002). Normal development of embryonic thalamocortical connectivity in the absence of evoked synaptic activity. *The Journal of Neuroscience, 22*(23), 10313-10323. https://doi.org/10.1523/JNEUROSCI.22-23-10313.2002

Momiyama, T., Sim, J. A., & Brown, D. A. (1996). Dopamine D1-like receptor-mediated presynaptic inhibition of excitatory transmission onto rat magnocellular basal forebrain neurons. *Journal of Physiology, 495*(1), 97-106. https://doi.org/10.1113/jphysiol.1996.sp021576

Muly, E. C., Szigeti, K., & Goldman-Rakic, P. S. (1998). D1 receptor in interneurons of macaque prefrontal cortex: distribution and subcellular localization. *The Journal of Neuroscience, 18*(24), 10553-10565. https://doi.org/10.1523/JNEUROSCI.18-24-10553.1998

Oeschger, F. M., Wang, W. Z., Lee, S., García-Moreno, F., Goffinet, A. M., Arbonés, M. L., … Molnár, Z. (2012). Gene expression analysis of the embryonic subplate. *Cerebral Cortex, 22*(6), 1343-1359. https://doi.org/10.1093/cercor/bhr197

Olsen, S. R., Bortone, D. S., Adesnik, H., & Scanziani, M. (2012). Gain control by layer six in cortical circuits of vision. *Nature, 483*, 47-52. https://doi.org/10.1038/nature10835

Osheroff, H. & Hatten, M. E. (2009). Gene expression profiling of preplate neurons destined for the subplate: genes involved in transcription, axon extension, neurotransmitter regulation, steroid hormone signaling, and neuronal survival. *Cerebral Cortex, 19*, i126-i134. https://doi.org/10.1093/cercor/bhp034

Ott, T., Jacob, S. N., & Nieder, A. (2014). Dopamine receptors differentially enhance rule coding in primate prefrontal cortex neurons. *Neuron, 84*(6), 1317-1328. http://dx.doi.org/10.1016/j.neuron.2014.11.012

Pavăl, D. (2017). A dopamine hypothesis of autism spectrum disorder. *Developmental Neuroscience, 39*(5), 355-360. https://doi.org/10.1159/000478725

Perrenoud, Q., Rossier, J., Geoffroy, H., Vitalis, T., & Gallopin, T. (2013). Diversity of GABAergic interneurons in layer Via and VIb of mouse barrel cortex. *Cerebral Cortex, 23*(2), 423-441. https://doi.org/10.1093/cercor/bhs032

Picciotto, M. R., Higley, M. J., & Mineur, Y. S. (2012). Acetylcholine as a neuromodulator: cholinergic signaling shapes nervous system function and behavior. *Neuron, 76*(1), 116-129. http://dx.doi.org/10.1016/j.neuron.2012.08.036

Poirier, M. A., Xiao, W., Macosko, J. C., Chan, C., Shin, Y. K., & Bennett, M. K. (1998). The synaptic SNARE complex is a parallel four-stranded helical bundle. *Nature Structural Biology, 5*(9), 765-769. https://doi.org/10.1038/1799

Popescu, A. T., Zhou, M. R., & Poo, M. (2016). Phasic dopamine release in the medial prefrontal cortex enhances stimulus discrimination. *PNAS, 113*(22), E3169-E3176. https://doi.org/10.1073/pnas.1606098113

Prensa, L. & Parent, A. (2001). The nigrostriatal pathway in the rat: a single-axon study of the relationship between dorsal and ventral tier nigral neurons and the striosome/matrix striatal compartments. *The Journal of Neuroscience, 21*(18), 7247-7260. https://doi.org/10.1523/JNEUROSCI.21-18-07247.2001

Rao, S. G., Williams, G. V., & Goldman-Rakic, P. S. (1999). Isodirectional tuning of adjacent interneurons and pyramidal cells during working memory: evidence for microcolumnar organization in PFC. *Journal of Neurophysiology, 81*(4), 1903-1916. https://doi.org/10.1152/jn.1999.81.4.1903

Rizo, J. & Südhof, T. C. (2012). The membrane fusion enigma: SNAREs, Sec1/Munc18 proteins, and their accomplices—guilty as charged. *Annual Review of Cell and Developmental Biology, 28*, 279-308. https://doi.org/10.1146/annurev-cellbio-101011-155818

Santana, N., Mengod, G., & Artigas, F. (2009). Quantitative analysis of the expression of dopamine D1 and D2 receptors in pyramidal and GABAergic neurons of the rat prefrontal cortex. *Cerebral Cortex, 19*(4), 849-860. https://doi.org/10.1093/cercor/bhn134

Seamans, J. K., Durstewitz, D., Christie, B. R., Stevens, C. F., & Sejnowski, T. J. (2001a). Dopamine D1/D5 receptor modulation of excitatory synaptic inputs to layer V prefrontal cortex neurons. *PNAS, 98*(1), 301-306. https://doi.org/10.1073/pnas.98.1.301

Seamans, J. K., Gorelova, N., Durstewitz, D., & Yang, C. R. (2001b). Bidirectional dopamine modulation of GABAergic inhibition in prefrontal cortical pyramidal neurons. *The Journal of Neuroscience, 21*(10), 3628-3638. https://doi.org/10.1523/JNEUROSCI.21-10-03628.2001

Seamans, J. K. & Yang, C. R. (2004). The principal features and mechanisms of dopamine modulation in the prefrontal cortex. *Progress in Neurobiology, 74*(1), 1-58. https://doi.org/10.1016/j.pneurobio.2004.05.006

Sherman, S. M. & Guillery, R. W. (2002). The role of the thalamus in the flow of information to the cortex. *Philosophical Transactions of the Royal Society of London, 357*(1428), 1695-1708. https://doi.org/10.1098/rstb.2002.1161

Sohal, V. S., Zhang, F., Yizhar, O., & Deisseroth, K. (2009). Parvalbumin neurons and gamma rhythms enhance cortical circuit performance. *Nature, 459*, 698-702. https://doi.org/10.1038/nature07991

Söllner, T. Bennett, M. K., Whiteheart, S. W., Scheller, R. H., & Rothman, J. E. (1993). A protein assembly-disassembly pathway in vitro that may correspond to sequential steps of synaptic vesicle docking, activation, and fusion. *Cell, 75*(3), 409-418. https://doi.org/10.1016/0092-8674(93)90376-2

Stagkourakis, S., Kim, H., Lyons, D. J., & Broberger, C. (2016). Dopamine autoreceptor regulation of a hypothalamic dopaminergic network. *Cell Reports, 15*(4), 735-747. http://dx.doi.org/10.1016/j.celrep.2016.03.062

Sutton, R. B., Fasshauer, D., Jahn, R., & Brunger, A. T. (1998). Crystal structure of a SNARE complex involved in synaptic exocytosis at 2.4 Å resolution. *Nature, 395*, 347-353. https://doi.org/10.1038/26412

Thompson, J. L., Yang, J., Lau, B., Liu, S., Baimel, C., Kerr, L. E., … Borgland, S. L. (2016). Age-dependent D1-D2 receptor coactivation in the lateral orbitofrontal cortex potentiates NMDA receptors and facilitates cognitive flexibility. *Cerebral Cortex, 26*(12), 4524-4539. https://doi.org/10.1093/cercor/bhv222

Tritsch, N. X. & Sabatini, B. L. (2012). Dopaminergic modulation of synaptic transmission in cortex and striatum. *Neuron, 76*(1), 33-50. http://dx.doi.org/10.1016/j.neuron.2012.09.023

Tsujino, N. & Sakurai, T. (2013). Role of orexin in modulating arousal, feeding, and motivation. *Frontiers in Behavioral Neuroscience, 7*(28), https://doi.org/10.3389/fnbeh.2013.00028

Vander Weele, C. M., Siciliano, C. A., Matthews, G. A., Namburi, P., Izadmehr, E. M., Espinel, I. C., … Tye, K. M. (2018). Dopamine enhances signal-to-noise ratio in cortical-brainstem encoding of aversive stimuli. *Nature, 563*, 397-401. https://doi.org/10.1038/s41586-018-0682-1

Vasistha, N. A., García-Moreno, F., Arora, S., Cheung, A. F. P. Arnold, S. J., Robertson, E. J., & Molnár, Z. (2014). Cortical and clonal contribution of Tbr2 expressing progenitors in the developing mouse brain. *Cerebral Cortex, 25*(10), 3290-3302. https://doi.org/10.1093/cercor/bhu125

Wang, J. & O'Donnell, P. (2001). D1 dopamine receptors potentiate NMDA-mediated excitability increase in layer V prefrontal cortical pyramidal neurons. *Cerebral Cortex, 11*(5), 452-462. https://doi.org/10.1093/cercor/11.5.452

Wang, W. Z., Oeschger, F. M., Montiel, J. F., García-Moreno, F., Hoerder-Suabedissen, A., Krubitzer, L., … Molnár, Z. (2011). Comparative aspects of subplate zone studies with gene expression in sauropsids and mammals. *Cerebral Cortex, 21*(10), 2187-2203. https://doi.org/10.1093/cercor/bhq278

Washbourne, P., Thompson, P. M., Carta, M., Costa, E. T., Mathews, J. R., López-Bendito G., Molnár, Z., …Wilson, M. C. (2002). Genetic ablation of the t-SNARE SNAP-25 distinguishes mechanisms of neuroexocytosis. *Nature Neuroscience, 5*(1), 19-26. https://doi.org/10.1038/nn783

Wegiel, J., Kuchna, I., Nowicki, K., Imaki, H., Wegiel, J., Marchi, E., … Wisniewski, T. (2010). The neuropathology of autism: defects of neurogenesis and neuronal migration, and dysplastic changes. *Acta Neuropathologica, 119*(6), 755-770. https://doi.org/10.1007/s00401-010-0655-4

Williams, G. V. & Goldman-Rakic, P. S. (1995). Modulation of memory fields by dopamine D1 receptors in prefrontal cortex. *Nature, 376*, 572-575. https://doi.org/10.1038/376572a0

Willsey, A. J., Sanders, S. J., Li, M., Dong, S., Tebbenkamp, A. T., Muhle, R. A., … State, M. W. (2013). Coexpression networks implicate human midfetal deep cortical projection neurons in the pathogenesis of autism. *Cell, 155*(5), 997-1007. https://doi.org/10.1016/j.cell.2013.10.020

Yan, J., He, C., Xia, J. X., Zhang, D., & Hu, Z. A. (2012). Orexin-A excites pyramidal neurons in layer 2/3 of the rat prefronal cortex. *Neuroscience Letters, 520*(1), 92-97. https://doi.org/10.1016/j.neulet.2012.05.038

Yang, C. R. & Seamans, J. K. (1996). Dopamine D1 receptor actions in layers V-VI rat prefrontal cortex neurons in vitro: modulation of dendritic-somatic signal integration. *The Journal of Neuroscience, 16*(5), 1922-1935. https://doi.org/10.1523/JNEUROSCI.16-05-01922.1996

Young, C. E. & Yang, C. R. (2004). Dopamine D1/D5 receptor modulates state-dependent switching of soma-dendritic Ca2+ potentials via differential protein kinase A and C activation in rat prefrontal cortical neurons. *The Journal of Neuroscience, 24*(1), 8-23. https://doi.org/10.1523/JNEUROSCI.1650-03.2004

Zheng, P., Zhang, X. X., Bunney, B. S., & Shi, W. X. (1999). Opposite modulation of cortical N-methyl-D-aspartate receptor-mediated responses by low and high concentrations of dopamine. *Neuroscience, 91*(2), 527-535. doi:10.1016/S0306-4522(98)00604-6

Zolnik, T. A., Bronec, A., Ross, A., Staab, M., Sachdev, R. N. S., Molnár, Z., Eickholt, B. J., & Larkum, M. E. (2023). Layer 6b controls brain state via apical dendrites and the higher-order thalamocortical system. *Neuron, 112*(5). https://doi.org/10.1016/j.neuron.2023.11.021

Zolnik, T. A., Ledderose, J., Toumazou, M., Trimbuch, T., Oram, T., Rosenmund, C., Eickholt, B. J., Sachdev, R. N. S., & Larkum, M. E. (2020). Layer 6b is driven by intracortical long-range projection neurons. *Cell Reports, 30*(10), 3492-3505. https://doi.org/10.1016/j.celrep.2020.02.044